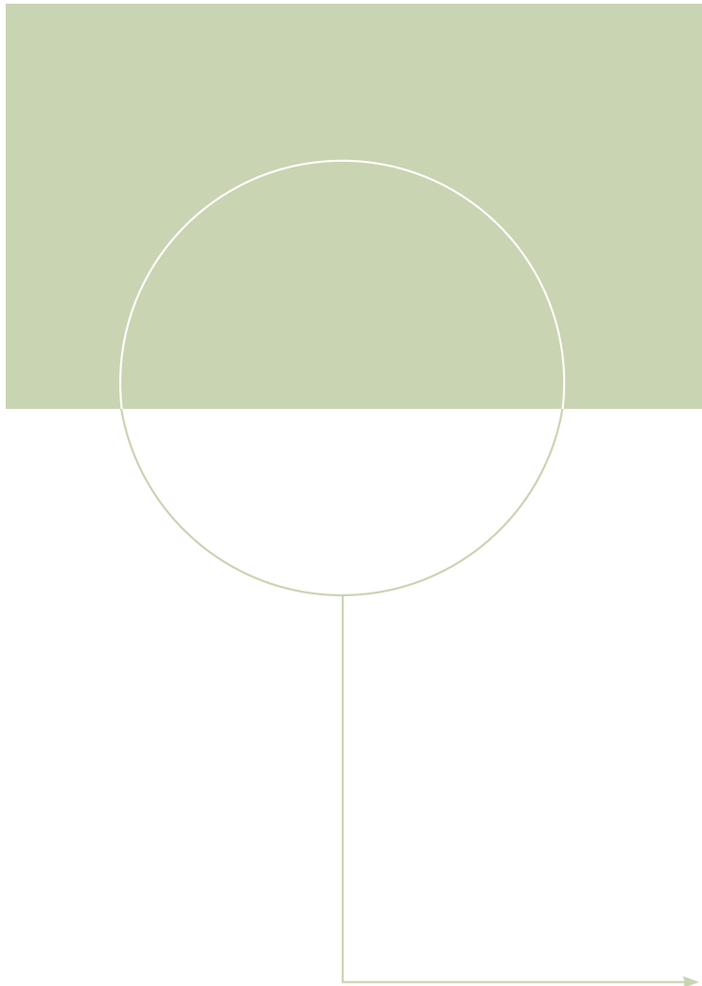

Master's thesis

2019

Simon Johan Nilsen Lingaas

NTNU
Norwegian University of
Science and Technology
Faculty of Engineering
Department of Energy and Process Engineering

Simon Johan Nilsen Lingaas

Heat-to-power conversion from variable surplus heat sources utilizing a thermal energy storage

June 2019

NTNU
Norwegian University of
Science and Technology

NTNU
Norwegian University of
Science and Technology

NTNU
Norwegian University of
Science and Technology

Heat-to-power conversion from variable surplus heat sources utilizing a thermal energy storage

Simon Johan Nilsen Lingaas

Master of Science in Energy and Environmental Engineering
Submission date: June 2019
Supervisor: Petter Nekså
Co-supervisor: Trond Andresen
Brede Andre Larsen Hagen

Norwegian University of Science and Technology
Department of Energy and Process Engineering

Norwegian University of Science and Technology

Faculty of Engineering Science and Technology
Department of Energy and Process Engineering

EPT-M

NTNU

MASTER WORK

for

Student Simon Johan Lingaas

Spring 2019

Heat-to-power conversion from variable surplus heat sources utilizing a thermal energy storage

Varme-to-kraft konvertering fra variable spillvarmekilder med integrert varmelager

Background and objective

In lack of competitive options, vast amounts of industrial surplus heat are dumped to the ambient all over the globe. If a local or internal need for heat exist, direct use of the heat will most often be a cost efficient option, but the local heat demand is often much lower than the amount of available heat from an industrial plant.

Many of the heat sources are very intermittent in nature, e.g. cooling of metal from foundries. These heat sources may be very attractive in temperature level but are challenging to utilise due to high energy output only in distinct periods. It is therefore of great interest to explore integration of some form of thermal storage for buffering in the overall energy capture and conversion system.

The FME HighEFF centre, where both NTNU and SINTEF Energy Research are partners, aims to develop new solutions for industrial surplus heat recovery and conversion.

The goal of this Master work is to systematically explore the potential benefit of thermal buffering in surplus heat recovery and conversion systems. The goal is to define suitable heat source characteristics, develop a numerical model for system analysis, and identify enhancement potential, dimensioning parameters for heat exchangers and energy storage, and describe observable trends in results.

The potential for improvement of the overall energy should be quantifiable. The heat source characteristics can be based on realistic conditions found in industry, or theoretical in order to isolate and emphasize certain aspects. The Master work will build on the modelling and work performed during the Project work.

The following tasks are to be considered:

1. Literature survey related to heat exchangers dominantly capturing radiative heat
2. Enhance the dynamic model developed during the Project work to describe the different elements of the heat recovery system, thermal storage and heat utilization part in more detail,

Address
N-7034 Trondheim
Norway

Location
K. Hejes vei 1b

Tel. +47 73 59 38 60
Fax +47 73 59 35 80
Org. no. NO 974 767 880

also including practical design elements and a possibility to make initial economic evaluation of a full system.
3. Validate the different parts of the model with information from literature and practical design considerations.
4. Implement a suitable control system for the different parts of the overall energy system
5. Utilise the model to investigate concepts for capture and utilization of intermittent heat sources both of high and medium temperatures, e.g. 1000'C and 400'C, and quantify and compare the potential for practical implementation and impact in the industry
6. Make a draft scientific paper based on the work performed
7. Propose a plan for further work

-- “ --

Department for Energy and Process Engineering, January 15, 2019

_____

Adjunct Prof. Petter Nekså
Supervisor

Co-Supervisor(s):
Brede A. L. Hagen, NTNU
Trond Andresen, SINTEF Energy Research

Summary

The goal of this work was to explore the potential benefit of thermal buffering in surplus heat recovery systems. The work examined the possibility to integrate a form of thermal energy storage into a heat recovery system to better handle heat sources of a highly variable nature. A thermal storage will enable a general disconnect between heat supply and demand, meaning the storage can be used to buffer excess heat during periods of high heat output from a heat source, which can be delivered later, once heat output from the heat source is lower. This could potentially be beneficial in heat recovery from a variable waste heat source, where the variations in heat would otherwise prove challenging for electrical power conversion. By integrating a thermal storage in a waste heat recovery system, such heat sources could become less troublesome in electrical power conversion use cases.

The potential for energy recovery from a variable heat source was explored using a case study. The case configuration and parameters were based on data and description of an existing silicon casting process at Elkem Salten, where large amounts of heat has to be removed as silicon is cooled from 1450°C to 25°C. This case fits the requirements of a variable heat source, as heat source temperatures will decline as the silicon is cooled, while the casting process is a batch process, where new, hot silicon is only added for cooling every second hour, meaning the heat released by the cooling silicon will fluctuate a lot during every two-hour period. To recover this heat, a heat recovery system was proposed. The proposed system consisted of a waste heat recovery unit (WHRU), a thermal energy storage and a power cycle, all connected by a closed loop where a heat transfer fluid is circulated.

A dynamic model of the heat recovery system was developed using a dynamic model formulation in the programming language Modelica. A literature study was conducted to gain insight into waste heat recovery units capable of recovering mostly radiative heat, which was helpful when deciding on the WHRU. The thermal storage consisted of a number of parallel heat transfer tubes embedded in a concrete volume, where heat is stored as the concrete is heated. The storage was chosen due to the simplicity of storage operation and the low cost of storage materials. In order to limit the scope of the work, the power cycle was not properly modeled. The potential for electrical power production was instead estimated through the available exergy transferred in the heat from the loop to the power cycle. The model was used to examine the proposed system, find a suitable system design and examine how the system design would affect heat recovery and the casting process itself, especially how the WHRU would affect silicon solidification rates. Some time was spent examining the viability of different control schemes, and an initial economic evaluation of the system was conducted.

The results showed that the integration of an energy storage proved effective at ensuring more stable operating conditions for the power cycle. A well-designed system would reduce the variations in heat and temperature experienced by the power cycle by over 85%, meaning power cycle operating conditions improved tremendously due to the integration of a storage. The system was at most found to produce 796 kWh of electric energy every two hours, which corresponds to 0.68% of the electric energy required in the silicon production process. It was also found that the proposed heat recovery unit could disturb the casting process. This should not happen, as that would impact the quality of the silicon product. Careful design of the heat recovery cycle, and especially the mold depth and surface area, was shown to be vital to ensuring proper casting conditions and solidification times. The system showed potential, both as it demonstrated the possibility to recover silicon casting heat, and because the integration of the storage proved successful at reducing cyclic variations in power cycle operating conditions.

Sammendrag

Målet med dette arbeidet var å undersøke den potensielle nytten av termisk buffring i et varmegjennvinningssystem. Arbeidet undersøkte muligheten for å integrere en form for termisk lagring inn i et varmegjennvinningssystem for å bedre håndtere varmekilder som er veldig variable. Et termisk lager kan gjøre det mulig å separere varmeforsyning og etterspørsel, noe som betyr at lageret kan brukes til å buffre overflødig varme i perioder med høy varmeeffekt fra en varmekilde som kan leveres senere når varmeproduksjonen fra varmekilden er lavere. Dette kan potensielt være fordelaktig ved varmegjenvinning fra en variabel varmekilde, der variasjonene i varme ellers ville vært utfordrende for elektrisk kraftkonvertering. Ved å integrere et termisk lager inn i et gjenvinningsanlegg for avfallsvarme kan slike varmekilder bli mindre utfordrende ved bruk til elektriske konverteringbruk. Et termisk lager kan gjøre det enklere å utnytte slike variable varmekilder.

Potensialet for energigjenvinning fra en variabel varmekilde ble undersøkt ved hjelp av et casestudie. Casekonfigurasjonen og parametrene var basert på data og beskrivelse av en eksisterende størkningsprosess ved Elkem Salten, hvor store mengder varme må fjernes mens silisium kjøles ned fra 1450°C til 25°C. Varmen som frigis fra silisiumet under kjølingen er svært variabel, noe som gjør at denne casen passer til dette masterarbeidet. Varmen frigitt fra silisiumet vil minke iløpet av støpingen mens silisiumet blir kaldere. Et varmegjenvinningssystem ble forslått for å gjenvinne denne varmen. Systemet bestod av en strålingsvarmeveksler (WHRU) for å fange silisiumvarmen, et termisk lager og en Rankine-syklus. En lukket sløyfe med et sirkulerende varmeoverføringsfluid vil overføre varmen mellom komponentene.

En dynamisk modell av varmegjenvinningssystemet ble utviklet ved hjelp av en dynamisk modellformulering i programmeringsspråket Modelica. Et litteraturstudie ble utført for å få innblikk i strålingsvarmevekslere, noe som var nyttig for å foreslå og modellere en WHRU. Det termiske lageret bestod av en rekke parallelle rør bygd inn i et betongvolum, hvor varme lagres ved at betongen blir varmet av fluidet i rørene. Lageret ble valgt grunnet hvor ukomplisert styringen av lageret vil være, og grunnet de lave kostnadene til betong. Rankine-syklusen ble ikke ordentlig modellert i et forsøk på å begrense omfanget av masterarbeidet. Potensialet for elektrisk kraftproduksjon ble istedenfor estimert fra eksergien i varmen som ble overført til Rankine-syklusen fra varmegjennvinningssystemet. Den ferdige modellen ble brukt til å undersøke potensialet til det foreslåtte systemet, finne et passende systemdesign og undersøke hvordan systemdesignet ville påvirke varmegjenvinning og størkningsprosessen til silisiumet. Effektiviteten av forskjellige kontrollsystemer ble undersøkt, og en enkel økonomisk evaluering av det foreslåtte systemet ble gjennomført.

Resultatene viste at integrasjonen av et energilager ville hjelpe med å sikre mer stabile driftsforhold for Rankine-syklusen. Et veldesignet system vil redusere variasjonene i varmeforsyning og temperaturer hos Rankine-syklusen med over 85%, som betyr at lageret klart forbedret driftsbetingelsene til Rankine-syklusen. Systemet ville produsere opp mot 796 kWh elektrisk energi per støkningsperiode. Dette tilsvarer 0.68% av den elektriske energien som kreves under produksjonen av silisiumet. Det ble fastslått at den foreslåtte varmegjennvinningsenheten vil påvirke størkningsprosessen, noe som ikke burde skje, da det vil påvirke kvaliteten til silisiumproduktet. Riktig utforming av varmegjennvinningssystemet, og da spesielt riktig valg av støpeformsdimensjoner vil være avgjørende for å sikre riktige støpebetingelser og størkningstider. Det forslåtte systemet har potensiale, både siden det demonstrerte muligheten for å gjenvinne størkningsvarmen til silisium, men også fordi det termiske lageret var et effektivt virkemiddel for å redusere sykliske variasjoner i driftsbetingelsene til Rankine-syklusen.

Preface

This work is my master's thesis, and it marks the conclusion of my five years as a student at the Norwegian University of Science and Technology. It has been carried out at the Department of Energy and Process Engineering, in collaboration with SINTEF Energy Research, as part of the FME HighEff.

I would like to thank my supervisors Petter Nekså, Trond Andresen and Brede Hagen for always being available for questioning, and for discussions to pave the way when I needed a direction. The discussions we have had and the interest they have shown in my work was tremendously helpful and always appreciated.

Table of Contents

List of Tables

List of Figures

Nomenclature

Symbols

A	Area, m^2
c	Specific heat capacity, $\mathrm{J}/(\mathrm{kg\,K})$
d	Silicon depth, m
d	Diameter, m
D	Tube pitch distance, m
E	Emitted radiation, W
E_b	Blackbody radiation, W
$F_{i\to j}$	Surface view factor
G	Irradiation, W
h	Specific enthalpy, $\mathrm{J/kg}$
h	Convection coefficient, $\mathrm{J\,K/m^2}$
h_{fus}	Heat of fusion, $\mathrm{W}/(\mathrm{kg\,K})$
J	Radiosity, W
k	Conductivity, $\mathrm{J}/(\mathrm{m\,K})$
k_i	PI controller gain
m	Mass, kg
$\dot{m}$	Mass flow, $\mathrm{kg/s}$
N	Number of
Nu	Nusselt number
p	Pressure, Pa
Pr	Prandtl number
R	Thermal resistance, $\mathrm{K/W}$
Re	Reynolds number
q	Net radiation heat transfer, W
$\dot{Q}$	Heat flow rate, kW
$t_{op,year}$	Yearly system operating hours, h
T	Temperature, K
T_i	PI Integral time constant
U	Internal energy, J
$\dot{V}$	Volume flow, $\mathrm{m^3/s}$
W	Work, kWh
$\dot{W}$	Power, kW

Greek symbols

α	Absorptivity
Δ	Difference
η	Heat recovery efficiency
η_{ex}	Exergy efficiency
ε	Emissivity
σ	Steffan Boltsmann constant
ρ	Density, $\mathrm{m^3/kg}$
ν	Kinematic viscosity

Subscripts

air	Air
avg	Time average
amb	Ambient
cv	Control volume
ex	Exergy
in	Control volume inlet
loss	Heat loss
L	Liquidus
out	Control volume outlet
rad	Radiation
S	Solidus
turb	Inlet of power cycle expander
wall	Side ”wall” of control volume

Abbreviations

FHP	Flat heat pipe
HTF	Heat transfer fluid
IRR	Internal rate of return
NPV	Net present value
TES	Thermal energy storage
WHRU	Waste heat recovery unit

Chapter 1

Introduction

1.1 Motivation

In order to reduce greenhouse gas emissions and lessen the effects of climate change from power production, it is vital to improve upon the energy usage in the industrial sector. This sector accounts for a large part of the global energy usage and is therefore a large contributor of emissions that may harm the environment, which means there are large potential benefits in improving upon how this sector consumes and utilizes energy. A characteristic of industrial energy usage is that much of the energy is needed for thermal processes. In the EU, thermal processes account for 70% of all energy used in the industry, and up toward a third of this heat is eventually lost (Bianchi et al., 2019). Recovering this heat would lead to better energy utilization and increased energy efficiencies, thus reducing emissions due to less need for energy. Lower industrial energy requirements could also prevent the need for the construction of new, now unnecessary power plants, which will all be associated with some unfortunate environmental consequences, be it additional from fossil fuel power plants or the environmental impact of a new hydroelectric dam. Cost savings is another potential benefit, as costs related to power requirements is often a substantial part of industrial expenses.

The Centre for an Energy Efficient and Competitive Industry for the Future (HighEFF), where both NTNU and SINTEF Energy Research are partners, aims to develop new solutions for industrial surplus heat recovery and conversion. Often, the waste heat to be recovered are intermittent or highly variable. These heat sources are challenging to utilize in a power conversion system due to their variations, but they can be attractive due to high energy content at certain intervals. Thus it is of interest to examine means to recover heat from such variable surplus heat sources, while reducing the variations in heat when releasing this heat to a power conversion system, making the heat source far more manageable for the conversion system.

This work will examine this by introducing a thermal energy storage (TES) into a heat recovery system. The storage will act as a buffer, storing heat during periods of high heat load, which will be delivered to the power cycle during periods with lower heat loads. It is of interest to examine the potential benefit to such a system and to examine the viability of a thermal storage in a surplus waste heat power conversion system. Gaining a better understanding into performance, viability, and dimensions of such a system will be helpful to better ascertain if this system can become a viable way to recover variable heat. If the thermal buffering introduced by the storage proves beneficial, systems such as this could pave the way for power conversion from heat sources which until now has been difficult to utilize.

1.2 Problem description

The objective of this Master work is to systematically explore the potential benefit of thermal buffering in an industrial waste heat recovery and conversion system. This will be done by focusing on the potential for heat recovery from the silicon casting process at Elkem Salten, where heat output from the silicon will decrease while the silicon is cooling. A system meant to recover this waste heat was proposed. A thermal energy storage will be integrated into the recovery system to act as a buffer to counteract the fluctuations in the heat recovered and to ensure a steady supply of heat to the electrical power conversion system. The proposed design will be viewed as an attempt to retrofit the current casting process to better recover waste heat, meaning the proposed system will generally try to adapt to the system in place, and it will not try to propose an entirely new silicon production process.

The proposed system must be modeled. As the objective is to examine the effect of a thermal storage, the model must be dynamic, not focusing on steady-state operation, but instead focusing on the transient behavior of an energy recovery system with a variable heat source. A literature survey will be conducted to gain some insight into current radiant heat exchangers, to better propose and model a waste heat recovery unit capable of recovering the mostly radiative heat released from the hot silicon. The model will focus on the dynamic behavior of this system, as the storage responds to the variations in heat loads from the silicon. The focus will be kept on the waste heat recovery unit and the effect of thermal buffering, while the dynamics of the power cycle will not be in focus. The entire power cycle will be imagined as an (Organic) Rankine cycle, but the modeling of the power cycle will be vastly simplified to limit the scope of the Master work. Other limitations will be the dynamics of the silicon. The mechanisms governing silicon solidification is quite complex, and a proper description of these mechanisms is outside the scope of this work. A simplification of this process was necessary, however concerns around how the silicon is affected by the waste heat recovery unit will be of interest.

Once the model has been developed, the various system components will be validated against similar components described in the literature. Then the model will be used to examine system behavior and how the integration of a storage will influence performance. An examination of how system parameters affect system behavior will be conducted in order to find a system design point where the system is well behaved and performs well. These parameters include the dimensions of the waste heat recovery unit and the layout of the thermal storage. Other aspects of the system will also be examined, such as the implementation of suitable system control schemes and an initial economic evaluation of the proposed system in order to evaluate the economic feasibility of such a system. All results will be quantified and presented as clearly and precisely as possible, and they will be analyzed and explained.

1.3 Background theory

1.3.1 Radiation heat transfer

Thermal radiation is a form of electromagnetic radiation emitted from all forms of matter with a temperature above absolute zero. The radiation intensity from a surface will depend on a variety of factors, such as the thermal properties of the emitting surface, and the temperature of the matter which emits radiation. At the same time, incident radiation onto a surface might be absorbed, reflected, re-emitted or transmitted through the surface, depending on the radiation properties of the surface.

The blackbody is an important concept in thermal radiation theory. Incorpera et al. (2005) defines a blackbody as a body that absorbs all incoming incident radiation, regardless of wavelength and direction. It also emits the most radiant energy for a prescribed temperature and wavelength. It is by definition a perfect emitter and absorber, and it is the standard which all other radiative surfaces is compared to. The Stefan-Boltzmann law describes the energy radiated from a blackbody:

$$\frac{E_b}{A} = \sigma T^4 \tag{1.1}$$

where E_b is the energy radiated from a surface with temperature T and surface area A, while σ is the Stefan-Boltzmann constant. Most surfaces are not blackbodies, and the energy radiated from these surfaces are often expressed as a fraction of the energy radiated from a blackbody at the same conditions:

$$\varepsilon = \frac{E}{E_b} = \frac{E}{\sigma T^4} \tag{1.2}$$

where ε is the emissivity of the surface, while E is the emitted radiation energy. Another important radiative property is the absorptivity, α, of a surface; the fraction of incident radiation onto a surface which is absorbed by the surface, again compared to a blackbody:

$$\alpha = \frac{G_{abs}}{G} \tag{1.3}$$

Here, G is the total incident radiation on the surface, while G_{abs} is the energy absorbed by the surface. Similarly, reflectivity is the fraction of incident radiation which is reflected off the surface. Assuming the surface is opaque, reflectivity will be:

$$\rho = 1 - \alpha \tag{1.4}$$

Emissivity, absorbtivity, and reflectivity are all properties of the surface material and will vary with surface temperature, radiation wavelength, and the radiation direction onto or from the surface. However, in this work all surfaces will be modeled as diffuse and gray, meaning radiative properties will be independent on direction and wavelength. Radiation calculations are greatly simplified if one assumes Kirchoff's law can be applied to all surfaces involved in the calculations. It states that $\varepsilon = \alpha$ where it is applicable.

As all matter above absolute zero emits thermal radiation, the *net* rate at which radiation is leaving surface i can be found by a radiation heat balance by the surface (Incorpera et al., 2005). At any surface, some irradiation will be absorbed ($\alpha_i G_i$), while some are reflected outwards ($\rho_i G_i$). At the same time, the surface will emit radiation based on the temperature of the surface (E_i). The net radiation, q_i, leaving surface i is therefore

$$q_i = A_i(E_i - \alpha_i G_i) = A_i(J_i - G_i) \tag{1.5}$$

where J_i is the surface radiosity, i.e. the total radiant energy leaving the surface. If one assumes the surface is opaque, diffuse and gray, the radiosity can be expressed as

$$J_i = E_i + \rho_i G_i = \varepsilon E_{bi} + (1 - \varepsilon) G_i \tag{1.6}$$

Then, solving Eq. 1.6 for G_i, and substituting into Eq. 1.5 gives

$$q_i = \frac{E_{bi} - J_i}{(1 - \varepsilon_i)/(\varepsilon_i A_i)}) \tag{1.7}$$

where the nominator can be seen as the heat transfer "driving force", while the denominator represents a surface radiative resistance.

The incident radiation onto surface i must originate from other radiative surfaces. G_i is therefore the sum of the incident radiation contribution from all radiative surfaces whose radiation strikes surface i. This is the basis for Eq. 1.8, which describes the total radiation heat transfer from a surface to all other radiative surfaces. Here, $F_{i \to j}$ is the view factor from surface i to j, which will be described in Subsection 1.3.2, while $q_{i \to j}$ is the net radiation heat transfer from i to j.

$$q_i = \sum_{j=1}^{N} \frac{J_i - J_j}{(A_i F_{i \to j})^{-1}} = \sum_{j=1}^{N} q_{i \to j} \tag{1.8}$$

Eqs. 1.7 and 1.8 are the basis for the thermal radiation network approach to radiation calculations. Using these equations, one can design a network of nodes, where each node corresponds to a radiating surface. A node will represent the radiosity of a surface, and Eq. 1.8 will be used to represent heat transfer between each node , while Eq. 1.7 is used to calculate net radiation into each node. For each node there are three parameters: q_i, T_i and J_i. Either surface temperature or net radiation heat flow rate must be known, meaning the network will be described by $2N$ equations for a network consisting of N surfaces. A more in-depth explanation of this method is provided by Incorpera et al. (2005).

1.3.2 View factors

In radiation heat transfer, the view factor, $F_{i \to j}$, is the portion of the radiation that leaves surface i that strikes surface j. It is a dimensionless number between 0 and 1, where 0 means no radiation leaving i will hit j, while a view factor of 1 means all radiation leaving i will strike j. The view factor value will depend on the geometries of each surface, as well as the placement of each surface relative to each other. There exists explicit equations for the calculation of view factors between simple surface geometries, such as between parallel plates or inside coaxial cylinders. Incorpera et al. (2005) provide an overview of some of these view factor equations. Often, view factors between more complex surface geometries can be constructed using known view factors between simple surfaces, and some view factor correlations, namely Eqs. 1.9, 1.10 and 1.11.

$$A_i F_{i \to j} = A_j F_{j \to i} \tag{1.9}$$

$$\sum_{j=1}^{N} F_{i \to j} = 1 \tag{1.10}$$

$$F_{i \to j,k} = F_{i \to j} + F_{i \to k} \tag{1.11}$$

1.3.3 Exergy

Exergy is the maximum useful work which can be extracted from a system as it is reversibly brought into equilibrium with its surroundings. It is the capacity of energy to do mechanical work (Gundersen, 2009). It is also a measure of energy quality, as various forms of energy are capable of varying degrees of mechanical work. This is especially important when it comes to thermal energy (heat), which is of a lower quality than many other forms of energy, such as mechanical motion or electricity. The exergy of heat is highly dependent on its temperature, with high-temperature heat having higher energy quality than low-temperature heat, thus having a higher potential of producing useful work.

The exergy of a heat stream represents the *maximum* amount of useful work which can theoretically be extracted, and it requires a reversible process to do so. No real process is reversible, as losses and irreversibilities will reduce the actual amount of useful work which can be recovered and. Nevertheless, the exergy of the heat is still a useful point of reference when estimating the potential of a heat stream in a heat recovery process.

Unlike energy, exergy can be destroyed. The exergy of heat is destroyed, or lost to us, when the source temperature is lowered and the energy quality of the heat is reduced. This is relevant in cases where heat is recovered or collected by an intermediary medium before it is transferred to a cycle to recover useful work. Due to the heat transfer to and from the intermediary medium, temperatures are lowered at the point where work is recovered, reducing the potential work from the heat. An exergy analysis can help quantify this effect.

The Carnot efficiency can be used to find the maximum available work which can theoretically be produced from a constant heat source. The work available from a heat source depends on the temperature of the heat, T_{hot}, the temperature of the surroundings, T_{amb} and the amount of heat available. The Carnot efficiency provides a measure of the theoretical maximum amount of work which can be produced by a heat engine between these two temperatures.

$$\eta_{carnot} = \frac{W_{max}}{Q} = \frac{T_{hot} - T_{amb}}{T_{hot}} \tag{1.12}$$

However, this work will focus on heat from sensible heat sources, where heat source temperatures are not constant, but continuously decreasing as heat is recovered. As such, the Carnot efficiency is modified to include a gliding heat source temperature, as shown in Eq. 1.13.

$$\eta_{system} = \frac{W_{max}}{Q} = 1 - \left(\frac{T_{amb}}{T_{hot,in} - T_{hot,out}} \right) \times \ln \left(\frac{T_{hot,in}}{T_{hot,out}} \right) \tag{1.13}$$

where $T_{hot,in}$ and $T_{hot,out}$ is the gliding temperature interval of the hot source, and W_{max} is the theoretical maximum work, i.e. the exergy of the heat.

1.3.4 The silicon production process

Silicon is commercially prepared by the reduction of silicon dioxide with carbon in a Submerged Arc Furnace (Børset, 2015). The raw materials are quarts (SiO_2) and carbonaceous reduction materials (C). The reduction material comes in to form of coke, coal, charcoal and wood chips. In addition, carbon electrodes are used (and consumed) in the Submerged Arc Furnace as electric current conductors. A simplified overall process reaction is:

$$SiO_2(s) + C(s) \rightarrow Si(l) + CO_2(g)$$

Once the furnace process is done, the product silicon has a temperature of 1600°C. The silicon is tapped from the bottom of the furnace before it is refined by slag treatment or gas purging. It is then poured into iron casting molds, where the silicon is to be cooled and solidified, with initial silicon temperatures of around 1450°C. This is the silicon casting process. When the silicon is sufficiently cooled, it is crushed into the desired particle sizes.

Temperatures above 1800°C are required in the furnace, reaching upwards of 2100°C at most. This is an energy-intensive process, and most plants use 11-13 kWh of electrical energy per kilogram of silicon produced (Børset, 2015). This corresponds to 45% of the total energy supplied to the process, while the energy contained in the raw materials and electrodes accounts for the rest. 32% of the input energy is contained in the product silicon, while the rest leaves the process as heat. Most of the heat leaves the process as heat in the off-gas from the furnace, but thermal energy is also lost by radiation and convection from the furnace walls, through cooling water, or as product heat (meaning thermal energy lost as hot silicon is cooled). Figure 1.1 shows the energy distribution of a typical silicon furnace, when scaled to a 10 MW electricity supply (Schei, 1998).

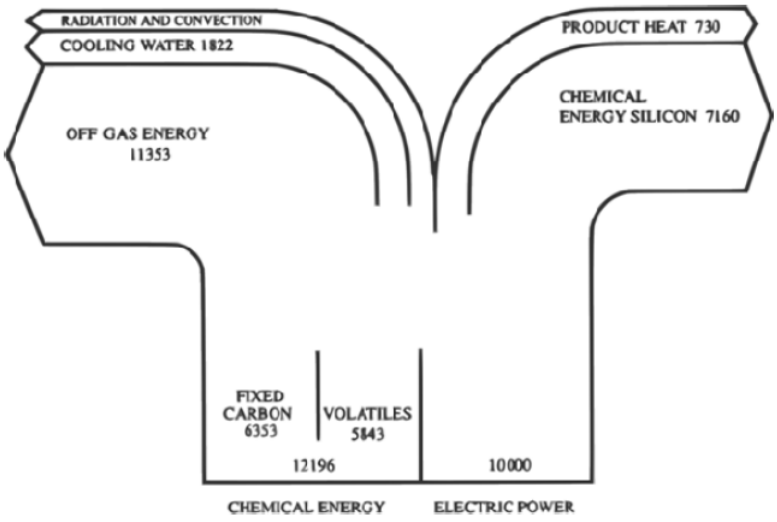

Figure 1.1: Sankey diagram for the energy flows in a 10 MW silicon furnace (Schei, 1998)

In the silicon casting process, liquid metal is poured into a metal mold and allowed to cool and solidified. The cooling rates and mold size will affect the microstructure of the silicon. This is the case for both silicon alloys and pure silicon. The rate of solidification will affect how long the silicon crystal formation will occur, and the longer it takes for the silicon to be fully solidified, the larger the silicon grain size will be (Benham et al., 2016). For instance, in ferrosilicon alloys with 75% silicon, the grain diameter is proportional to the local solidification time to the power of one third (Tveit, 1988).

Too fast cooling rates will lead to silicon grains that are very small, which cause dust, or fines, to be lost once the silicon is crushed after the casting process. The yield is reduced, but the small grains means there will be a homogeneous distribution of impurities in the silicon, which is advantageous in the silicon alloy industry. If silicon cooling rates are too slow, silicon grains will become too large, causing impurities to gather in the cracks between grains. This buildup of impurities in the cracks will lead to a nonhomogeneous distribution of impurities, which is undesirable in the silicon production industry (Benham et al., 2016). The cooling rate is not thought to affect the silicon in any meaningful way once it is fully solidified, meaning the

silicon cooling rate must be carefully controlled until it is done solidifying, as the cooling rate until this point will be critical in ensuring the quality of the end product.

The thermal energy lost as product heat will be of special interest in this work. As can be seen in Figure 1.1, about 3.3% of the total process energy input will eventually end up as product heat. This is not an insignificant amount of energy and it represents high-temperature thermal energy which is not usually recovered, meaning there is a potential for heat recovery, and thus a potential to increase energy efficiencies and energy savings. It can also be seen from the figure that the thermal energy in the off-gas is far more substantial than the thermal energy contained in the product heat. But heat recovery from the off-gas heat has already been implemented in many plants, it has received much more research, and far more commonplace than heat recovery from product heat. It is of interest to investigate heat recovery from a part of the process which has not received much attention before.

1.4 Summary of project work

This work is a continuation of a project done during the autumn of 2018. The objective of the project was to create a dynamic system model to describe heat recovery from an intermittent, discontinuous heat source. The heat source would also be decided on, and the effect of changing system parameters was to be explored and analyzed.

The primary reason for analyzing the heat recovery from an intermittent heat source was to examine the potential benefits of using a thermal storage to store excess heat. The thermal storage was thought to be able to act as a thermal buffer: storing some heat while the system experienced periods of high heat supply, then delivering the stored heat once the supply of heat lowered or disappeared. This way heat could be more evenly distributed, and highly variable heat sources could become easier to handle, making them more suitable for energy recovery.

The dynamic model was created from scratch in the modeling language Modelica. This was done to ensure full understanding of the system dynamics, and to be properly familiarized with the Modelica language. The project focused on the dynamics of the system, often simplifying the behavior of system components to decrease model complexities. The thermal storage concept chosen was a passive, sensible concrete storage, where a heat transfer fluid would pass through pipes embedded in a block of concrete. Heat would be transferred between the fluid and storage concrete depending on their temperatures.

One of the project objectives was to propose an intermittent heat source, which was used to explore the potential of the model as part of a case study. The heat source was the heat released from silicon as it cooled during the industrial production of silicon. Heat loads would initially be high, but they would continuously decrease as silicon temperatures lowered. In the dynamic model, a heat recovery unit would collect the silicon heat and deposit it to a heat transfer fluid. The fluid would be brought through the thermal storage, before heat was transferred to a power cycle, meant to produce electric power from the silicon heat. The heat transfer fluid would then be brought back to the silicon heat recovery unit, meaning the heat transfer would flow in a loop. This also means the charging and discharge of the storage would be governed by system temperatures, without any means to mechanically control it. The layout of the project work system is shown in Figure 1.2

Once the system was modeled, an analysis into which parameters affected system performance was conducted. The heat capacity of the storage was primarily found to affect how much the system fluctuates. A higher heat capacity meant more heat was stored per Kelvin increase

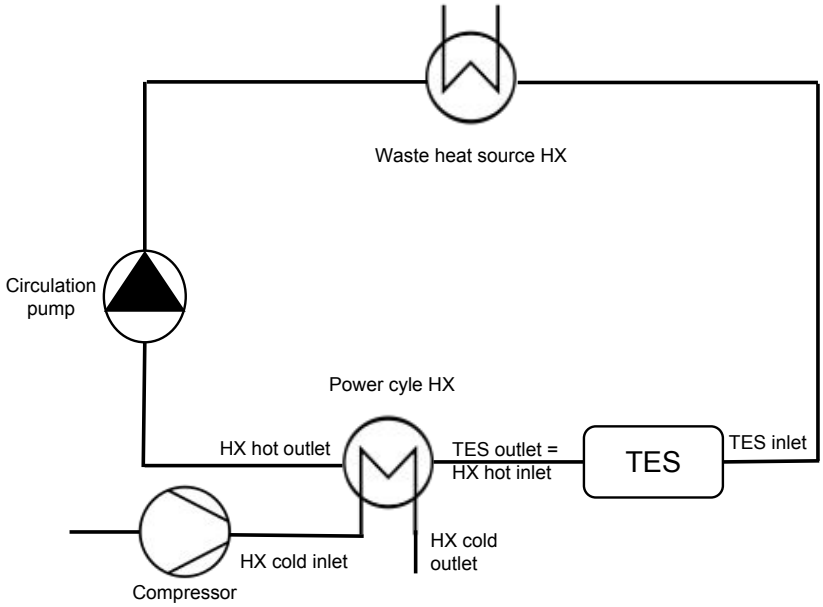

Figure 1.2: Project work system schematic

in temperature, meaning less temperature fluctuations, which in turn meant less variation in the heat delivered to the power cycle. The overall heat transfer coefficient (UA-value) of the storage would primarily govern how much heat is transferred to and from the storage, and how sudden the storage could adapt to sudden changes in temperatures and heat loads. A higher UA-value would mean the storage was better able to buffer heat during high peak loads, and better able to deposit heat during periods of heat deficiency. This effect would propagate throughout the entire loop, and it would lead to lower temperature variations in the system, which also lead to a more even deposit of heat to the power cycle.

The UA-value governing heat transfer from the loop to the power cycle was also examined. An increase in UA-value would increase power cycle temperatures, while decrease loop temperature, due to the increase in heat transfer from the loop to the power cycle. A decrease in UA value would act the opposite way, decreasing power cycle temperatures while increasing the loop and storage temperatures, while also reducing the heat recovered.

System mass flows were the final parameters which were analyzed. Unlike the other parameters, mass flow rates are not an aspect of the system which must be decided as it is designed. They can be changed during operation, meaning they can be used to actively control system operation. Changing the mass flow rate in the loop did not affect system behavior greatly. An increase in mass flow rate would decrease temperature changes throughout system components, but otherwise system performance changed very little. Changing the mass flow rate of the power cycle affected the system much more. An increase in power cycle flow rates would increase heat flows to the power cycle, which would decrease system temperatures. It would also decrease power cycle temperatures out of the heat exchanger.

The system analyzed in the project work was found to produce 48.4 kWh of electric energy per tonne silicon produced, which meant it produced 0.44% of the electric energy needed during the silicon process. The dynamic model behaved well, but a variety of simplifications and assumptions made while creating the model meant it would be a priority to improve upon the model during the Master's work, in order to make a model which would better describe the system heat transfer and performance.

Chapter 2

Literature Review

A literature survey focused on heat exchangers predominantly capturing radiant heat was conducted as part of this thesis. It was conducted in order to improve knowledge surrounding such collectors, to gain an understanding of how such heat collectors are designed, and to use the findings from this survey when deciding and modeling a heat exchanger meant to collect primarily radiant heat from an industrial waste heat source. The subject of radiant heat collectors is primarily found in the literature as part of studies into collector technologies for use in solar concentrated power. As such, time was spent investigating these technologies, to see if they could prove applicable in an industrial heat recovery setting. Time was also spent reading up on already proposed industrial heat recovery systems mainly focused on radiant heat. Findings from this survey are summarized in this chapter.

2.1 Radiation heat collectors in the solar power industry

In the literature, the most prevalent radiant heat collectors are heat exchangers involved in the capture of solar energy. A multitude of different collector technologies exists, designed for different applications and temperature ranges. Kalogirou (2014), and Sarbu and Sebarchievici (2017) provide a detailed account of available solar thermal collection technologies, some of which are summarized below.

There are two types of solar collectors: non-concentrating and concentrating collectors. A non-concentrating collector utilizes the same area for intercepting and absorbing the solar radiation, while a concentrating solar collector intercepts the solar irradiation with reflective surfaces, focusing the sun's beam radiation onto a smaller receiving area, increasing the radiation flux, thus making concentrating collectors suitable for high-temperature applications. Non-concentrating collectors are not suitable for high-temperature applications because the solar thermal energy per surface area is too low.

2.1.1 Flat-plate collector

The flat-plate collector is a non-concentrating collector usually used in collection systems designed for operation at temperatures below 100°C. It is mostly used for applications such as solar water heating, building heating, air conditioning, and industrial process heat. In a flat-plate collector, solar radiation passes through a transparent cover and impinges on an absorber

surface. Much of the energy is absorbed by the absorber plate and is transferred to a heat transfer fluid in fluid tubes connected to the absorber plate. To avoid conduction losses, both the underside and sides of the plate are insulated. The transparent cover serves several functions. It reduces convection losses from the absorber plate by restraining the stagnant air between the plate and the cover. It also reduced radiation losses from the collector: The cover is designed so that it is transparent for the shortwave radiation from the sun, but nearly opaque to the longwave thermal radiation emitted by the absorber plate. Thus the longwave radiation will be reflected off the inside of the plate, before being reabsorbed by the plate. The flat-plate collector is inexpensive, with no moving parts, and capable of capturing both beam and diffuse radiation.

2.1.2 Evacuated tube collector

Evacuated tube collectors are another non-concentrating solar collector. As with the flat plate collector, it can collect both diffusive and direct radiation. Due to measures taken to reduce heat losses, it is able to operate at higher temperatures than the previously flat-plate collector. Kalogirou (2014) reports evacuated tube collector operating temperatures of up to 200°C. The evacuated tube consists of a heat pipe inside a vacuum-sealed tube, which enables high-efficiency heat exchange using liquid-vapor phase change materials, which makes the heat pipe a highly efficient thermal conductor. It contains a small amount of fluid which undergoes an evaporating-condensing cycle. The fluid is evaporated by the solar heat and is then transported to a heat sink region, where the fluid is condensed, releasing its latent heat to some other heat transfer fluid. The vacuum-sealed tube encompassing the heat pipe helps to reduce heat losses by limiting convection and radiation heat losses. The heat pipe itself is a sealed copper pipe which is attached to black copper fins to increase radiation absorption area. At the top of the heat pipe, protruding out of the vacuum-sealed tube is a metal tip which contains the heat pipe condenser. The layout of an evacuated tube is further described in Figure 2.1. An evacuated tube collector consists of several evacuated tubes mounted side by side. Each of the heat pipe condensers is placed in a heat exchanger, where the heat released the heat pipe condensers is transferred to a heat transfer fluid flowing through the exchanger, usually water or glycol. The evacuated tube collectors are usually produced with outer diameters ranging from 30 to 100 mm and lengths of around 2 m.

2.1.3 Concentrating solar collectors

Concentrating solar collectors enable higher energy delivery temperatures. The solar concentration is done by a *concentrator*, an optical system which directs beam radiation from a large area onto the smaller solar *receiver*, which absorbs the solar radiation. Compared to a flat-plate collector, a concentrating collector can achieve higher thermodynamic efficiencies due to higher working fluid temperatures. The receiver area is smaller, which leads to smaller heat loss areas, a reduction in heat losses, and increasing thermal efficiencies. In addition, reflecting surfaces are structurally simpler than flat-plate collectors and require less material. A concentrating solar collector plant requires less area of solar collecting surface, resulting in the cost per unit area of the solar collecting surface to be lower than that of the flat-plate-collector. Some disadvantages are also present: Little to no diffuse radiation is collected, some form of tracking system is required to enable the solar collector to follow the sun, and the solar reflecting surfaces will need periodic cleaning and maintenance to avoid a reduction in solar reflection onto the receiver surface.

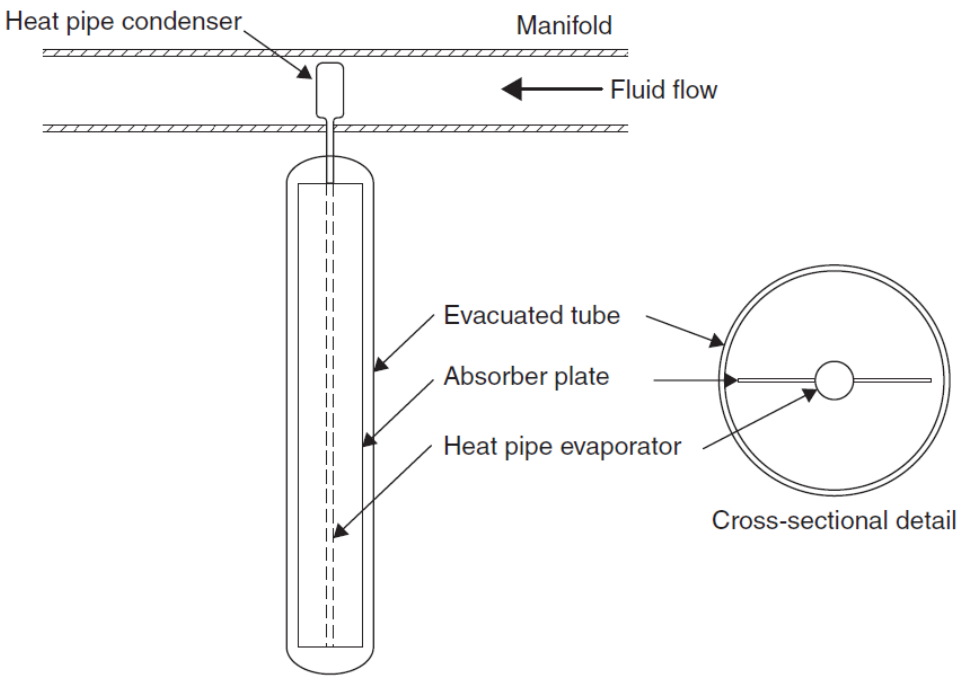

Figure 2.1: Layout of a single evacuated tube (Kalogirou, 2014)

Several different designs exist for solar concentrating collectors. The most important parameter in concentrating collectors is their concentration ratios, which is the ratio between the solar concentrator area and the receiver area. Concentration ratios vary from single digit concentration to central receiver plants with concentration ratios in the thousands. Higher concentration ratios result in higher temperatures at which energy can be delivered, but also stricter requirements for the concentrator performance. Two different concentrating solar collectors will be described.

2.1.4 Parabolic through collector

Parabolic through collectors consists of a sheet of reflective material bent into a parabolic shape and a tubular receiver stationed in the focal line of the parabolic concentrator. The receiver consists of a black metal tube covered with a glass tube to reduce convective heat losses. Figure 2.2 describes the setup. A solar tracking mechanism ensures that the parabola is pointed towards the sun at all times. Single axis sun tracking is used, rotating the collector parallel to the axis of the receiver. Long collectors modules are most often produced because of this. Beam radiation from the sun is reflected off the reflective surface of the concentrator onto the receiver tube. The concentrated radiation heats the fluid circulating inside the receiver, converting solar radiation into usable heat. It is a low cost, mature technology, capable of reaching fluid temperatures as high as 400°C or as low as 50°C. The fluid flowing through the receiver varies depending on the temperature desired for its intended application. Water is often used as the heat transfer fluid, and thermal oils are used in the upper part of the collector's temperature range (Buehler et al., 2016). CO_2 has been proposed as the working fluid in a parabolic through power plant utilizing a supercritical CO_2 Rankine cycle (Qiu et al., 2017). Parabolic through collectors are the dominant solar collector technology utilized for power production purposes. At the end of 2016, there was close to 5 GW_e of operational concentrated solar power capacity. 13% of

this capacity was from central-receiver power plants, while the rest was predominantly from parabolic through plants (Ho, 2017).

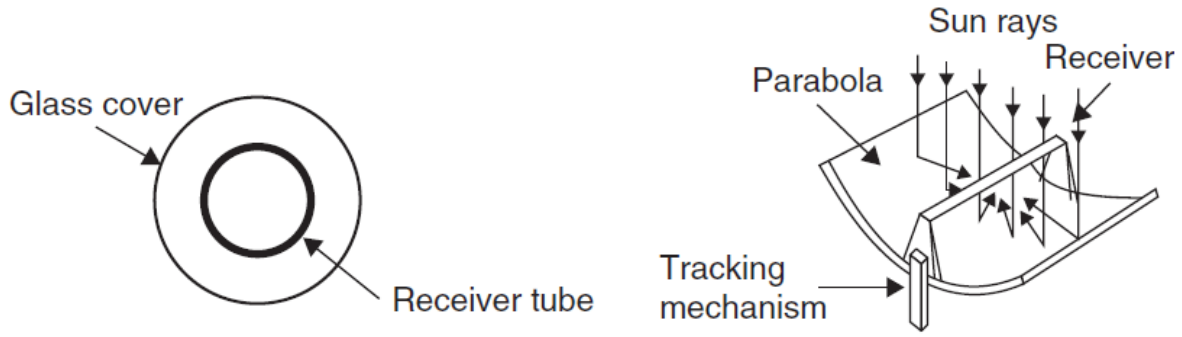

Figure 2.2: Parabolic Through Collector (Kalogirou, 2014)

2.1.5 Central receiver systems

A central receiver system, also called a heliostat field, is a concentrating solar collector with a very high concentration ratio, used to attain receiver temperatures above 1000°C. To attain such high temperatures, thousands of flat or slightly concave, sun-tracking mirrors (heliostats) are used to reflect solar beam radiation, reorienting all the concentrated solar flux toward a central receiver mounted on a tower. The heat absorbed by the receiver is transferred to a circulating fluid, which is used to produce power. Figure 2.3 describes such a plant.

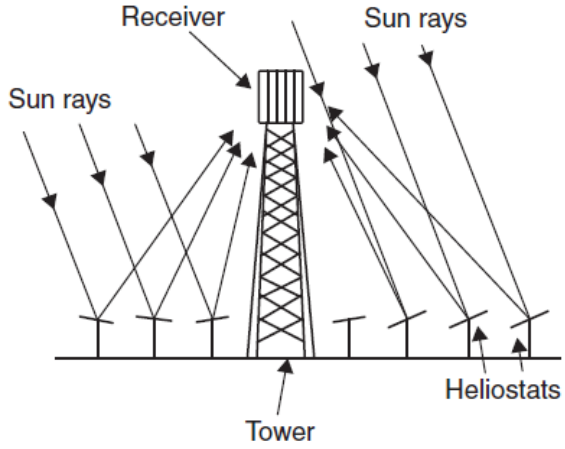

Figure 2.3: Schematic of a central receiver heliostat system (Kalogirou, 2014)

There are several designs available for the central receiver. According to Ho and Iverson (2014), there are a number of important features required in these receivers. The materials used in the heat transfer must be low-cost and durable, to ensure that they can withstand high concentration ratios. The heat transfer fluids must be able to withstand temperatures above 650°C, while the receiver must have a high solar absorptance, as well as low radiative and convective heat losses to ensure high thermal efficiencies. The central receiver designs can be categorized as either gas receivers, liquid receivers or solid particle receivers.

Gas receivers are characterized by the radiation heat being transferred to a hot gas. Such receivers are capable of achieving the highest heat transfer fluid temperatures of any central receiver (>1000°C), they can use inert and environmentally friendly gases, and heat transfer fluids utilized are low cost compared to other receiver configurations. However, they also have low thermal conductivity, flow instabilities, and often the need for costly equipment if high-pressure gases are involved. There are a number of different gas receiver technologies, each collecting the radiation heat through different means.

Volumetric air receivers use porous structures that are irradiated by concentrated sunlight. Gas flows through the porous structure and is thus heated by irradiation. The gas temperature will depend on the porous structure of the receiver: metals can result in temperatures between 800 and 1000°C, ceramic structures can reach 1200°C, while SiC can reach up to 1500°C. The temperature of the porous surface leads to significant radiative losses. Collector efficiencies range from 50 to 90%.

Tubular receivers consist of gas flowing through a mesh of tubes, where the concentrated solar beam radiation heats the tubes, which then heats the gas inside. An advantage of this is the ability to control the tube geometry. The tubes can be configured in ways to enable reflected irradiance to be trapped rather than lost to the environment, reducing radiative losses. Outlet temperatures of the gas are 700-800°C, with collector efficiencies upwards of 85%.

Microchannel gas receivers are enclosed plates with many small channels running through the plate. They operate much like the tubular gas receiver, but the plate configuration increases the surface area between the gas heat transfer fluid and the irradiated receiver walls. Collection efficiencies of up to 90% and outlet gas temperatures of 700°C are expected.

Liquid receivers utilize liquid as the heat transfer fluid. The state-of-the-art liquid receivers utilize a eutectic mixture of sodium and potassium nitrate as the heat transfer fluid, the so-called "Solar Salt". It has a relatively low freezing point of 200°C and is usable as heat transfer fluid at temperatures upwards of 600°C. According to Ho (2017), liquid receiver designs are tubular, similar to the tubular gas receiver. Most of the research into liquid receivers focus on the heat transfer fluid, rather than the receiver design itself. To reach temperatures higher than 600°C, other heat transfer fluids are researched, such as halide salts and liquid metals. As of now, solar salt remains dominant as heat transfer fluid, and tubular solar salt receivers are the most common central receiver design in commercial power plants.

Solid particle based technologies is not a commercially viable technology, but it has received some attention from researchers. In these receivers, sand-like ceramic particles fall through a cavity receiver, where they are directly irradiated by concentrated solar radiation. The solar irradiation heats the ceramic particles, which is then stored in an insulated particle storage tank, or used to heat a secondary working fluid for a power cycle, as seen in Figure 2.4.

2.2 Radiant heat recovery exchangers in the industry

2.2.1 Heat recovery from steel cooling

Jouhara et al. (2017) examined the possibility to recover waste heat in the steel making industry. They designed a heat recovery system meant to recover heat from hot steel rods during the steel cooling process. To enable this heat recovery, they designed a heat recovery system based on a flat heat pipe (FHP) exchanger. The flat heat pipe was designed to recover heat mainly by thermal radiation from heat sources with temperatures greater than 500°C. Thermal radiation

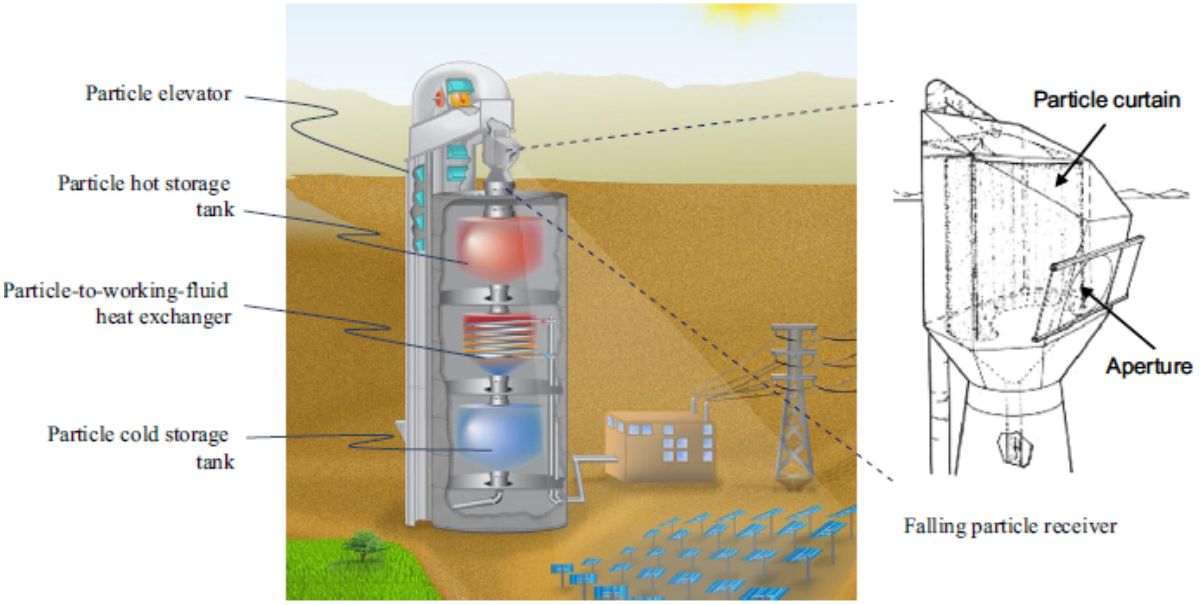

Figure 2.4: Schematic of a falling particle receiver system, with storage tank and secondary fluid heat exchange (Ho and Iverson, 2014)

was absorbed at the outer surface of the FHP, before the heat is transferred to the FHP evaporator through the surface wall. The heat vaporizes the heat pipe working fluid, which then flows upwards to the condenser, where it condenses as heat is delivered to the cooling fluid via a shell and tube heat exchanger. Once the working fluid is condensed, it flows back to the heat pipe evaporator due to gravity. A theoretical investigation into the performance of the FHP was conducted and a prototype was built to validate the results, and both laboratory and industrial tests were conducted. The prototype consisted of a single flat heat pipe exchanger, with a surface area of 1 m^2. Laboratory experiments were done using electrical heaters, with heater temperatures of 500-580°C, water flow rates of 0.42 L/min and inlet water temperatures of 11°C. Industrial tests were done on a production line during the cooling process of steel wires from 450°C to ambient, by placing the radiant heat exchanger above the manufacturing line. Figure 2.5 describes the design of the flat pipe heat exchanger and how it is placed above the hot metal during the industrial tests.

The theoretical investigation was conducted by implementing a model of the flat heat pipe exchanger to predict the performance of the FHP heat exchanger. The thermal network analogy method was used in the implementation of the model, both to describe the radiation heat absorbed on the plate and the behavior of the heat pipe. Results from the model and experiments showed very similar results, with water outlet temperatures ranging from 63 to 85°C, and an average heat transfer rate between 4.1 and 5.7 kW for the experimental tests, while the industrial tests achieved average heat transfer rates of 11.6 kW. The numerical model did not take into account the heat transfer by forced convection from the hot air above the steel wires, which caused the model result to somewhat deviate from the experimental results. The model results were found to deviate at most 6.77%, which was deemed an acceptable uncertainty value. The authors predicted a total of 700 kW of wasted heat could potentially be recovered from the industrial plant used in these experiments if similar flat heat pipe exchangers were installed along the entirety of the cooling production line.

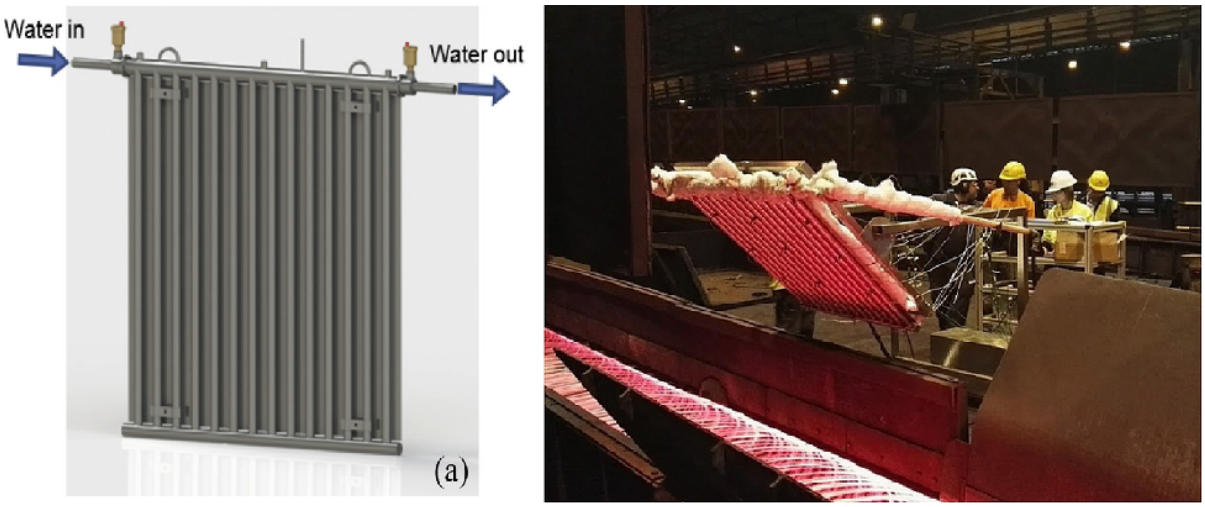

Figure 2.5: The radiative flat heat pipe heat exchanger (Jouhara et al., 2017)

2.2.2 Heat recovery from the ceramics industry

Delpech et al. (2019) sought to recover heat from the cooling process in the ceramics industry. The heat recovered were to be reused in the drying stage of the ceramics manufacturing process. This drying process occurs in a ceramics roller hearth kiln, where clay is heated by electric heaters before it is cooled to ambient temperatures. The implementation of a radiative heat pipe ceiling was investigated to recover heat inside such a kiln. The heat recovery system was composed of ten parallel heat pipes with diameters of 28 mm, connected by a bottom pipe, as well as a condenser section on the other end, where heat is transferred to the coolant medium (water). The system was designed for an operating pressure of 100 bars and was made of stainless steel. Figure 2.6 shows a model of the recovery system, as well as its integration in a kiln.

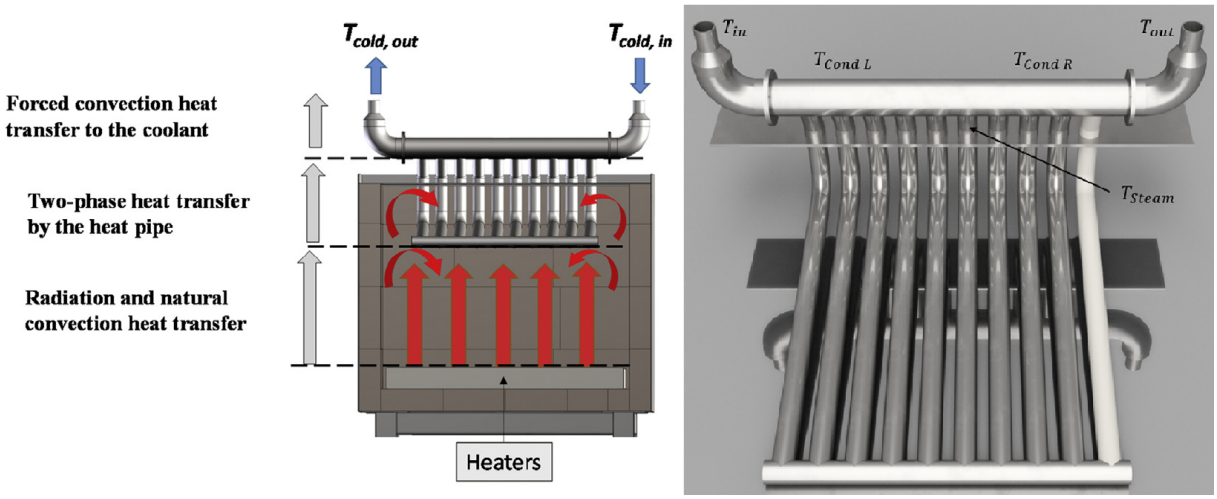

Figure 2.6: Description of the radiative heat pipe recovery system in a ceramics kiln (Delpech et al., 2019)

A theoretical model of the heat transfer was made. As with the model made by Jouhara et al. (2017), it utilizes the thermal network analogy, but special care was made to properly model the influence of the kiln on the heat released by the hot ceramic, as the hot ceramic will emit heat to the heat pipe, but also to the kiln walls. The heat pipe will absorb heat from both the hot ceramics and the hot walls, which was imperative to include in the analysis. The authors greatly simplified the thermal network by assuming the kiln was fully insulated, which meant all heat absorbed by the wall was reradiated and would eventually be absorbed by the heat pipes. Convective heat transfer was also included in this model. Experimental tests were also conducted, using heaters instead of hot ceramics, at temperatures ranging from 200°C to 500°C while varying the coolant volume flow. Experimental heat transfer rates varied depending on the heater temperatures, but reached upwards of 3000 W at 500°C heater temperatures and as low as 400 W at 200°C heater temperatures, while the heat pipe efficiencies ranged from 26 to 42%. Model results mostly agreed with the experimental results, diverging at most 15% from each other. Thermal radiation was found to be the dominating heat transfer mechanic at higher temperatures, and the water flow rate was not found to impact heat transfer rates significantly.

2.2.3 Heat recovery from rotary kilns

Caputo et al. (2011) proposed a radiant heat recovery exchanger to recover radiant heat lost through the surface of a rotary kiln. During cement production, the outer surface of the rotary kiln reaches temperatures of 400°C. Due to these high temperatures and the large size of the kilns, surface heat losses accounts for 8-15% of the total heat input. To recover this heat they proposed an external heat exchanger which were to surround the rotary kiln as a secondary shell, acting as a heat exchanger for a heat transfer fluid (water). Along this shell, an array of pressurized water-carrying tubes arranged in a longitudinal pattern would transfer heat from the shell to the pressurized water. The heat recovered were to be used in a district heating network, with returning water temperature of 90°C.

A mathematical model of the heat recovery system was made. A differential kiln element was modeled, by setting up the energy balances for the air in-between the kiln and shell surface, as well as for the water on the shell side, as shown in Figure 2.7. Convective heat transfer from the kiln to the air ($dq_a^{c''}$) and from the air to the shell surface ($dq_a^{c'}$) was modeled using Nusselt number correlations assuming forced convection. If air velocity was set sufficiently low, the convective heat transfer coefficient assumed to be similar to that of free convection (about 5 $\mathrm{W}/(\mathrm{m}^2\,\mathrm{K})$). Radiation heat transfer ($dq_{H_20}^i$) was modeled as two grey bodies with different emissivities. All radiation heat from the kiln will hit the shell surface as the rotary kiln and the heat recovery kiln is schematized as two coaxial cylinders with infinite length, simplifying the description of the radiation heat transfer.

The effect of forced convection on heat recovery was investigated. In cement manufacturing, auxiliary blowers are used to control the kiln surface temperature. The presence of such blowers in this recovery system would enable the airflow to move in a co-current or counter-current fashion in relation to the water flow, enabling forced conduction and thus higher convective heat transfer coefficients. This lead to increasing air temperatures, increasing the amount of sensible heat discharged as the air leaves the heat recovery system. While an increase in convection heat transfer would increase the air temperature, the air temperature would still be below the water temperature most of the time, meaning the increased air temperature would not result in more heat transferred to the water side. In cases were kiln surface temperatures were very high and air flow was flowing counter-current to the water flow, air temperatures at the air outlet would

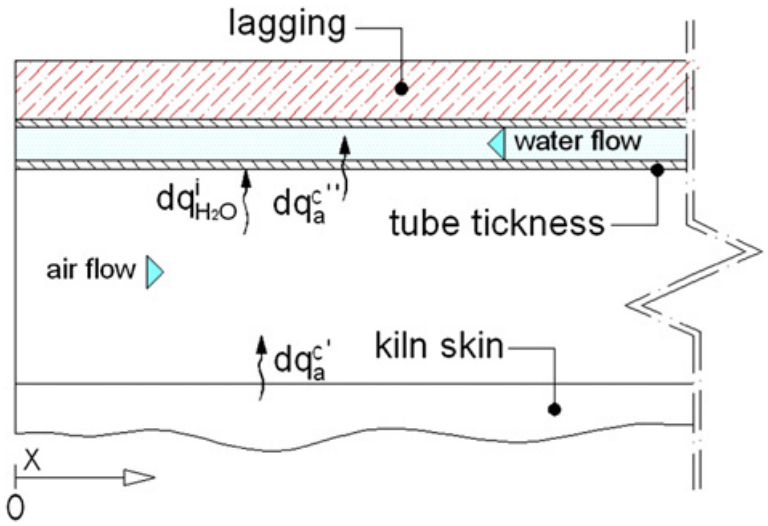

Figure 2.7: The differential kiln element (Caputo et al., 2011)

be hotter than water temperatures, but even in this case the heat transferred to the water from the hot air would be small compared to the radiant heat transfer. The forced convection proved to reduce heat uptake by the water, reducing water outlet temperatures, because more of the kiln heat was discharged out of the recovery system in the form of heated air. Thus, forced convection proved detrimental to heat recovery. The effect of kiln surface temperature was also investigated. A 20 m heat recovery exchanger would able to recover 1750 kW with an average kiln wall temperature of 400°C, while only 250 kW could be recovered with a kiln having a 200°C wall temperature.

Du et al. (2018) also investigated heat recovery from rotary kilns in the cement industry, and proposed a radiant heat recovery exchanger placed on the outside of the rotary kiln, primarily recovering radiant heat. The heat recovery system consisted of a radiant heat exchanger similar to that proposed by Caputo et al. (2011), i.e. a shell fitted with heat transfer pipes covering the rotary kiln as an outward shell. Above the rotary kiln, coiled tubes were placed to recover the heat from convection heat transfer. The heat transfer fluid was water, and water was heated from 20-30°C to 58-70°C during the testing. In these tests, it was found that convection heat transfer did prove beneficial to the heat recovery, most likely due to the lower water temperatures present in the recovery systems, which would increase the driving forces for the convection heat transfer. It was found that the heat recovery system did not disturb the cement production in any significant manner, and the recovery system helped make the shell temperature uniformly distributed along the rotary kiln. A focus on radiant heat exchange was proposed on the hotter side of the rotary kiln, while a greater emphasis on the coiled pipe convective heat transfer exchangers should be emphasized in areas where kiln surface temperatures are lower.

2.3 Remarks

The literature provided several insights into radiative heat recovery exchangers. Firstly, most radiation heat exchangers encountered in the concentrated solar power industry will not be applicable for the use case imagined in this project work. This primarily concerns the concentrating heat exchangers. There will neither be space nor possibility to use concentrating technologies, and many of the receiver systems were very complex and expensive. However,

some of the non-concentrating solar collectors were more promising. Most of these exchangers were limited to low-temperature application because the influx of solar radiation was too low for high-temperature application to be possible. If utilized with a more energy intense heat source, they could be used to achieve higher temperature heat. However, the design of these collectors is still more complex than some of the ones proposed for industrial use, and there are benefits to keeping system complexity down, both to keep investment cost and maintenance costs low. The abundant use of glass as part of collector design would also be problematic in an industrial scenario, due to the increased need for cleaning and maintenance.

Another important insight was that there is already some heat recovery from industrial waste heat sources which primarily focused on radiant heat recovery. But all the cases which were described in this chapter utilized the recovered heat for low-temperature applications, below 110°C. Very little focus was given to heat sources with higher temperatures, and no attempt was found attempting electric power conversion with heat recovered from such a source. However, they did in detail describe their models and heat collector design, which was found to be very useful when proposing and modeling a heat recovery system in Chapter 3. In addition, no focus was aimed towards cases with a variable waste heat source, as all the industrial case studies investigated waste heat sources with a steady supply of heat.

Chapter 3

System overview and model details

3.1 Case

This work is based around the silicon casting process at the Elkem Salten silicon plant. The goal is to examine the potential of recovering heat as liquid silicon, initially at 1450°C, is cooled, solidified and further cooled till it reaches its target temperature of 25°C. The heat recovered will be transferred to a Rankine cycle to generate electric power.

Silicon is produced in a Submerged Ark Furnace at Elkem Salten. After the furnace and the subsequent refinement processes are completed, silicon will be poured into suitable molds for cooling. Here, 9000 kg of silicon is poured into molds once every two hours, a pouring process which takes 30 minutes due to the amount of silicon. Once it has been poured into molds, it is cooled, first using air, then cooling water once silicon temperatures approach 1000°C. Once the content of the molds is sufficiently cold, it is removed from the molds and crushed before further refinement. The molds used for casting are placed beside each other on a rotating carousel, shown in Figure 3.1. After a mold is filled with liquid silicon, the carousel rotates, allowing a new mold to be filled. As more molds are filled, the casting mold is moved further and further around the carousel. The mold will eventually reach a section of the carousel where water will be used to accelerate the cooling process, and once silicon temperatures are sufficiently low, the silicon will be removed from the mold, having completed the casting process.

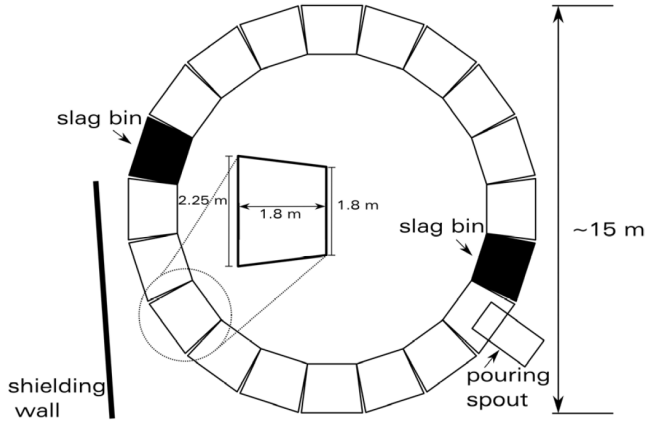

Figure 3.1: Schematic of the silicon casting process, showing the casting ladle, moulds and shielding wall as it currently stands at Elkem Salten (Børset, 2015)

The silicon releases large amounts of heat as it is cooled, heat which is not utilized in any way today. This work will propose and examine a system to better utilize this heat, by recovering the product heat and use it as a heat source for a power production cycle. But to properly design a heat recovery system based on this process, there are some important considerations to be made. A heat recovery system around the casting process faces the very real possibility of disturbing or changing the silicon cooling rate. As was discussed in Subsection 1.3.4, the rate at which the silicon solidifies will affect its microstructure, i.e. the silicon grain size. Thus, it is of utmost importance to design any recovery system in a way which does not negatively affect the microstructure, by ensuring the silicon is cooled at the proper rate until all silicon has solidified. A heat recovery system that negatively affects cooling rates will not be accepted, as it will reduce silicon yields, thus negatively affecting the primary purpose of this silicon *production* plant.

While the silicon cooling rate must be taken into account as to not disturb the silicon process, another priority must be to recover as much heat as possible from the casting process, in order to maximize the power production potential of this system. As new molds are filled with silicon every two hours, heat recovery from each batch of silicon will be limited to a two-hour period.

The properties of the silicon used in this work are shown in Table 3.1[1]. While this work refers to it as silicon, the properties used in this work is actually those of a high purity ferrosilicon, meaning solidification will occur over a temperature interval, shown in the table as the solidus and liquidus temperature. The thermal conductivity will affect the thermal gradient in the silicon and does in reality vary with temperature. The conductivity is noticeably higher before the silicon is solidified than after. Its value will therefore depend on whether it is fully solidified or not. k_l will be used for silicon temperatures above the solidus temperature, while k_s will be used otherwise (Benham et al., 2016).

Table 3.1: Properties of ferrosilicon with 75% silicon purity

Property	Unit	Value
Density, ρ	$\mathrm{kg/m^3}$	3200
Specific heat capacity, c_p	$\mathrm{kJ/(kg\,K)}$	0.812
Heat of fusion, h_{fus}	$\mathrm{kJ/kg}$	1100
Thermal conductivity before solidification, k_l	$\mathrm{W/(m\,K)}$	44
Thermal conductivity after solidification, k_s	$\mathrm{W/(m\,K)}$	23.5
Convective heat transfer coefficient, h_{air}	$\mathrm{W/(m^2\,K)}$	10
Solidus, T_S	°C	1205
Liquidus, T_L	°C	1350
Emissivity, ε	–	0.55

It is important to note that the thermal values in Table 3.1 are not necessarily the same as the properties of the silicon produced at Salten Elkem. These values were chosen to represent silicon similar to the silicon produced at Elkem, but some deviation from actual silicon properties values must be expected. This in turn means that the results attained from this model are not completely comparable to the Elkem plant.

[1]Data taken from www.matweb.com (FeSi 75 0.025 Ti High Purity Ferrosilicon), Tveit (1988), and Benham et al. (2016)

3.2 System overview

In order to better utilize the heat released as silicon is cooled, a heat recovery system was proposed. In this heat recovery system, silicon heat will act as the heat source for a Rankine cycle. The system is based on a waste heat recovery unit (WHRU), a thermal energy storage (TES) and a power cycle connected in a closed loop. A heat transfer fluid (HTF) flows through the loop, transferring heat between the system components. Heat is first transferred to the loop by a WHRU meant to capture the radiation and convective heat released by the silicon. Then, the HTF passes through a thermal storage, before depositing heat onto a power cycle, which utilizes the captured silicon heat to generate power. A concept sketch of the system is shown in Figure 3.2.

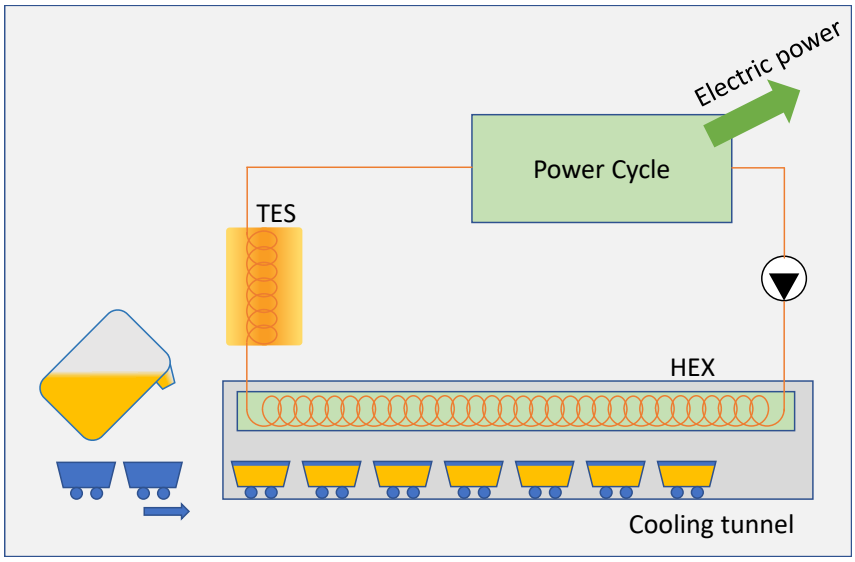

Figure 3.2: Concept figure of the proposed heat recovery and conversion system

The components that make up the proposed heat recovery system will be described in this section, while the modeling and mathematical description of the system are presented in Sections 3.4 to 3.9.

The WHRU uses the radiative and convective heat released by the silicon to heat a heat transfer fluid. The inspiration for the heat collector is two of the radiative heat recovery systems described in Section 2.2, namely the flat pipe heat exchanger system from Jouhara et al. (2017), which recovered heat from hot steel wires, and the radiant heat recovery system proposed by Caputo et al. (2011) to recover heat from a rotary kiln.

The WHRU was imagined as a heat shield, or tunnel, placed above the casting molds, with the loop HTF fluid flowing through an array of pipes inside the tunnel walls. The molds would move through the tunnel either by a carousel, as is currently the case at Salten, or in a straight path, similar to the system described by Jouhara et al.. Radiation and convection heat from the mold would heat the tunnel walls, which would in turn heat the fluid inside the pipe array. The heat transfer fluid would enter the tunnel walls at the end of the tunnel, where the silicon is at its coldest, pass through the length of the tunnel and leave at the start, where silicon has just been poured into molds. The tunnel is open in both ends, and air blowers are installed to control the flow of air through the tunnel, which can be used to better control the silicon cooling rate.

Silicon is poured into molds for 30 minutes once every two hours. In addition, heat transfer rates will be highest when the silicon is at its hottest, while temperatures and heat flow rates will

be significantly lowered towards the end of each casting cycle. This results in a heat recovery system with a highly variable heat source, where both source temperatures and heat flow rates change drastically throughout the casting process. Such a heat source is not suitable for power generation, as the highly variable heat source temperature would shift the operating point of the power cycle turbine away from its design point This results in off-design operation, which is bad for the power cycle performance. In addition, the system would have to be designed for peak loads, making the system severely oversized during the end of a casting cycle, when silicon temperatures are low and heat transfer rates are at its lowest. The power produced by the power cycle would be very variable, possibly even discontinuous, if the silicon is cooled quickly enough.

To mitigate the fluctuations caused by the heat source, a thermal energy storage was included in the heat recovery loop. It is meant to store excess heat delivered to the loop as silicon heat transfer rates are high, which can then be deposited to the power cycle once silicon temperatures and heat transfer rates have declined. By using the thermal storage as a buffer, it will help reduce fluctuations in both temperature and heat transfer rates onto the power cycle, ensuring a more stable power production, and less variations in the power produced.

The thermal storage chosen in this project was a sensible storage with high-temperature concrete as the storage material. It consists of a bundle of steel tubes encased in concrete. The loop HTF will flow through the storage immediately after the WHRU. If silicon heat output is high, the temperature of the HTF will be higher than the concrete, thus transferring some of the surplus heat to the storage. If instead HTF temperatures are low, due to low silicon heat outputs, concrete temperatures will be higher than the HTF, thus some of the storage heat will be transferred to the HTF. The storage will in both cases help reduce the thermal variations caused by a variable heat source. As can be seen from Figure 3.2, there is only one loop for both heat supply and extraction between the loop and the TES, meaning the rate of heat transferred to or from the storage is entirely dependent on the temperature of the concrete and the heat transfer fluid, meaning there are few to no means of actively controlling when the storage should store or deposit heat. On the other hand, the primary function of this storage, reducing thermal variations encountered by the power cycle, will be achieved without a need for any active storage control.

The power cycle is imagined to be a Rankine cycle, where heat is delivered from the heat recovery cycle to generate electric power. The Rankine cycle is not the focus of this thesis, and will therefore not be examined or described in any detail. In its stead, a component estimating power production as a fraction of available exergy will be used to estimate the potential for power production while modeling and simulating the system.

The proposed system utilizes one loop for both charging and discharging of the thermal energy storage, unlike most other sensible storage solutions, where separate loops for charging and discharging are present. An example of such a system is shown in Figure 3.3. In such a system, one can more easily control the system behavior, by cutting of storage charging at a set storage temperature, or stopping storage discharge once the heat transfer fluid goes below a set temperature. In addition, the fluid flowing through the storage will change directions during charging and discharging periods, which enables better thermal stratification, thus it will maintain a hot and cold side in the storage material. Such a system is also more complex, as it requires more control systems and valves to properly manage the system, and would likely lead to higher maintenance costs due to the increased complexity. Such a system would also most likely be operated as a set of storage modules in parallel, to enable some storage modules to be charged while others supply heat to the heat sink, as simultaneously charging and discharging the storage is difficult.

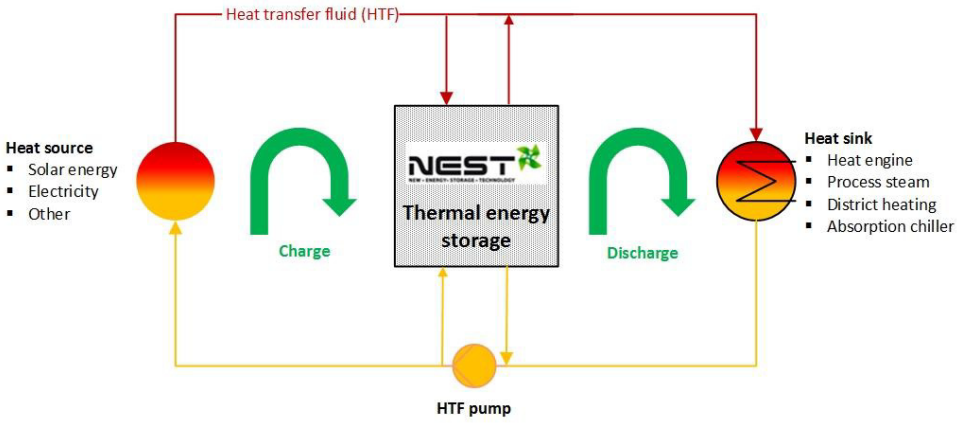

Figure 3.3: An example system where TES charging and discharging are separated (Bergan and Greiner, 2014)

A one loop solution simplifies modeling and operation, and reduces the amount and complexity of control systems necessary for proper operation of the system. The loop will also help maintain a higher loop temperature, which will be beneficial in regards to the power cycle, where higher temperatures are associated with higher cycle efficiencies. Higher temperatures in the loop could also lead to less heat recovery, as the temperature difference between the silicon heat source and casting molds and loop heat transfer fluid is smaller. However, this reduction in the temperature difference will be less impactful in this scenario than in many heat transfer scenarios, as the heat flow from the mold will be dominated by radiant heat. Radiant heat transfer depends on the source temperature to the fourth power, meaning heat recovery will be less impacted by high loop temperatures when compared to a case where other heat transfer mechanics is dominant.

3.3 Modelica

The model of the system was made using the Modelica modeling language, with Dymola being used as the interface for modeling, compiling and simulation. Modelica is a high-level declarative language for describing mathematical behavior. It is often applied to engineering systems and can be used to describe the behavior of different types of engineering components. These component models can then be connected into larger systems, enabling easy modeling of complex physical systems. As a declarative modeling language, Modelica does not require the user to implement numerical solvers for the numerous equations necessary to model every component in a system. The user needs only focus on the mathematical description of the component, while Dymola will handle the numerics.

Another major advantage of the Modelica language is the possibility to create models using a graphical approach. Modelica is often best utilized as an object-oriented modeling tool. It is often beneficial to mathematically describe simple models detailing a single mechanism, and then combining these single models using a graphical interface, where components can be seen as blocks which can be connected to other components. The system components are created by the user or found in preexisting component libraries. The most well-known library is the Modelica Standard Library (MSL), an open source component library containing a number of component models in various engineering domains, as well as purely Boolean and mathematical

components. The `Modelica.Blocks` and `Modelica.Thermal` libraries are both a part of MSL and have both been utilized in this work.

Connecting two or more components requires the use of connectors. A connector is a way for one component to exchange information with another component. In Modelica, connectors for physical systems contains two distinct classes of variables. "Across" variables are the first class of connector variables. Differences in across variables across a component will cause a component to react. Examples include temperature, pressure, and voltage. The other connector variable class is "flow" variables. These variables usually represent the flow of some conserved quantity such as mass flow rate, momentum, or energy. The flow of these flow variables is usually a result of the difference in across variables through a component model.

In this work, the component models are mostly describing heat transfer or fluid flow, thus components utilizing thermal and fluid connectors are often necessary. Temperature is the across variable in heat transfer connectors. A difference in temperature between two heat transfer connectors will result in an exchange of heat, which is the flow variable in heat transfer components. In fluid flow component connectors, pressure will act as an across variable, where a pressure difference results in mass flow, the flow variable. In addition, specific enthalpy acts as an across variable, while enthalpy flow rate will act as a flow variable for the fluid flow energy balance.

Once connectors are used to connect two or more components, Modelica will generate equations to connect the components. A balance equation will govern the flow variables: The sum of all flow variables which are connected will equal zero. All connected across variables will equal each other. A direct analog to these connector equations is Kirchhoff's laws used in electrical engineering. The sign convention in Modelica stipulates that a positive value for a flow variable represent the flow of the conserved quantity *into* a component.

3.4 Fluid flow modeling

Fluid flow is an integral part of many component models encountered in this work. A fluid flow model is required to model the flow of heat transfer fluid in the heat recovery loop, the power cycle working fluid and the air flow in the heat recovery tunnel. Fluid flow will be modeled by using components found in the `Modelica.Thermal.FluidHeatFlow` library, in which fluid behavior is modeled with constant fluid parameters. The component HeatedPipes in this library forms the basis for all fluid flow modeling in this work.

The HeatedPipe component describes a single fluid control volume. Two fluid flow connectors (FlowPorts) constitutes the fluid flow into and out of the control volume, while a heat transfer connector (HeatPort) represents the heat exchange through the walls of the pipe. As the fluid is modeled with constant fluid parameters, enthalpy is defined as $h = c_p T$, while the fluid is incompressible. Thus, Eqs. 3.1 and 3.2 is the governing equations of the fluid control volume, describing the mass and energy balance.

$$\dot{m}_{in} + \dot{m}_{out} = 0 \tag{3.1}$$

$$\dot{m}_{in} h_{in} + \dot{m}_{out} h_{out} + \dot{Q}_{wall} = \frac{dU}{dt} = m_{cv} c_v \frac{dT}{dt} \tag{3.2}$$

Here, T is the temperature at the control volume outlet, m_{cv} is the mass of the control volume, while $\dot{Q}_{wall}$ is the heat flow through the pipe wall, and its value is decided by a heat transfer component connected to the HeatPort connector (see Section 3.5). The inlet temperature can

be found by $T_{in} = h_{in}/c_p$. The temperature involved in calculating $\dot{Q}_{wall}$ is the fluid outlet temperature, T_{out}. The pressure drop through the control volume is described by Eq. 3.3.

$$\Delta p = p_{in} - p_{out} = f(\dot{V}_{flow}) \tag{3.3}$$

$f(\dot{V}_{flow})$ is the pipe pressure drop as a function of the volumetric flow rate. This work does not focus on the pressure drop through the system. Δp was set to zero to reflect this.

As the HeatedPipe represents a single control volume, it is often necessary to represent a pipe as several HeatedPipe components connected in series, thus discretizing the pipe to provide a better representation of the pipe behavior along the pipe length. Figure 3.4 illustrates three HeatedPipe components connected in series. The blue lines correspond to connections between HeatedPipe connectors, while the red lines are meant to illustrate a between the HeatedPipe heat ports to external components describing the heat transfer to or from the pipe. Due to the connectors, the outlet pressure, temperature and specific enthalpy of one control volume will be set equal to the inlet pressure of the previous control volume, while the change in these parameters across each control volume is decided by Eqs. 3.1, 3.2 and 3.3.

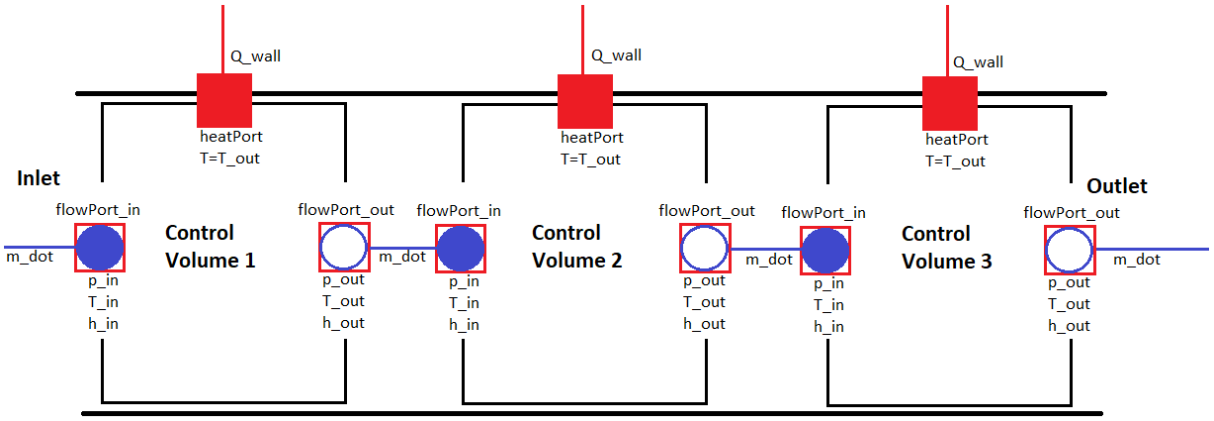

Figure 3.4: Three fluid control volumes connected in series

3.5 Heat transfer components

This work describes a number of different heat transfer mechanisms. It is necessary to describe the heat flow from the hot silicon to the heat recovery loop, the heat transferred to and from the thermal storage module, and heat transferred from the heat recovery loop to the power production cycle. A number of different heat transfer components were required to describe these mechanisms in a satisfying manner.

3.5.1 Radiation heat transfer

The initial temperature of hot silicon is 1450°C during casting. Radiation heat transfer will be the dominant method of heat transfer at such high temperatures, which both Jouhara et al. (2017) and Du et al. (2018) observed while recovering waste heat from hot surfaces. Thus it is necessary to properly model the radiation heat transfer as it occurs between the hot silicon, the heat recovery tunnel, and the surroundings

The radiation was modeled using the approach described in Subsection 1.3.1, i.e. it was modeled as a thermal radiation network. Three surfaces were included in the model: the silicon surface as it is cooled (Surface 1), the tunnel walls (Surface 2), and the surroundings (Surface 3). Not all of the radiation emitted by the silicon surface is intercepted by the tunnel walls, some of the radiation will "miss" the tunnel walls by hitting the openings of the tunnel, which is synonymous with the radiation hitting Surface 3. The surrounding surface area is therefore represented by the inlet and exit tunnel surface area. As little to no heat is reradiated from the surroundings back to the tunnel or silicon, Surface 3 is also regarded as a blackbody ($\varepsilon_3 = 1$). The thermal radiation network is shown in Figure 3.5, with the HeatPort locations drawn in red. Notice how there is no surface radiative resistance associated with Surface 3, a result of the blackbody property of this surface, which results in the surface radiative resistance being zero.

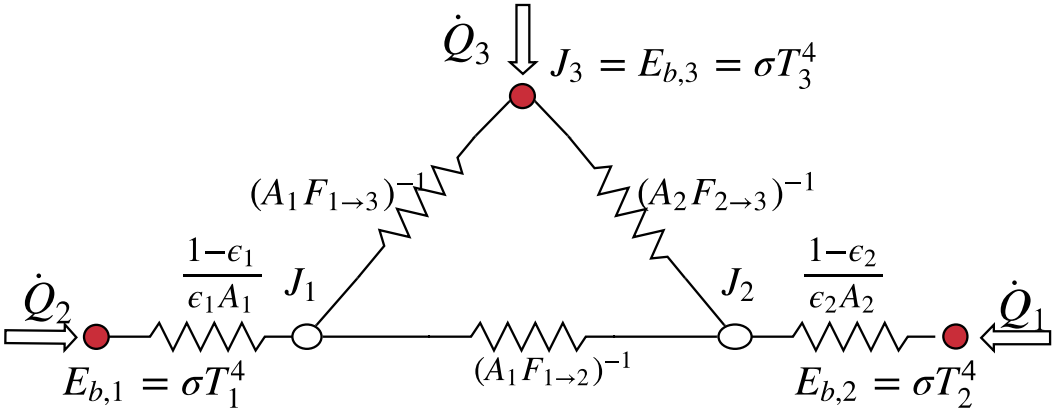

Figure 3.5: The thermal radiation network used to describe radiation heat transfer

The radiation component in Modelica consisted of three heat transfer connectors, where each connector would be connected to a component representing one of the three surfaces involved in the radiation heat transfer. The radiosity (J_1, J_2, J_3) of each surface is found by Eqs. 3.4, 3.5, and 3.6, which are the energy balances around each node, based on Eqs. 1.7 and 1.8.

$$\frac{\sigma T_1^4 - J_1}{\frac{1-\varepsilon_1}{\varepsilon_1 A_1}} = \frac{J_1 - J_2}{\frac{1}{A_1 F_{1\to2}}} + \frac{J_1 - J_3}{\frac{1}{A_1 F_{1\to3}}} \tag{3.4}$$

$$\frac{\sigma T_2^4 - J_2}{\frac{1-\varepsilon_2}{\varepsilon_2 A_2}} = \frac{J_2 - J_1}{\frac{1}{A_1 F_{1\to2}}} + \frac{J_2 - J_3}{\frac{1}{A_2 F_{2\to3}}} \tag{3.5}$$

$$\frac{\sigma T_3^4 - J_3}{\frac{1-\varepsilon_3}{\varepsilon_3 A_3}} = \frac{J_3 - J_1}{\frac{1}{A_1 F_{1\to3}}} + \frac{J_3 - J_2}{\frac{1}{A_2 F_{2\to3}}} \tag{3.6}$$

Because the surface radiative resistance is zero at Surface 3, Eq. 3.6 is simplified by multiplying both sides of the equation with $\frac{1-\varepsilon_3}{\varepsilon_3 A_3} = 0$, which results in Eq. 3.7.

$$\sigma T_3^4 - J_3 = 0 \tag{3.7}$$

The temperature of each connector are T_1, T_2, and T_3, while the radiation heat flow through each connector is the net heat flow from each surface, and is defined as:

$$\dot{Q}_{rad,1} = q_1 = \frac{\sigma T_1^4 - J_1}{\frac{1-\varepsilon_1}{\varepsilon_1 A_1}} \tag{3.8}$$

$$\dot{Q}_{rad,2} = q_2 = \frac{\sigma T_2^4 - J_2}{\frac{1-\varepsilon_2}{\varepsilon_2 A_2}} \tag{3.9}$$

$$\dot{Q}_{rad,3} = q_3 = q_{3\to1} + q_{3\to2} = \frac{J_3 - J_1}{\frac{1}{A_1 F_{1\to3}}} + \frac{J_3 - J_2}{\frac{1}{A_2 F_{2\to3}}} \tag{3.10}$$

The surface areas involved in the radiation heat transfer vary depending on the dimensions of the heat recovery tunnel and molds. The radiation view factors ($F_{i\to j}$) will depend on WHRU dimensions. The heat recovery tunnel in this work is assumed to be rectangular, which simplifies view factor calculations. Incorpera et al. (2005) provides explicit formulas for the view factors between two rectangular plates, both perpendicular plates sharing one common edge and two rectangular, parallel plates. These formulas, combined with the view factor rules described in Subsection 1.3.2, enables the calculation of all necessary view factors.

3.5.2 Thermal resistors

Besides radiation heat transfer, both convection and conduction heat transfer occurs in this system. Components capable of describing both these phenomenons are required. The heat flow components are modeled as thermal resistors. It consists of two thermal connectors, while the heat flow through the component is defined as:

$$\dot{Q} = \frac{\Delta T}{R} \tag{3.11}$$

here R is the thermal resistance in the component, while ΔT is the temperature gradient across the heat transfer component, i.e. the temperature difference between the thermal connectors. The value of the thermal resistance could be set as constant, which was done in cases of pure conduction heat transfer, or its value could be decided by a heat transfer coefficient correlation.

3.6 Silicon heat source

The silicon acts as a heat source for the heat recovery cycle by releasing heat as it is cooled from 1450°C. In this work, the silicon contained in the casting molds will be modeled as a thermal mass whose temperature decreases as heat is released. Heat transfer from the mold surface is modeled using the radiation and convection models described in earlier sections, while heat transfer throughout the silicon depth will be included in the silicon model. This approach is similar to the one-dimensional modeling approaches of Benham et al. (2016) and Tveit (1988), but modifications had to be made when implementing the model using the Modelica language.

In Modelica, a thermal mass is another word for a thermal capacitor, in which a net heat input into the capacitor will result in an increase in capacitor temperature, while a net heat output from the capacitor will result in a decrease in capacitor temperature. The thermal capacitor is described by Eq. 3.12, where $C = mc_{p,tot}(T)$ is the heat capacity of the capacitor.

$$C\frac{dT}{dt} = \sum \dot{Q}_{in} \tag{3.12}$$

However, there are two important aspects of the silicon behavior that has to be taken into account when using thermal capacitors as the basis for modeling. The silicon will solidify as it is cooled, i.e. a phase change will occur. This phase change is accompanied by additional heat

released from the silicon, its heat of fusion. This must be accounted for, as the heat of fusion accounts for a substantial part of the total heat released during the silicon cooling. In addition, the thermal gradient throughout the silicon must be included in the silicon model, to properly gauge the silicon solidification front through the casting mold.

To include the heat of fusion in the silicon model, the heat capacity of the capacitors will be adjusted in the solidification temperature interval. The solidification will happen between the liquidus and solidus temperatures (T_L and T_S, see Table 3.1). Assuming the heat of fusion (h_{fus}) is released in a uniform manner across the solidification interval, the specific heat capacity of the silicon is adjusted to:

$$c_{p,tot} = \begin{cases} c_p, & T < T_S \\ c_p + \frac{h_{fus}}{T_L - T_S}, & T_S \leq T \leq T_L \\ c_p, & T > T_L \end{cases} \tag{3.13}$$

The casting molds are considered well insulated, with no heat transfer occurring through the mold floors or sidewalls. As the molds are wide, long and shallow, heat flow in the mold will be dominated by flow through the depth, meaning a one-dimensional heat transfer model can be used (Benham et al., 2016). In this work, heat transfer from the molds only occurs through the top of the molds, on the interface between the hot silicon and the air above. A thermal gradient in the molds will be present, due to the silicon thermal resistance. As a one-dimensional heat transfer model is used, silicon temperatures are assumed to only vary in one direction: coldest at the top where heat is transferred away from the mold, while hottest close to the mold floor.

To represent this, the silicon molds were modeled as thermal networks consisting of N thermal capacitors, with resistors connected in between. Each capacitor, or node, represents a layer in the silicon mold with uniform temperature. The total silicon mass contained in the mold is divided equally between all the capacitors. An example thermal network with 4 temperature nodes are shown in Figure 3.6. Node 4 (shown in red) doubles as the Modelica HeatPort connector and is therefore the topmost layer of the mold silicon. T_4 is therefore the coldest temperature node, while T_1 is hottest. $\dot{Q}_{in}$ is positive for a heat flow *into* the mold due to Modelica sign conventions.

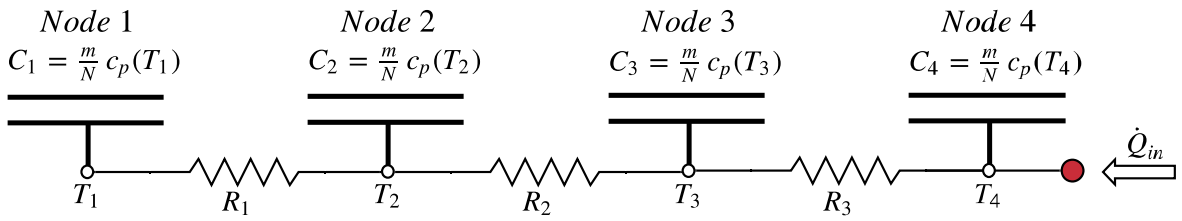

Figure 3.6: The thermal network for the silicon in a casting mold with $N = 4$ temperature nodes

The thermal resistors represent the thermal conductivity of the mold silicon, and the thermal resistance will vary with the volume of silicon in the molds, and with the mold geometry. The molds all have a square surface area, and the depth of the silicon depends on the amount of silicon pored into each mold. As such, the thermal resistance of mold i is:

$$R_i = \frac{d_i}{kA} \tag{3.14}$$

$$d_i = \frac{m}{\rho A N} \tag{3.15}$$

where d_i is the depth of each silicon node layer, m is the mass of silicon in the mold, k is the conductivity of the silicon, ρ is the silicon density, N the total number of nodes, while A is the silicon surface heat transfer area.

3.7 Waste heat recovery unit

The WHRU component describes several important aspects of this system. It utilizes radiation and convection heat transfer components to model the heat transfer from each mold to the WHRU and it models the loop heat transfer fluid inside the tunnel walls. It also controls the timings of each mold, to ensure that each mold is poured with hot silicon at the right time and that each mold is placed in the tunnel for the determined duration.

3.7.1 Tunnel heat transfer

The modeling of the tunnel heat transfer is done in a similar fashion as the model presented by Caputo et al. (2011) in Subsection 2.2.3. Radiation heat is transferred from the molds to the radiation shield/tunnel wall. Unlike the work done by Caputo et al., the radiation heat transfer also describes the radiation heat which does not impact the tunnel walls, but instead leaves the tunnel altogether, transferring heat into the surroundings. At the same time, convective heat transfer is present between the hot silicon and the air inside the tunnel, and between the tunnel air and the tunnel walls. The external tunnel surface is assumed to be insulated by a layer of glass fiber, to reduce the heat losses from the external tunnel surface. Auxiliary blowers are used to control the air flow rate inside the tunnel, providing air circulation while keeping the air temperature under control.

As auxiliary blowers are used, forced convection will be present. The Gnielinski correlation is used to decide the forced convection coefficient. But, if the air velocity is sufficiently low, free convection is assumed, at which point convection coefficient correlating to free convection is used. Gnielinski's correlation is meant for turbulent flow in tubes, not flow in square tunnels, but the correlation was used regardless, utilizing the hydraulic diameter while calculating the Reynolds number and Nusselt number. Gnielinski's correlation in shown in Eq. 3.16.

$$Nu_D = \frac{h_{forced} d_{hyd}}{k} = \frac{(f/8)(Re_D - 1000)Pr}{1 + 12.7(f/8)^(1/2)(Pr^{2/3} - 1)} \tag{3.16}$$

where f is the Darcy friction factor. Assuming a smooth tunnel surface, the friction factor can be found from:

$$f = (0.79ln(Re_D) - 1.64)^{-2} \tag{3.17}$$

The Gnielinski correlation is valid for

$$0.5 \leq Pr \leq 2000$$
$$3000 \leq Re_D \leq 5 \times 10^6$$

then, the final air heat transfer coefficient is decided by

$$h_{air} = max\{h_{free}, h_{forced}\} \tag{3.18}$$

Figure 3.7 shows the tunnel heat transfer, as it is modeled in Dymola. "port_mold" and "port_ambient" are the heat flow ports, where the silicon mold and ambient surroundings will be connected. Both "HTFflow" and "airFlow" are HeatedPipe components, and represent the flow of heat transfer fluid in the tunnel wall and air flow through the tunnel. "convection1" and "convection2" are thermal resistors representing the air convective heat transfer, where the thermal resistances are decided by "forcedConvection", which calculates the air convective coefficient from Eqs. 3.16 and 3.18. As the surface areas involved in the mold-to-air and air-to-tunnel heat transfer are different, h_{air} is multiplied by the mold or wall surface area in components "A_tunnel" and "A_mold" to decide the thermal resistance of the two convective heat transfer components involved with the tunnel air heat transfer. The radiation heat transfer is modeled using the Modelica radiation component discussed in Subsection 3.5.1. The surroundings are modeled as a blackbody, and the tunnel wall and mold surface as grey surfaces with different emissivities and surface areas. "wallLoss" is a thermal resistor representing heat loss from the external tunnel wall. Its thermal resistance is decided by the thickness of the insulating layer, the thermal conductivity of the thermal layer, and the air free convection coefficient.

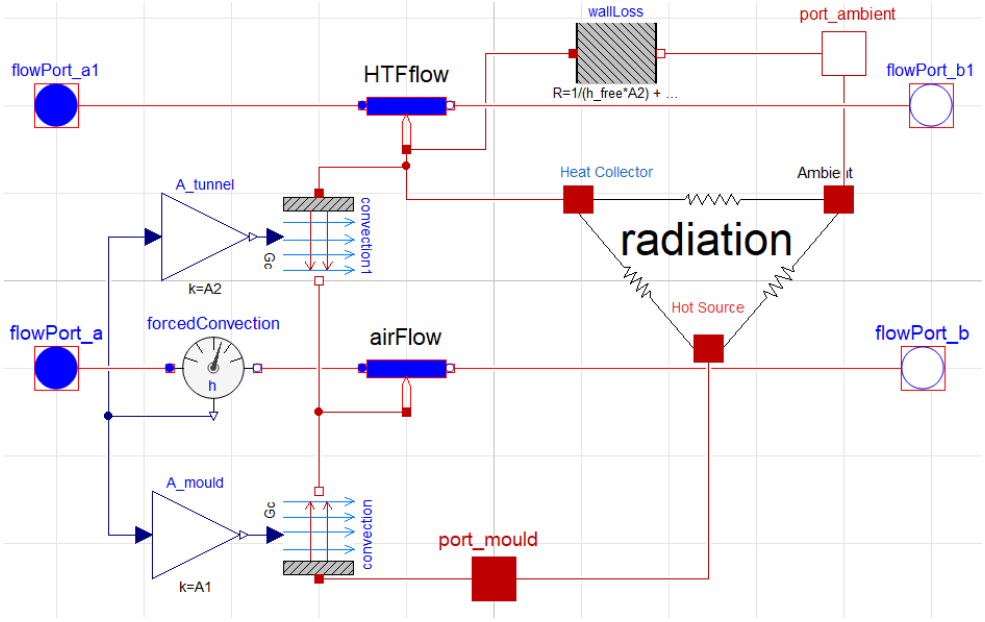

Figure 3.7: Tunnel heat transfer, as modeled in Dymola

3.7.2 Complete WHRU component

The heat transfer component described above describes only a cross section of the WHRU, and is aptly named "TunnelSegment". To model the entirety of the tunnel, multiple TunnelSegments were connected in series. In addition, silicon molds and a representation of the surroundings (ambient temperature) were included to complete the component.

Figure 3.8 shows the graphical representation of the entire tunnel component in Dymola, named "TunnelDiscrete". The component named "tunnelSegment[]" in the center of the figure is the component described in Subsection 3.7.1, while "mould[]" is the component described in Section 3.6, describing the heat released from a casting mold filled with silicon. The square brackets in their name signify that these components are arrays of identical components. The tunnelSegment components are connected in series, thus discretizing tunnel behavior, while

each mold component is connected to a section of the tunnel. The flowPorts connects the tunnel heat transfer fluid to the rest of the heat recovery loop.

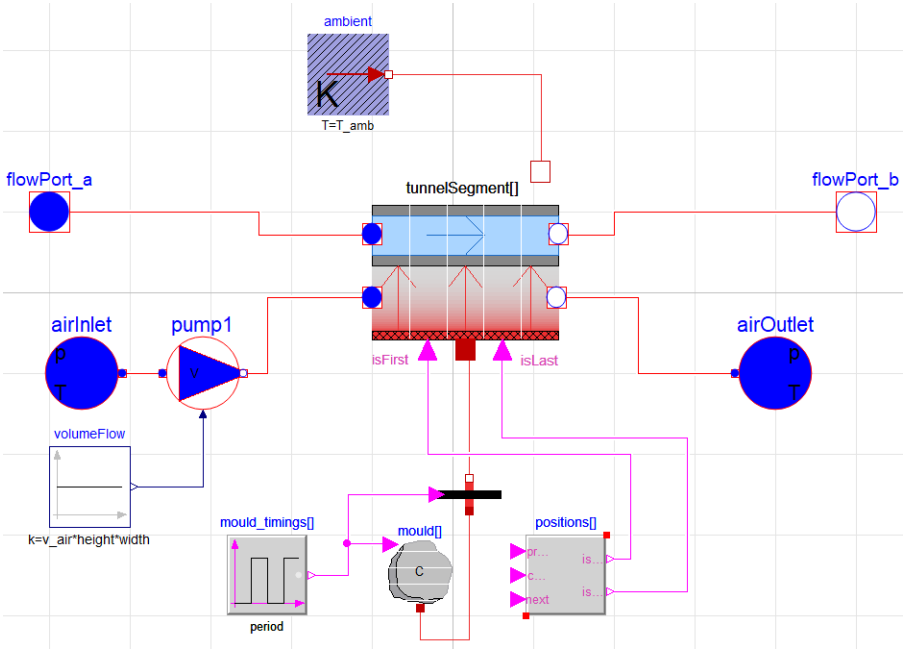

Figure 3.8: The entire waste heat recovery unit (tunnel), as modeled in Dymola

To control the air flow, "airInlet" and "airOutlet" represent the inlet and outlet flow of air from the tunnel, while "pump1" controls the air volumetric flow rate into the tunnel. To represent the surrounding temperature, "ambient" is set to 25°C and is connected to each tunnelSegment.

During the initial part of the casting process, 30 minutes are spent pouring 9000 kg of silicon into a number of casting molds, meaning it is important to control when each mold is initiated, when each mold is brought beneath the heat recovery tunnel, and when each mold is removed from the tunnel. The "mould_timings" components control these aspects for each mold. A mold is initiated at 1450°C once silicon is poured into said mold. While a mold is moving beneath the heat recovery tunnel, mold heat transfer is described by the tunnelSegment component. Once the mold has moved out from beneath the tunnel, the heat flow from the mold component is blocked, since heat is no longer transferred from the mold to the tunnel. The "positions" component controls the position of each mold beneath the tunnel. This was necessary in order to simulate each tunnel being moved through the tunnel as new molds are poured with silicon, as this will affect the view factor experienced by each mold.

The view factors between the mold, tunnel openings, and the tunnel surface will change as the mold moves through the tunnel. In this work, the view factors were calculated for a mold underneath the tunnel by the tunnel opening. The tunnel view factors were assumed to change linearly as the mold passed through the tunnel, while the view factor between the mold and tunnel wall was found to be very close to 1 at the middle point of the tunnel. As such, $F_{1\to2}$ was modeled to increase linearly from its initial value at the tunnel opening to 1 as it passes the middle point of the tunnel, at which point it would start to revert toward its initial value as it approaches the tunnel exit. The opposite will be the case for $F_{1\to3}$ and $F_{2\to3}$, which will be highest by the tunnel openings, and zero by the tunnel halfway point.

3.8 Thermal storage component

The thermal energy storage component describes the behavior of the concrete storage. The component was based on the work presented by Jian et al. (2015). A modeling approach for a sensible thermal storage system was proposed there, and its validity was tested against experimental data. The proposed model was found to be quite accurate when compared to the experiments.

Jian et al. proposed to model the sensible storage system by using the lumped capacitance assumption. The lumped capacitance assumption is valid when the internal thermal resistance of the storage material is low compared to the convective thermal resistance of the heat transfer fluid transferring heat to the material (low Biot numbers, $Bi = hL/k \leq 0.1$). With low Biot numbers, the heat conduction inside the body is much greater than the heat convection away from its surface, leading to negligible temperature gradients inside the body. However, concrete thermal conductivity is low, rendering the lumped capacitance assumption void. An effective heat transfer coefficient was introduced, which, alongside a modified lumped capacitance model, was valid for larger Biot numbers. This in turn made the lumped capacitance assumption viable for the concrete storage model.

The storage module consists of a cuboid-shaped concrete block containing a tube bundle with a triangular pitch, where each pipe is surrounded b a concrete volume in the shape of a hexagonal prism, see Figure 3.9a. To simplify the analysis, the hexagonal prism shape of the storage was substituted with a cylindrical shape, with the same cross-sectional area, as shown in Figure 3.9b, where $d_o^2 = 2\sqrt{3}D^2/\pi$.

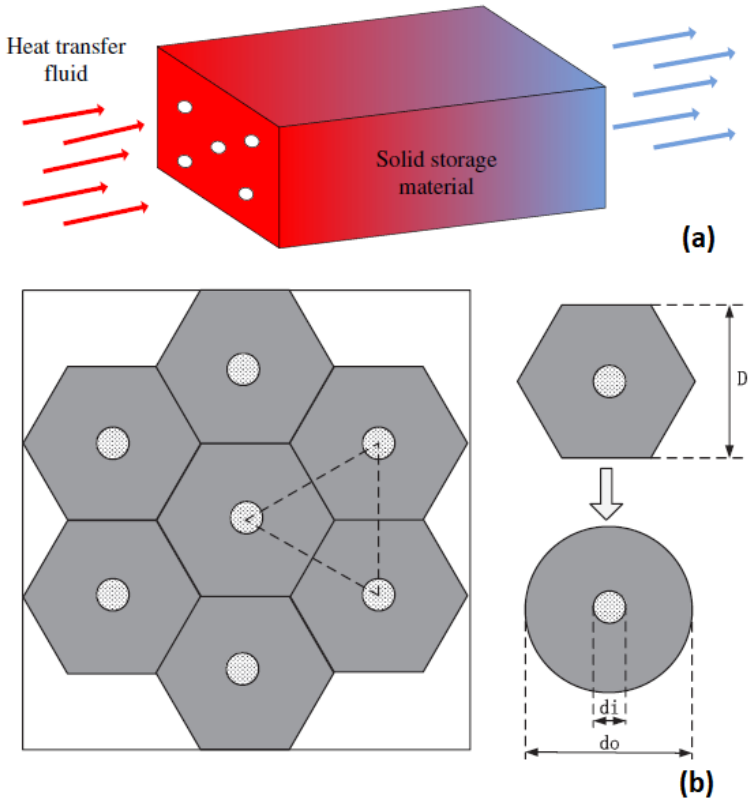

Figure 3.9: **(a)** The layout of the thermal storage unit. **(b)** Storage geometry and model simplification (Jian et al., 2015)

In addition to the lumped capacitance assumption, it was also assumed that thermal conduction in the axial direction was negligible and that there are no heat losses from the storage to the surroundings. The thermal resistance in the heat transfer pipes was neglected, as the thermal conductivity of the pipes is much higher than that of the concrete. It was also assumed that every tube and their surrounding concrete behave the same way.

The effective heat transfer coefficient proposed by Jian et al. is:

$$\frac{1}{h_E} = \frac{1}{h} + \frac{1}{k}\frac{4ab^4 \ln\frac{b}{a} - 3ab^4 + 4a^3b^2 - a^5}{4(b^2 - a^2)^2} \tag{3.19}$$

where $a = d_i/2$, $b = d_o/2$, h_E is the effective heat transfer coefficient, k is the concrete thermal conduction coefficient, while h is the fluid heat transfer convection coefficient. In this equation, $\frac{1}{h}$ is the contribution of the fluid convection on overall heat transfer, while the rest describes heat transfer through the concrete surrounding each tube.

When implementing the storage model in Modelica, only a single tube and its surrounding concrete were modeled. By doing this, modeling was simplified to that of a fluid flowing inside a tube embedded in a concentric cylinder of high-temperature concrete, as shown in Figure 3.10. To model the entire storage, the tube was scaled up by multiplying the tube dimensions by the number of pipes in the storage module, a method recommended by Zaversky et al. (2014).

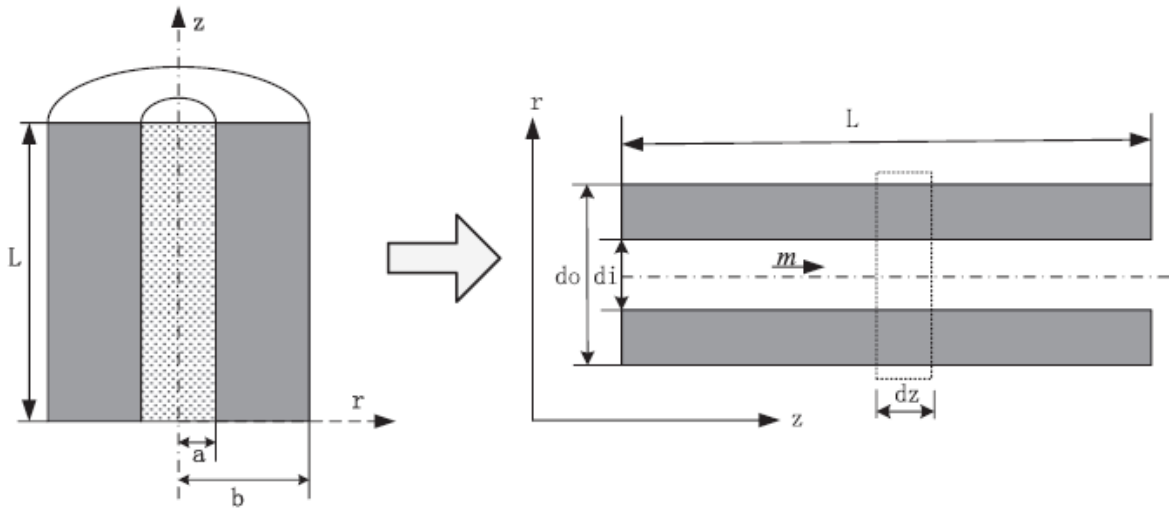

Figure 3.10: Thermal storage control volume (Jian et al., 2015)

Figure 3.11 shows the storage model as it appears in Dymola. The concrete is modeled as a thermal capacitor, "heatCapacitor[]", which is governed by Eq. 3.12. To include the changing temperature of the storage in the axial direction, the storage is represented as N_{TES} thermal capacitors, each having an equal fraction of the total storage heat capacity. The heat transfer to and from the capacitors is described by N_{TES} heat resistors, "heatTranfer[]". Each capacitor is connected to a thermal resistor, which is then connected to "HTFflow[]", which are HeatedPipe components describing the behavior of the heat transfer fluid. The thermal resistance in each resistor is decided by the "storageHeatTransfer" component, which calculates the effective heat transfer coefficient proposed by Jian in Eq. 3.19. The Gnielisnki correlation, Eq. 3.16, is used to find the fluid forced convection coefficient, while the FlowPorts connects the fluid flow with the rest of the heat recovery loop. Table 3.2 lists the thermal properties of the concrete used in this work.

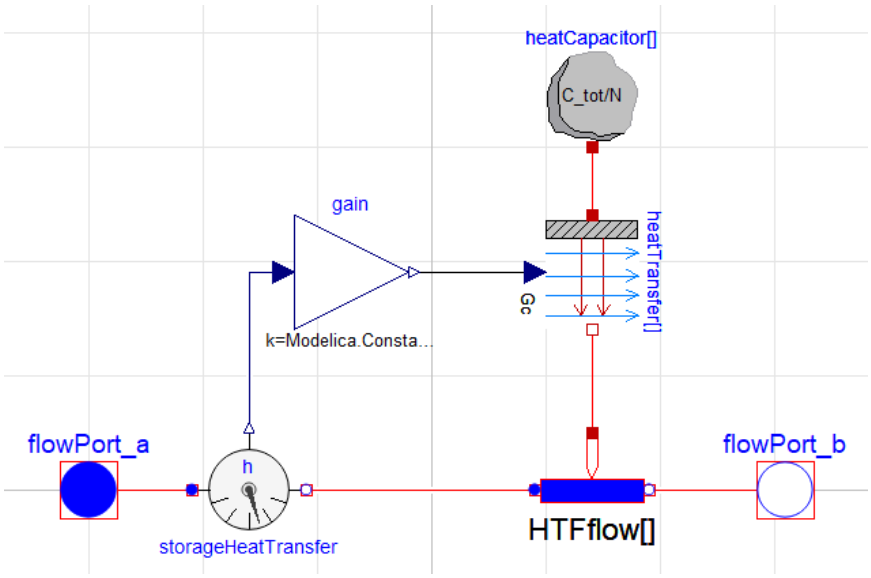

Figure 3.11: The thermal storage, as modeled in Dymola

Table 3.2: Concrete properties (Jian et al., 2015)

Property	Unit	Value
ρ	$\mathrm{kg/m^3}$	3100
c_p	$\mathrm{J/(kg\,K)}$	1180
k	$\mathrm{W/(m\,K)}$	2.65

3.9 Estimator for electricity generation

The heat recovered from the silicon is transferred from the heat recovery loop through a heat exchanger into a power production cycle to produce electricity. The power cycle was imagined to be a Rankine cycle. The scope of this work does not encompass proper modeling of this Rankine cycle. Nevertheless, there is a need to estimate the potential for electricity production from this system. In addition, a heat sink must be connected to the loop heat exchanger to properly model the heat transferred out of the loop.

To include both of these aspects in the model, the cold side of the loop heat exchanger was modeled as a fluid flow with a user-defined inlet temperature and mass flow rate. Heat transferred to the cold side of the loop heat exchanger was considered the heat transferred to the imagined Rankine cycle. This is not an optimal approximation, as the heat exchanger model does not include the phase change usually encountered in a steam Rankine cycle, meaning temperature profiles and heat transfer characteristics will deviate from expected behavior. However, as the fluid model utilized in this work did not support phase change, it was the best available modeling option. The cold side inlet heat exchanger temperature was set to 100 °C.

The heat exchanger transfers heat from the heat recovery loop to an external power production cycle. It is modeled as a simple counter flow heat exchanger, where the heat transfer characteristics are decided by its UA value. The Modelica component is shown in Figure 3.12.

The heat exchanger is divided into N_{hx} control volumes, to better represent the spatial temperature gradient throughout the heat exchanger. It is modeled as two series of fluid volumes, one for the hot fluid flow and one for the cold flow. Thermal resistors are connected between the

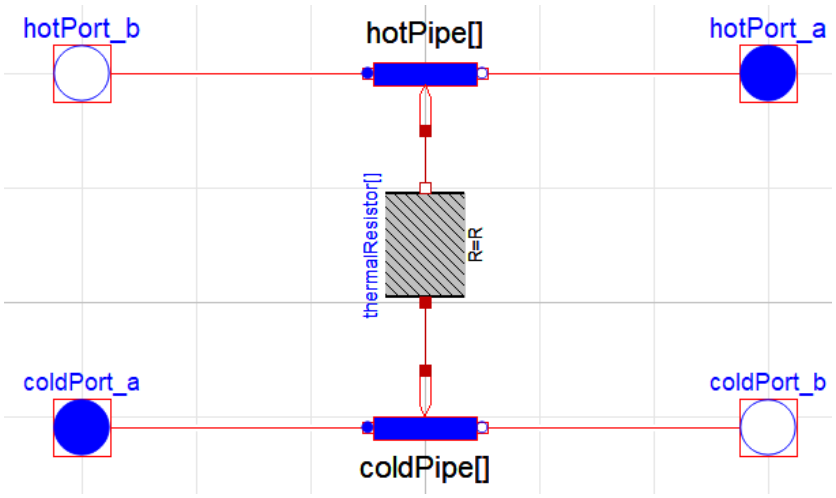

Figure 3.12: Simple heat exchanger, as modeled in Dymola

hot and cold fluid volumes to describe the heat transfer. Each resistor has a thermal resistance R_i of:

$$R_i = N_{hx} R_{tot} = \frac{N_{hx}}{UA} \tag{3.20}$$

To find an estimate for the amount of electric power produced by the power cycle, the constrained gliding temperature Carnot efficiency was used - see Eq. 1.13. This Carnot efficiency was used to determine the exergy available to the Rankine cycle. Exergy is the maximum useful work which can be extracted from a system as it is brought into equilibrium with a heat reservoir/heat sink, and is therefore an indicator of the maximum possible electric power which can be generated. However, no real, reversible process will ever be able to extract all available exergy, so in this work it was assumed that 50% of all exergy available to the Rankine cycle on the hot side of the loop heat exchanger is lost during heat transfer and power generation. The estimated power, $\dot{W}_{el}$, produced from the Rankine cycle is estimated to be:

$$\dot{W}_{el} = \eta_{system} B \dot{Q}_{HX} \tag{3.21}$$

Here, $\dot{Q}_{HX}$ is the heat transferred through the loop heat exchanger to the Rankine cycle, $B = 0.5$ is the fraction of the exergy which will be converted to electrical power, while η_{system} is the gliding, constrained Carnot efficiency from Eq. 1.13, where $T_{hot,in}$ and $T_{hot,out}$ is the hot inlet and outlet temperature in the heat exchanger, while T_{amb} is the ambient temperature.

3.10 Overview

Figure 3.13 displays the entire system as it appears in Dymola, with all main components connected in a loop. Components to further control the behaviour of the system, such as PI-regulators, are not shown here.

In addition to the air flowing through the heat recovery tunnel, there are two fluids in this system, namely the heat recovery loop fluid and the power cycle working fluid. The far most common working fluid in commercial Rankine cycles is water/steam, which was chosen as the power cycle working fluid. The loop heat transfer fluid would need to withstand high temperatures, to ensure high Rankine cycle efficiencies. Maximum temperatures at peak heat load were

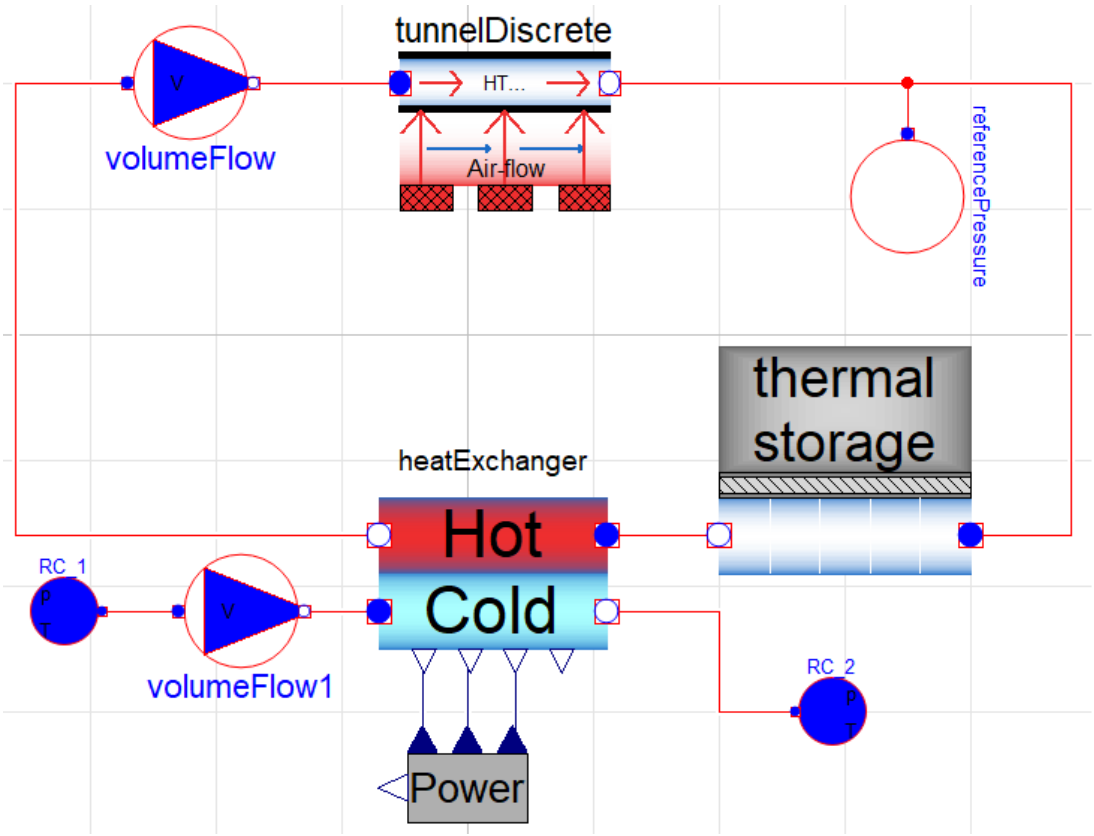

Figure 3.13: The heat recovery system, as it appears in Dymola

well above 500°C. Thermal oils have often been proposed as the heat transfer fluid in thermal storage concepts in the literature, but they are often not thermally stable above 400°C, which excluded their usage in this work. Molten salts, often used in concentrated solar power, would be more suitable with an active storage system, where the molten salt could act as both storage medium and heat transfer fluid. These salts would also complicate system operation due to their high freezing point. Instead, high-pressure CO_2 was chosen as the loop HTF. It can withstand high temperatures, is readily available and is cheap. HTF fluid pressure could be optimized to improve performance. Higher HTF pressures would result in higher fluid thermal capacitance per volume unit, as densities and specific heats increases. The thermal conductivity would also rise with pressures. However, an increase in pressure also corresponds to a need for thicker tube walls to withstand the elevated pressures, which will lead to higher investment costs. The CO2 properties used in this work will assume a system pressure of 70 bar. The fluid properties used in the model are tabulated in Table 3.3.

The behavior of this system is highly dynamic, and its behavior will depend on the initial temperatures of the storage. The system will require some time to reach its cyclic steady state. This refers to the system conditions that result in system temperatures at the beginning of a cycle to match up with the temperatures at the end of a cycle, resulting in identical subsequent cycles. This will be the system's operational point when operated over extended periods of time. For no cyclic change in the storage temperature, there must be en equilibrium between the overall heat supplied to the system during a casting cycle and the overall heat released from the system to the power cycle. The cyclic steady state can found by initializing the system and allowing the system to instill itself towards its operational state over some cycles of operation. Once the

Table 3.3: Fluid parameters used in simulations

		Fluid		
Property	Unit	CO_2	Steam	Air
p	bar	70	20	1.013
ρ	$\mathrm{kg/m^3}$	55.13	3.26	0.736
c_p	$\mathrm{J/(kg\,K)}$	1156	2128	1027
c_v	$\mathrm{J/(kg\,K)}$	934	1631	739
k	$\mathrm{W/(m\,K)}$	0.047	0.055	0.038
ν	$\mathrm{m^2/s}$	5.39×10^{-7}	7.46×10^{-6}	3.5×10^{-5}

cyclic steady state has been found, the system can be initialized using the storage temperatures encountered at the starting point of such a period, meaning subsequent simulations could avoid the search for the steady state. Table 3.4 provides an overview of the model parameters, explaining which parameters are set constant throughout all simulations, and which are available for tuning. The silicon parameters tabulated in Table 3.1 are used in all simulations.

Table 3.4: System parameters and their value

Property	Unit	Value
Duration of a casting cycle	s	7200
Time to empty ladle in molds	s	1800
Mold time underneath tunnel	s	variable
Ambient temperature	°C	25
Silicon initial temperature	°C	1450
Silicon mass per cycle	kg	9000
Number of molds per cycle	–	10
Tunnel surface emissivity	–	0.8
Conductivity, tunnel insulation	$\mathrm{W/(m\,K)}$	0.055
Thickness, tunnel insulation	m	0.01
Tunnel length, width, height	m	variable
Loop HTF mass flow rate	$\mathrm{kg/s}$	variable
Air mean velocity	$\mathrm{m/s}$	variable
TES storage capacity	$\mathrm{J/K}$	variable
TES tube inner diameter	mm	variable
TES tube pitch distance	mm	variable
TES number of HTF tubes	–	variable
Heat exchanger cold inlet temperature	°C	100
Rankine cycle mass flow rate	$\mathrm{m/s}$	variable
Heat exchanger UA-value	$\mathrm{W/K}$	variable

Chapter 4

Model validation

To ensure that the component models described in Chapter 3 behaved as they should, it was important to validate the Modelica model against other works. This was done in order to gain confidence in the model's behavior. No work describing a similar system in its entirety was found, so instead a validation of each component was performed by using the Modelica system components to replicate experiments or models described by others, and examine how the Modelica components perform in comparison. Verifying that the behavior of the Modelica components resembles the behavior described in other works will affirm the validity of the model components, making it more reasonable to assume that the Modelica components will behave as they should during full system simulations. Some deviations in system behavior will be expected, both due to the rather simple models used in this work, and due to the component models often having to be somewhat retrofitted to fit with the specifications of the other systems.

The thermal storage model and silicon casting mold model were compared against experimental data to ensure that they behaved as one should expect. For the silicon mold model, it was important to validate the silicon behavior and establish a baseline cooling rate. For the TES system, it was important to check if the thermal response was realistic. Most experimental measurements from a concrete energy storage have been conducted at lower temperatures than what will be utilized in this work, but validating storage behavior at lower temperatures will still help to confirm the validity of the storage model. No comparable experimental results were found for the heat recovery tunnel, so the behavior of the model was compared against simulated results from another paper.

4.1 Silicon model

The silicon cooling rate during solidification affects the quality of the silicon end product, as discussed in 1.3.4. While this work focuses on heat recovery from silicon, it will still be of utmost importance to maintain proper cooling rates until the silicon is fully solidified. The measure for proper cooling rate in this work will be the solidification time: the time required for silicon in a mold to be fully solidified. It is assumed that silicon is cooled correctly if the solidification time in the recovery system is similar to the time currently needed for solidification at Elkem Salten without a heat recovery system installed.

It was therefore necessary to find the solidification time at Elkem. Once found, it would act as the baseline for all further results, and any modification to the casting process would need to maintain this solidification time in order to be even considered as a real alternative. Cooling

rates will depend on the desired properties of the product silicon. The solidification time will, as a result, vary from plant to plant. Temperature measurements from a previous project work were used to find an estimate for the solidification time at Elkem.

Lobo (2009) used thermal imaging to measure the surface temperature of silicon in the molds along the casting carousel at Salten Elkem. The temperatures of nine molds were measured, where the hottest silicon appears to be very recently poured into a mold, while the coldest of the measured silicon was poured approximately 30 minutes ago. Assuming all nine molds were poured at equidistant time intervals, one could use the temperature measurements to plot the surface temperature through the first 30 minutes of the casting period.

While the surface temperatures are useful for deciding the onset of solidification in a mold, it does not show the solidification time, as the silicon below the surface is hotter than the surface silicon. To find the total solidification time, a simulation using the silicon mold component was performed, simulating the casting conditions at Elkem Salten with no heat recovery system. Radiation and air convective cooling were present until 30 minutes into the casting process, at which point water cooling was introduced. This simulation, and the measurements done by Lobo is shown in Figure 4.1. The silicon properties are as tabulated in Table 3.1, with a mold silicon surface area of $2.03 \times 1.8\ \mathrm{m}^2$ (Lobo, 2009). Water cooling was assumed to have a heat transfer coefficient of 1000 $\mathrm{W}/(\mathrm{m}^2\,\mathrm{K})$. The simulated mold contained 1000 kg of silicon.

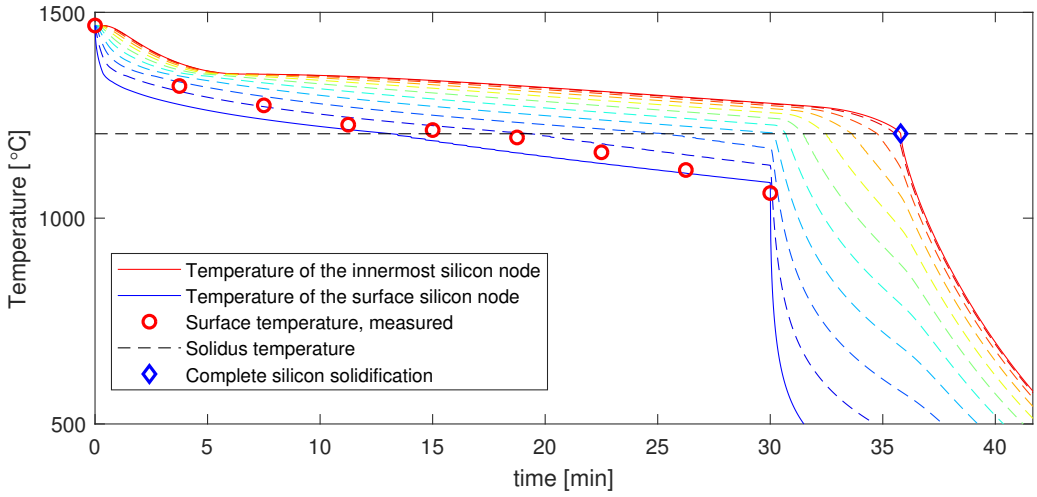

Figure 4.1: Comparison between simulated silicon surface temperatures using Dymola and experimental measurements by Lobo (2009)

From Figure 4.1 it can be seen that the estimated solidification time is approximately 36 minutes, while the surface of the mold reached the solidus temperature in 13.2 minutes. The figure also shows that the surface temperatures simulated by the mold fit fairly well with the measured surface temperatures. While it is not a perfect fit, the deviations from the measurements are not large. The measured surface temperatures will stay between the simulated temperature of the surface silicon node, and the silicon temperature 15% into the silicon depth.

A comparison was made between silicon measurements from Tveit (1988) and the silicon model to further verify the behavior of the silicon model. Tveit measured the temperatures in ferrosilicon alloys as it was cooled from 1340°C in iron casting molds. Figure 4.2a shows the measurements. The temperature sensors were located within silicon depth: 23 mm, 51 mm and 68 mm from the topmost silicon. Heat transfer occurred from the air-silicon surface, and

through the bottom of the mold, as the mold was not fully insulated. These measurements were used to verify the behavior of the silicon mold model. The thermal properties of the silicon measured by Tveit differ from the ones used in this work, so the temperature profiles were not expected to match up. A comparison between the two would all the same point to whether or not the silicon behavior predicted by the model simulations is sensible.

The Modelica component models discussed in the previous chapter was used to recreate Tveit's experiments. Some modifications were necessary to include heat transfer from the bottom of the casting mold. Heat flow through the mold was implemented as resistors, representing the thermal resistance through insulation and the iron mold, and thermal capacitors, representing the thermal mass of the iron mold, allowing the initially cold iron to be heated by its hot content. The simulation results are shown in Figure 4.2b. The values used in the simulation were given by Tveit (1988), page 124-126.

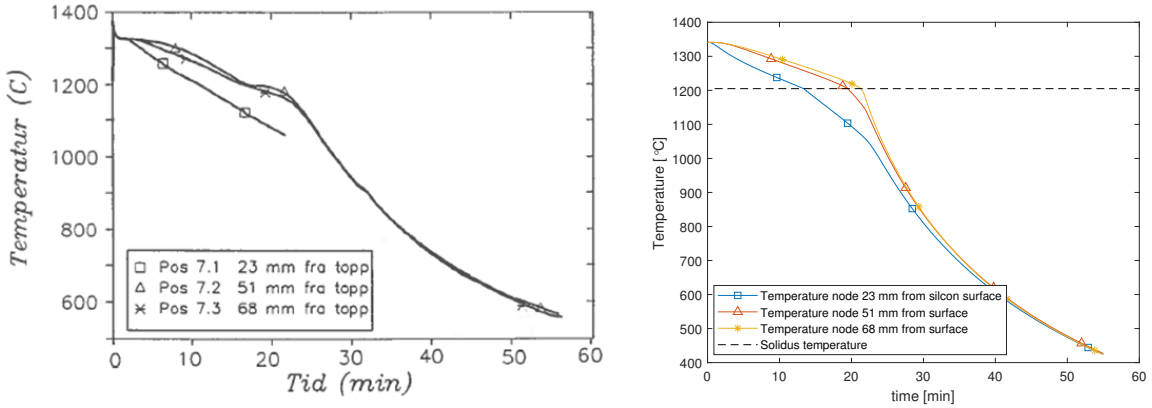

(a) Experimental temperature measurements of a ferrosilicon alloy by Tveit (1988)

(b) Replicating Tveit's experiment in Dymola using the silicon mold component model

Figure 4.2: Comparison of experimental temperature measurements and simulation results

There are some differences in the temperature profiles of Figures 4.2a and 4.2b. Initial silicon cooling rates are somewhat faster in the measured data-set, while the simulated results are cooled further, with a final temperature 120°C lower than the measured temperatures. The temperature profiles as a whole are very similar, and the differences can mostly be explained by differences in silicon properties. Nevertheless, the behavior of the silicon model seems to coincide sufficiently well with Tveit's measurements of actual silicon cooling behavior, as the overall temperature profiles and the time needed for solidification are very similar.

4.2 Validation of thermal storage performance

The thermal storage model was validated by comparing the storage response against experimental data from the literature. Doretti et al. (2019) conducted experiments to measure the behavior of a concrete thermal storage, as a way to validate their own numerical storage model. The experimental storage module consisted of four steel pipes encased in concrete, with thermal oil as the heat transfer fluid. The dimensions of the storage was $0.2 \times 0.2 \times 4$ m, it contained 390 kg concrete, and the heat transfer fluid used was a thermal oil. The properties of the concrete and thermal oil was provided by Doretti et al. (2019). The TES model was adjusted to match

the experimental setup, and the simulation and measured results were compared. Figure 4.3 shows the temperatures found by experimental measurements and from Dymola. It is primarily the experimental data in Figures 4.3a and 4.3c that is of interest (black lines). The concrete temperature shown in these figures was the average temperature of the storage.

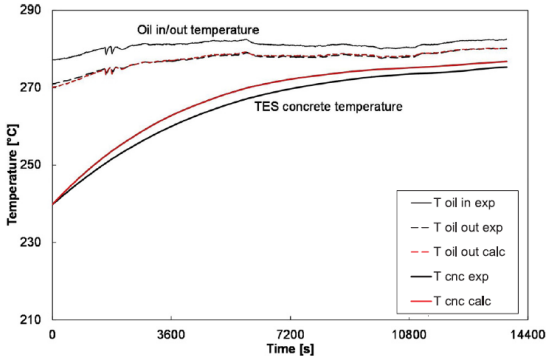

(a) Storage charging temperatures, experimental measurements (Doretti et al., 2019)

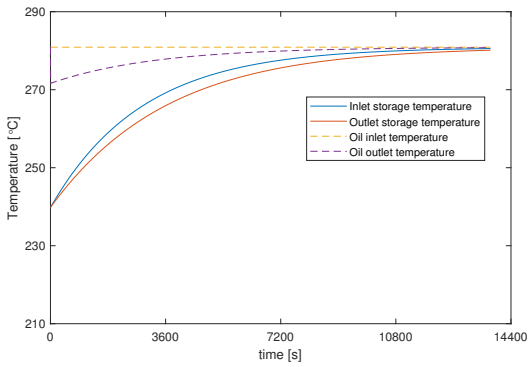

(b) Storage charging temperatures, as simulated in Dymola

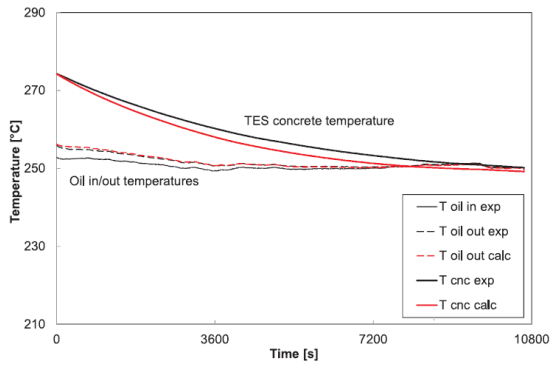

(c) Storage discharging temperatures, experimental measurements (Doretti et al., 2019)

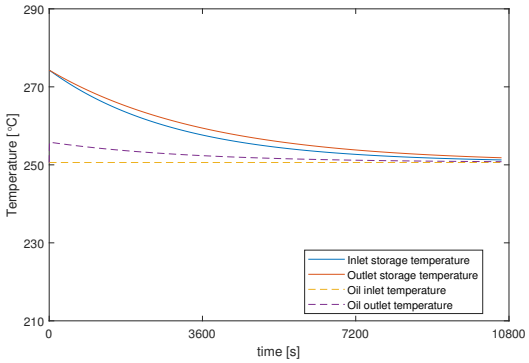

(d) Storage discharging temperatures, as simulated in Dymola

Figure 4.3: Comparison between measurements of an experimental concrete storage module and simulated recreation using the Dymola TES model (Doretti et al., 2019)

All in all the model performed admirably. However, some deviations were always present due to the model not accounting for thermal losses to the surroundings. Net heat flow rates into the storage were as a result a bit too high in the storage compared to the experimental data points, while net heat flow rates out of the storage module were a bit too low during storage discharge. This appears to be the reason why storage and fluid temperatures would not converge toward the same temperature in Figure 4.3a, while they do in Figure 4.3b. Other potential sources for deviations are the differences in storage geometry and the constant fluid properties used by the Modelica model. The TES model assumes the behavior of through all the steel pipes are equal, which is a valid assumption when there is no heat loss through the storage walls and there are considerably more pipes in parallel through the storage. This could also explain the differences in the results. Finally: constant fluid parameters simplify modeling and reduce simulation times, but it also neglects changes to fluid properties which could cause changes to heat transfer. Large changes in temperature could for instance change the overall heat transfer coefficient between

the storage and heat transfer fluid.

4.3 Validation of heat recovery tunnel behavior

No experimental data was found which could have been used to validate the waste heat recovery system's performance. Instead, the tunnel was modified to simulate radiant heat recovery from a rotary kiln, as simulation results from such a system have been described in the literature previously by Caputo et al. (2011), a study described in Subsection 2.2.3. The design of the WHRU was inspired by this work and is therefore quite similar, so the WHRU component could easily be modified to resemble the kiln system by changing the tunnel dimensions, source temperature and the thermal properties of the heat source and tunnel wall. No radiation losses were included, and the heat recovery fluid was pressurized water. The air flow between the rotary kiln and radiation heat recovery was simulated both as flowing counter-current and co-current to the heat transfer fluid. A comparison between the reference model results and the Dymola model is shown in Figure 4.4.

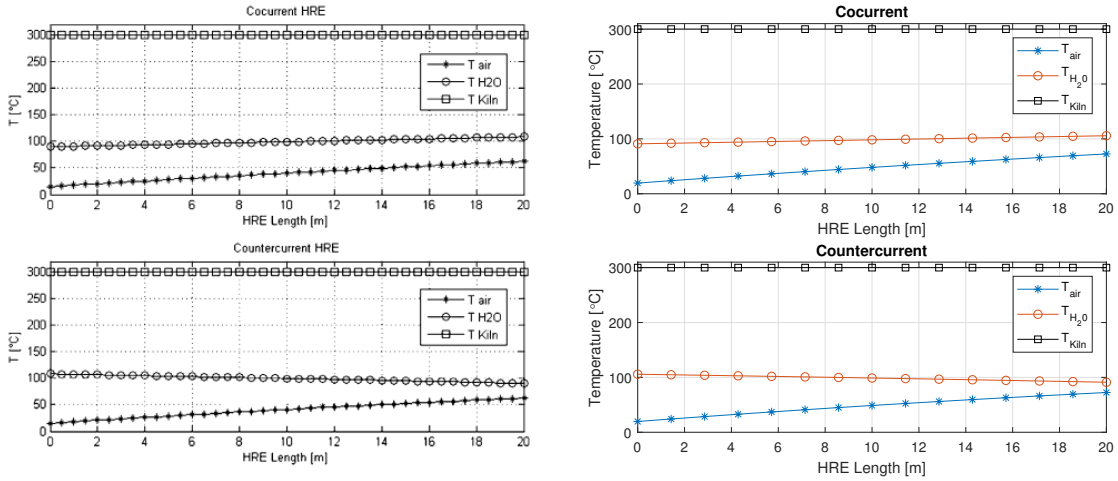

(a) Heat recovery from a rotary kiln, as modeled by Caputo et al.

(b) Replication of the rotary kiln heat recovery model using Dymola

Figure 4.4: Using the work of Caputo et al. (2011) to validate tunnel heat recovery behaviour

Figure 4.4 shows a comparison between the models when tested with an air velocity of 1 $\mathrm{m/s}$. Some thermal properties were not listed in the paper, so approximate values were used. The behavior of the two models are quite similar, but outgoing air temperatures are too high, while water temperatures are too low in the Dymola replication. The deviation between the two models also shows itself in the overall power transferred from the kiln: the Dymola model underestimated the heat transferred to the water by 19% while overestimating the heat transferred to the air by 8%. The reference model estimated a heat recovery efficiency of 64.5%, while the Dymola model estimated an efficiency of 61%. The operating conditions of the tunnel during silicon heat recovery will be quite dissimilar from the kiln recovery system it was compared to, but tunnel behavior was shown to behave quite as expected at these low temperatures. While this is no guarantee for the component's behavior at higher temperatures, it does inspire confidence in the heat recovery component.

Chapter 5

Results

5.1 Silicon exergy

As this work aims to produce power from silicon heat, a measure of the exergy contained in hot silicon was a valuable metric. It could be used as a point of comparison when analyzing the efficiencies of any proposed system, as the silicon exergy symbolized the absolute maximum potential work which could theoretically be extracted from the silicon heat, assuming no losses or irreversibilities. The silicon properties tabulated in Table 3.1 were used to express how much energy is stored due to the temperature of the silicon. Using 25°C as reference temperature, one can show how much heat has been released while silicon is cooled from 1450°C. Then, Eq. 1.13 is used to measure the exergy content in this heat, thus estimating the remaining exergy and heat in the silicon casting molds at any given temperature. This is shown in Figure 5.1.

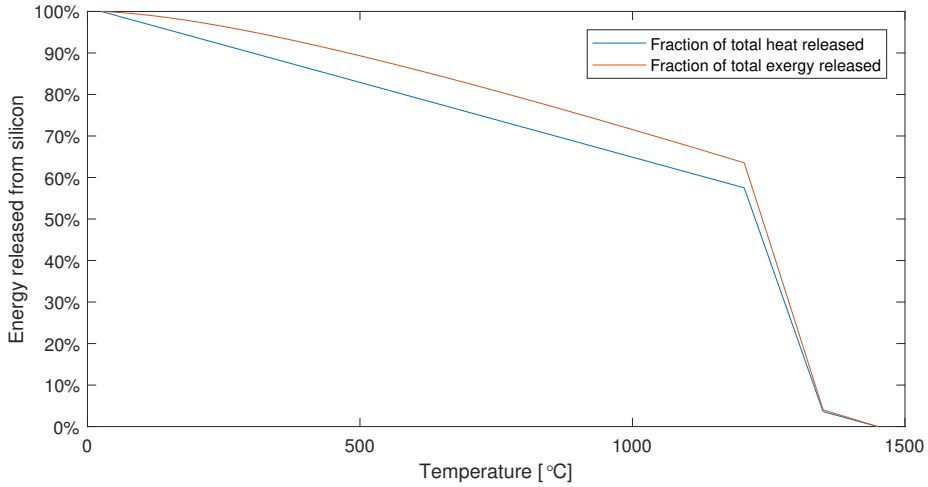

Figure 5.1: Heat and exergy released from silicon as it is cooled from 1450°C to 25°C

As seen here, most of the exergy is contained in the higher temperature region of the silicon. Once solidification has occurred, 65% of available exergy will have been released from the silicon, while nearly 90% of all available exergy has been released once the silicon reaches 500°C. It was calculated that 9000 kg of silicon will release 5.6 MWh of heat as it is cooled to 25°C, 71.8% of which can be considered exergy. Since the thermal storage and loop HTF usually

maintain a somewhat high temperature, silicon will not be cooled to 25°C while underneath the heat recovery tunnel. This exergy analysis shows that this matters very little from a heat recovery perspective, as very little exergy is left to be recovered at the lowermost temperature levels.

5.2 Model behavior

The model results will differ greatly depending on the chosen system parameters, but its behavior will retain some characteristics during all simulations. To describe these characteristics, a baseline system was created, with system parameters as described in Table 5.1. The baseline system will also be used as a point of comparison when system modifications are introduced, and when the effects of changing system parameters are examined.

Table 5.1: System parameters for the baseline case

Property	Unit	Value
mold time underneath tunnel	s	6480
Tunnel length	m	21.8
Tunnel width	m	2
Tunnel height	m	1
Loop HTF mass flow rate	kg/s	15
Air mean velocity	m/s	1
TES storage capacity	MJ/K	50
TES tube inner diameter	mm	15
TES tube pitch	mm	90
TES number of HTF tubes	–	620
Rankine cycle mass flow rate	kg/s	3
Heat exchanger UA-value	kW/K	10

The baseline system was simulated with constant loop and power cycle mass flow rates and with no additional control systems affecting system behavior. Under these conditions, system behavior will converge towards the systems cyclic steady state, which is regarded as its operating point. All system comparisons will therefore be done at each system's cyclic steady state. Cyclic steady state is assumed when initial temperatures of each system component coincide with their temperature during the end of the same casting cycle, meaning the operation of the system will be identical for subsequent casting cycles. The temperature profiles and primary heat flow rates of this baseline system are shown in Figure 5.2, describing the behavior of the loop WHRU, thermal storage, power cycle heat exchanger and one of the silicon molds. As was shown when discussing the system layout, the heat recovery tunnel is connected to the thermal storage, which is then connected to the heat exchanger, which loops back to the heat recovery tunnel. As such, tunnel HTF outlet temperature will always match storage HTF inlet temperatures, while storage HTF outlet temperatures will match heat exchanger hot side inlet temperature, and so on.

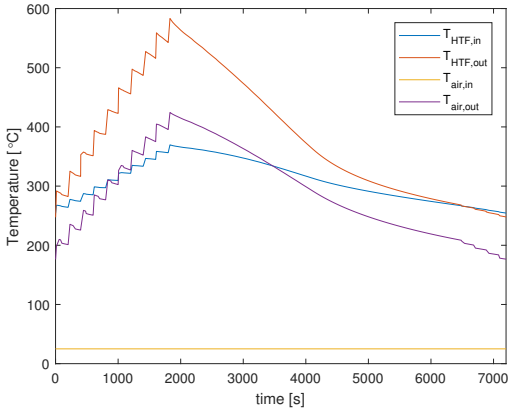

(a) Temperature profiles of the WHRU

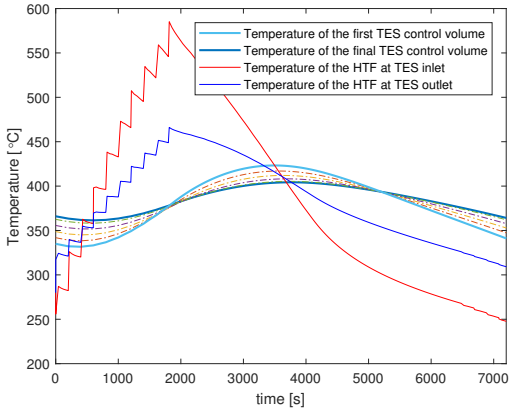

(b) Temperature profiles of the TES

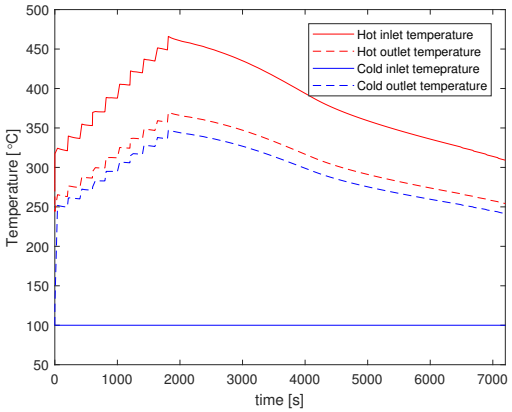

(c) Temperature profiles of the loop-Rankine cycle heat exchanger

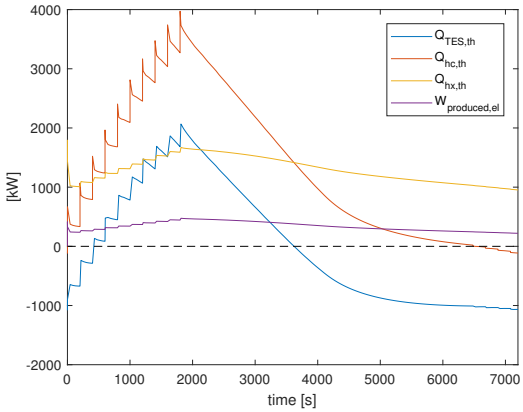

(d) System heat flow rates and the estimate for power production

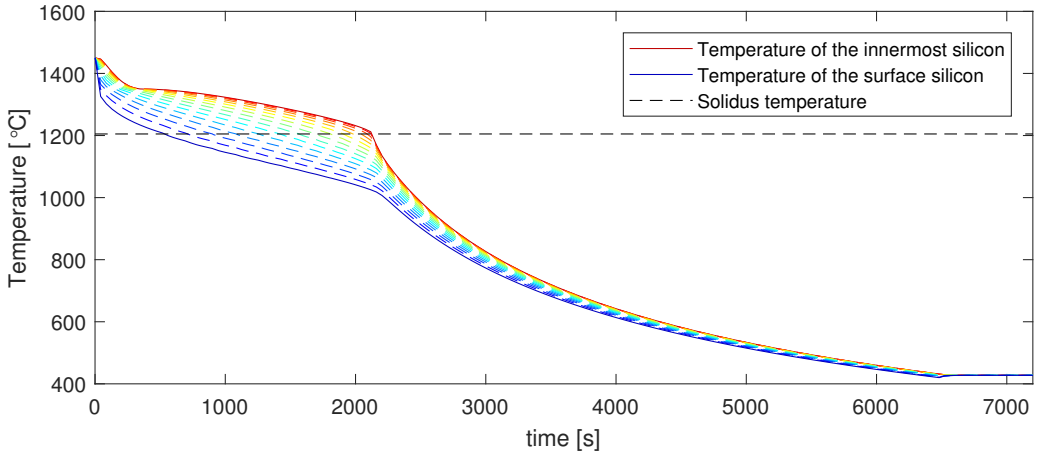

(e) Temperature profile of silicon underneath the heat recovery tunnel

Figure 5.2: Behaviour of the baseline system

Figure 5.2 describes a very dynamic system, where temperatures and heat loads change throughout the entire cycle. During the initial 30 minutes of the casting cycle, 10 casting molds are filled with hot silicon and placed underneath the tunnel at equidistant time steps. This correlates to the spikes in system temperatures and heat flows seen throughout Table 5.1. The spikes are also caused by the sudden formation of a temperature gradient in the silicon molds. The entire mold is initiated at 1450°C, but silicon temperatures close to the surface experiences a fast initial temperature decline, as seen in Figure 5.2e, while the temperature of silicon deeper in the mold experience a slower temperature decline. The silicon temperature profile shown here corresponds to the silicon first placed underneath the tunnel. The solidification time in this simulation is 35.5 minutes, which closely matches the target solidification time of 36 minutes decided in Section 4.1. Each of the ten casting molds in this simulation was kept underneath the heat recovery tunnel for 6480 s, i.e. 90% of the casting cycle duration. Further water cooling of the silicon mold is not included in the model, meaning the final silicon temperatures of 427°C merely reflects the silicon temperature as it is removed from the tunnel. Additional cooling might be necessary if the silicon must be even colder before it is crushed.

Heat flow rates to the recovery tunnel continue to increase as more and more silicon is placed underneath the tunnel for heat recovery, and it starts to decrease once all silicon has been placed underneath the tunnel. Heat flow rates will at this point start to continuously decrease as silicon temperatures decline, and eventually, heat flow rates will further decrease as silicon is moved out from underneath the tunnel heat recovery unit. Figure 5.2d shows how storage and heat exchanger flow rates relate to tunnel recovery heat. As heat flow rates to the tunnel increase, heat flow into the storage material increases alongside it. Positive storage flow rates signify a net heat input to the storage, meaning the storage temperatures are increasing, and the storage is charging. While some of the recovered heat is immediately transferred through the loop to the power cycle, a substantial part of the recovered heat is stored in the TES, which will later be supplied to the Rankine cycle, once silicon temperatures have lowered. Discharging of the storage commences once storage temperatures are higher than the loop HTF temperatures.

In Figure 5.2d, it can be seen that the heat flow through the heat recovery tunnel is slightly negative towards the end to the casting cycle. It happens when the silicon molds are removed from the tunnel, meaning the heat source transferring heat to the tunnel is no longer there. At the same time, air is still flowing inside the tunnel, meaning the loop heat transfer fluid will heat the colder air, thus transferring heat from the tunnel HTF to the air, explaining negative tunnel heat flow rates.

As the heat transferred from the heat recovery loop to the Rankine cycle fluctuates, so does the temperature on the Rankine cycle side of the heat exchanger. The outlet temperature varies between 241°C and 347°C during a cycle, with the hotter temperatures coinciding with peak silicon heat transfer rates. High temperatures and heat flows are correlated to high estimated power production, while the low temperatures and heat exchanger heat flow rates coincide with periods of less electricity generation.

While the simulation shows highly variable heat flow rates from the silicon heat source, it estimates a much less variable power production, which is thanks to the thermal storage. The storage enables continuous electricity production, and this system is estimated to produce an average of 338 kW of electric power, but it fluctuates between 221 kW and 481 kW. The power production varies greatly, but the inclusion of a thermal storage avoids discontinuous power production, which would have nearly been the case without a storage. This system was shown to recover 54.6% of the heat transferred from the hot silicon, while it converted 16.7% of all available exergy in the silicon to electric power (exergy efficiency). This corresponds to

74.9 kWh of electric energy generated per tonne silicon produced, which is merely 0.58% of the electric energy needed in the production of this silicon.

The baseline system's main characteristics are summarized in Table 5.2. As seen from Figure 5.2, system performance will continuously change throughout the entire casting cycle, making it difficult to compactly describe system performance. The characteristics listed below provide a measure for some of the more important aspects of the system. Power production per casting cycle will provide a measure of the overall potential of this system, and is important because producing electric power is the overall objective of this heat recovery system, and because a larger electricity production will mean more willingness to invest in the system. At the same time, it is of interest to ascertain how much the power production will fluctuate throughout a normal casting cycle, as it would be beneficial to reduce this fluctuation. This is also why the temperature of the power cycle turbine is an important system characteristic. Less fluctuations here will simplify power cycle operation. Storage temperatures are of interest due to the thermal limitations of the concrete. Heat and exergy efficiencies describe how well the system recovers the silicon heat, while the solidification time will describe how the system affects the silicon process.

Table 5.2: Main system characteristics of the baseline system performance

Property	Unit	Value
Power produced per cycle, W	kWh	676.2
Variation in power produced, $\Delta\dot{W}$	kW	259.6
Average power cycle turbine temperature, $T_{turb,avg}$	°C	292.1
Variation in power cycle turbine temperature, ΔT_{turb}	°C	106.2
Average storage temperature, $T_{TES,avg}$	°C	383.6
Maximum concrete temperature, $T_{TES,max}$	°C	426.6
Total exergy recovery, η_{ex}	%	16.7
Cycle heat recovery efficiency, η	%	54.6
Solidification time, t_s	min	36.0

Chapter 6

Analysis

The behavior of the model components was validated in Chapter 4 and a description of model behavior was presented in Chapter 5. Now, the model will be used to investigate the behavior of the proposed heat recovery system. These investigations will be used as the basis for choosing a system design. But to properly choose system design parameters it is vital to understand how these parameters affect system performance and behavior. This has already been done for some parameters in the project work preceding this Master's thesis (Lingaas, 2018), which was summarized in Section 1.4. The system modeled in this work differs from the system discussed in the project work, but how the system reacts to changes in parameters has stayed mostly the same, meaning the effect of changing mass flow rates, UA-values and storage heat capacities will be the same in this work.

The model has undergone substantial modifications to better and more accurately describe the system behavior since the project work. This has also led to certain changes in how system parameters will affect loop behavior. In the project work, storage heat capacity and overall UA-value could be decided separately. This is no longer the case, as the storage UA-value will depend on the dimensions of the storage. The size of the storage, but also the dimensions and pitch of the heat transfer tubes will affect the storage UA-value. Other changes to behavior compared to the project work system is the heat recovery tunnel. Due to a better implementation of system dimensions, thermal losses will now be affected by the dimensioning of the tunnel. Air flow through the tunnel was also not included in the project work. The impact of the waste heat recovery system on silicon casting conditions was also not considered during the project, but will be brought into focus now.

To gain a better understanding of the system and changes introduced to the system since the project work, an investigation into some system parameters effect on system behavior was carried out. System parameters already investigated in the project work will not be investigated anew. Once these parameters have been thoroughly investigated, system design parameters will be proposed. An examination into system control schemes was done, and an initial economic evaluation of the design system was conducted.

6.1 The effect of a thermal storage on system performance

It is of interest to compare the performance of this system up against a similar system without a thermal storage, as a means to ascertain the effect of the thermal storage on system performance. While a storage will lower variations in system performance throughout a casting cycle, it also introduces another potential loss in exergy throughout the heat recovery loop. A thermal storage means heat has to be transferred from the loop to the storage and transferred back to the loop from the storage, and in both of these cases there is a need for a temperature difference between the loop HTF and storage to drive this heat flow. However, this will also lead to a decrease in system temperatures, so while the energy is conserved, temperatures are lowered, meaning exergy is destroyed. A system with no thermal storage would therefore be able to deliver heat with a higher net exergy content than a system with a thermal storage. However, a system with no thermal storage would be far more variable. This is shown in Figure 6.1, which shows a comparison between the baseline system and the exact same system with no thermal storage. Figure 6.1a shows the outlet temperature on the power cycle side of the heat exchanger, while Figure 6.1b shows the estimation for power production from each system.

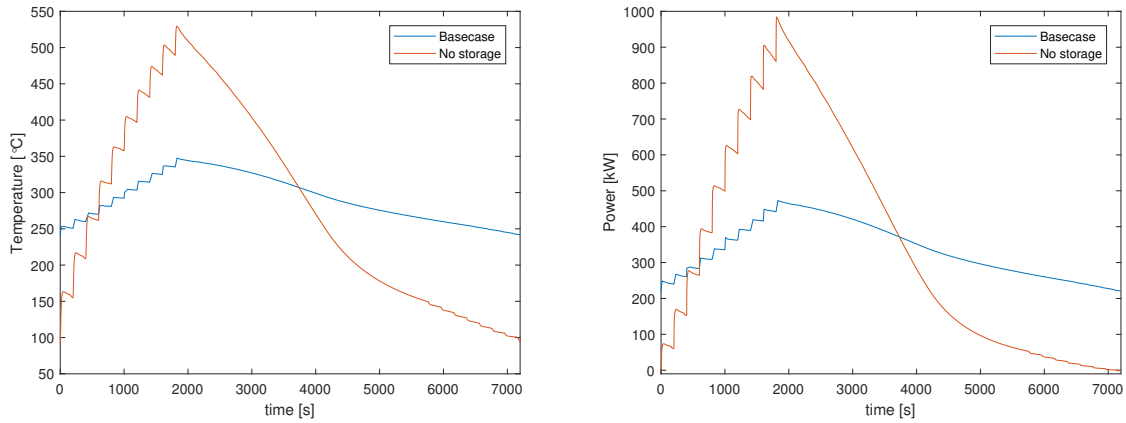

(a) Heat exchanger outlet temperature on the power cycle side

(b) Estimated power production from both the storage and no-storage systems

Figure 6.1: Comparison showing the effect of a thermal storage on system performance

As can be seen in Figure 6.1, the inclusion of a thermal storage have reduced variations experienced by the power cycle to a very large degree. In a system with no storage, the temperature variations encountered at the hot side of the power cycle would go from 429.6°C to 106.0°C throughout a casting cycle, while the variation in estimated power production would go from 984.6 kW to 252 kW. This is a reduction in variations by respectively 75.3% and 74.4% as a direct result of the storage. However, the total estimate for power produced through a casting cycle slightly favors the system without a storage, which produced 706.4kWh, while the storage system produced 676.2 kWh. It is important to keep in mind that the estimate for power production in this work is based on the exergy in the heat transferred from the loop to the power cycle, and nothing else, as seen in Section 3.9. Recall, estimated electrical conversion was set to be 50% of the available exergy in the heat sent to the power cycle. This means that the reduction in estimated power in actuality shows a reduction in the exergy recovered by the system, meaning the introduction of a thermal storage led to a destruction of exergy. The reduction in exergy in the storage system was 5% compared to the system without a storage.

This is primarily explained by the no-storage system delivering more heat to the power cycle at higher system temperature, which is beneficial for the exergy delivery. Less heat is delivered at low system temperatures, where exergy efficiencies will be low (see Eq. 1.13). At the same time, total heat recovered from the silicon are very similar between the two systems.

Not considered when estimating electrical power production is the effects of a power cycle design point and losses due to operating the power cycle away from this design point. As neither of storage system or no-storage system manages to provide constant conditions for the power cycle, off-design losses will be present in both systems. But these losses will be far greater in the system with no storage, as the variations in heat, temperature, and exergy content are far greater here. Variations are much lower in the storage system, meaning it is far more likely that electric power conversion is feasible from the storage system compared to the no-storage system.

6.2 Design of the thermal energy storage

The storage design will be decided by the total storage heat capacity, the heat transfer tube diameter, the tube pitch distance and the number of tubes, as seen in Figure 3.9. Once these four design parameters are decided, the volume of concrete needed in the storage is decided by the total storage heat capacity. The tube pitch decides how much concrete will surround each heat transfer tube, which alongside the number of parallel tubes will decide the cross-sectional area of the storage. Then, storage length is set to provide enough volume for the concrete material while accounting for the volume occupied by the embedded heat transfer tubes. Changing any of these design parameters will change how the storage behaves, which will have an effect on the entirety of the heat recovery system. From the project work (Lingaas, 2018), it is already known how system performance will change with changes to overall storage heat capacity and UA-value, as summarized in Section 1.4, but it is of interest to examine how storage UA-value will be affected by changes to all of the design parameters, as this was not examined during the project work. Thus, to understand how the storage dimensions and layout affect storage heat transfer, some time was spent examining this relationship.

The average fluid velocities through the thermal storage will depend on the total cross-sectional flow area available in the heat transfer tubes. This area will depend on the storage inner tube diameter and the number of tubes, which means fluid velocities will depend on the same parameters, as seen in Figure 6.2. The figure shows how adding additional heat transfer tubes or increasing tube diameters leads to lower fluid velocities.

The effect of changing the inner tube diameter on the storage heat transfer coefficient was examined in Figure 6.3. Here, tube pitch and storage heat capacity were kept constant and equal to that of the baseline system, while the number of tubes and tube diameter was varied. Since storage length and cross-sectional area are both in part decided by the number of tubes and tube diameter, they will change with the design parameters.

In Figure 6.3a it can be seen that h_E, the storage heat transfer coefficient, will decrease with increasing tube diameters and number of tubes. On the other hand, Figure 6.3b shows the overall storage UA-value reacting differently. While the UA-value of storages with lower tube diameters will change relatively little with a change to the number of tubes, a storage with a large tube diameter will experience a large increase in UA-value when using fewer heat transfer tubes through the storage. Keep in mind that a decrease in tube numbers will mean an increase in tube length, as tube pitch and storage heat capacity was kept constant. This means

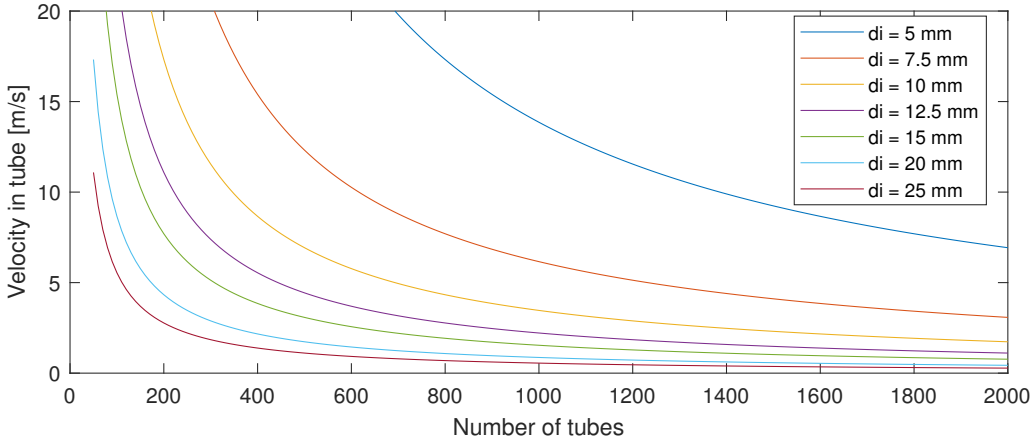

Figure 6.2: Fluid velocities through the thermal energy storage

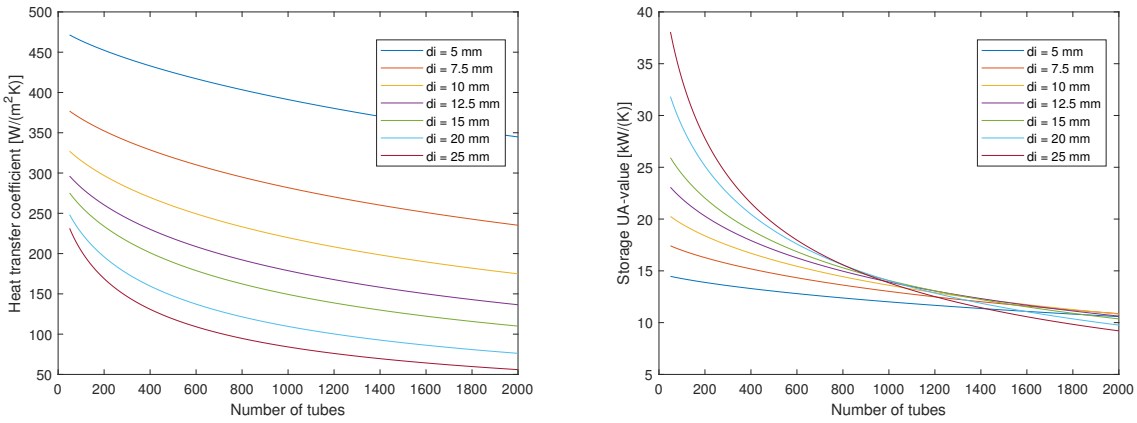

(a) Effective heat transfer coefficient, h_E

(b) Overall UA-value of the storage unit

Figure 6.3: Storage heat transfer coefficients as a function of the number and diameter of heat the transfer tubes.

that the number of tubes and the storage length are inversely related, as more tubes necessitate a shorter storage to maintain the desired heat capacity/concrete mass. This also means the heat transfer area between the HTF and the storage remains constant for any set inner diameter in Figure 6.3, no matter the number of tubes. This is very beneficial for the UA-value of large diameter tubes: While the effective heat transfer coefficients are lower compared to tubes with low diameters, heat transfer areas are much bigger. However, larger pipe diameters are more expensive and the increased tube diameter means the tubes displace a part of the storage volume which would otherwise be filled with concrete, which leads to a longer storage unit to maintain the right concrete mass. Thus the storage performs better, but it becomes more expensive due to it requiring both longer and wider heat transfer tubes.

The tube pitch distance will also affect storage behavior. Figure 6.4a shows the overall UA-value as the tube pitch distance varies between 50 and 140 mm while the inner diameter is kept constant. As can be seen here, UA-values increase when the distance between heat transfer tubes is reduced. Also seen from the figure is that UA-values decrease as the number of heat transfer tubes increases, as was the case when analyzing the effect of different inner

diameters. However, a reduction in tube pitch will increase the amount of heat transfer tubing in the storage, and it will increase the length of the storage unless additional tubes are added in parallel. Very low tube numbers and pitch distances would result in storage lengths being far too long for the storage to make sense, as shown in Figure 6.4b.

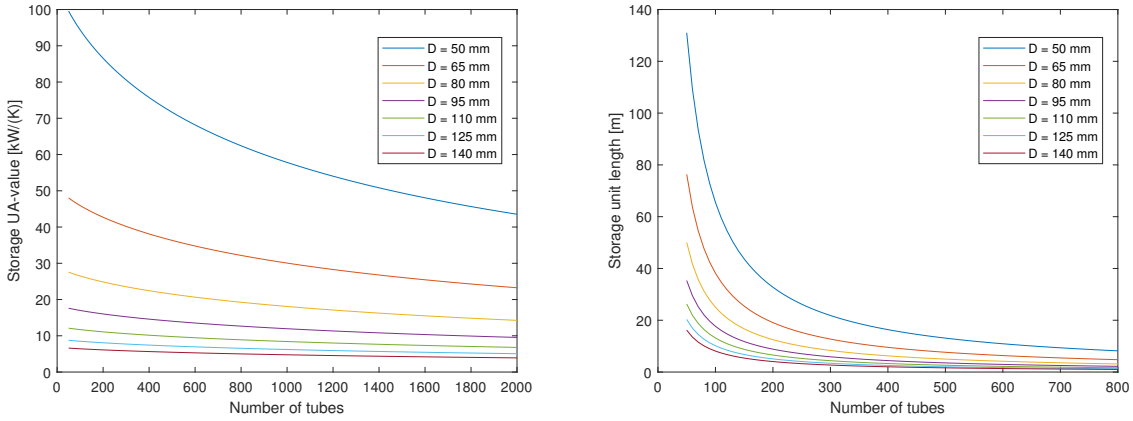

(a) Storage UA-value

(b) Storage length

Figure 6.4: Storage overall UA-value and unit length as a function of the number and diameter of heat the transfer tubes

Through Figures 6.2, 6.3, and 6.4, it has been shown that the storage behavior will be affected by the storage design parameters. Storage dimensions were shown to have a large effect on the overall storage heat transfer coefficient, meaning a good storage design will potentially have a large positive effect on storage behavior. Heat recovery systems with large storage UA-values was in the project work linked to systems that were able to keep changes to power cycle temperatures and heat loads as low as possible (Lingaas, 2018). This was due to the storage being better able to store heat during periods of high silicon heat flow, while also being better at depositing the stored heat during the latter parts of the casting cycles. Large UA-values also meant the storage would "react" faster to sudden changes in temperatures. This in turn kept the temperature of the HTF flowing out of the storage and into the power cycle heat exchanger much less variable, which induced less variations in the power cycle, leading to a more even production of electrical power. A comparison from the project work is shown in Figure 6.5, where the operation of a similar storage is simulated twice, both having the same heat capacity, but having very different storage UA-values, which showcases the benefit of large storage overall heat transfer coefficient.

Ensuring a large overall heat transfer coefficient in the storage will therefore be beneficial for the overall system operation, and it has been found that storage UA-values will increase with lower pitch distances, wider tube diameters, and higher fluid velocities. However, using storage design parameters which improves heat transfer conditions will also increase storage costs. An increase in storage costs was found to be linked to an increase to tube diameters and reduction in tube pitch, as both increase the amount of heat transfer tubing needed in the storage, which will material costs. However, as concrete as storage material is relatively inexpensive compared to most alternatives, a slight increase in investment cost can be worth it to improve storage performance.

In both Figure 6.3 and 6.4 it was shown how storage heat coefficients would increase as the number of heat transfer tubes were reduced. This is explained by Figure 6.2: as the number of

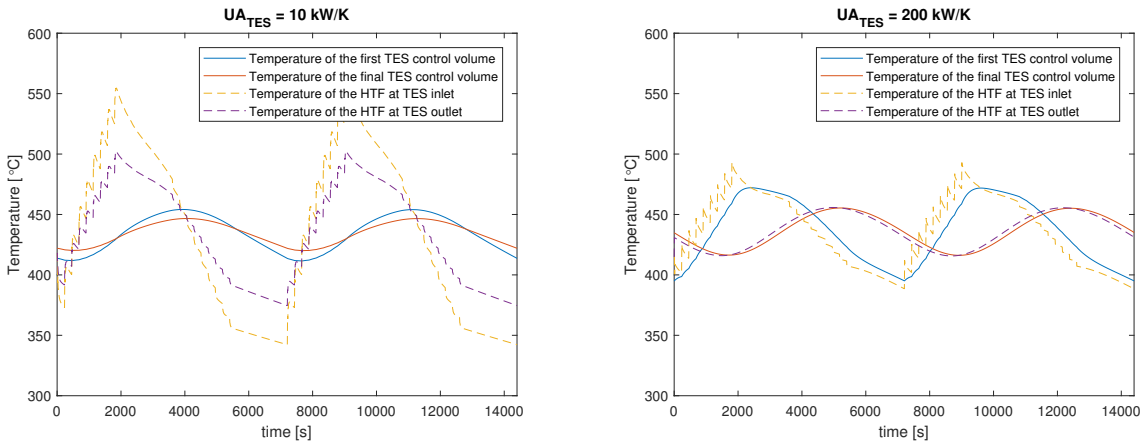

(a) Storage temperature profile with a low UA-value

(b) Storage temperature profile with a very high UA-value

Figure 6.5: Comparison of a TES with high and low UA-value (Lingaas, 2018)

tubes through the storage is reduced, fluid velocities will increase. An increase in fluid velocities will lead to a more turbulent pipe flow, meaning Reynolds numbers will increase. As the fluid convection coefficient is found through Gnielinski's correlation (Eq. 3.16), an increase to the Reynolds number will lead to an increase in the fluid convection coefficient. Finally, an increase to the fluid convection coefficient will positively affect storage heat transfer through Eq. 3.19, as the fluid convection coefficient contributes to the overall storage heat transfer.

When testing the storage at different tube diameters, it was apparent that large tube diameters are to be preferred when seen from the perspective of storage performance. The large increase in storage heat transfer area appears to more than make up the reduction in storage heat transfer coefficient, especially if there are relatively few heat transfer tubes through the storage. To maximize the storage UA-value, it has been shown large tube diameters and few pipes in parallel are preferable, as long as pitch distance is kept constant. However, too few heat transfer pipes should be avoided, as it would lead to a storage that with a low cross-sectional area and a longer storage unit, which would both require more space than strictly necessary, and lead to a storage with a large surface area. The Dymola model assumes an adiabatic storage surface, meaning no storage loss, but a larger surface area will in reality be accompanied by an increase in heat losses, which would lower the effectiveness of the storage or cause a greater need for insulation to reduce storage losses. To reduce the need for insulation, it would be beneficial to try to reduce the storage surface area per unit storage volume. Thus, in order to reduce potential surface losses, one should keep the storage length from becoming too long.

The tube pitch distance was shown to be very influential in storage heat transfer, with shorter tube pitches improving storage behavior considerably. However, a shorter tube pitch will also necessitate a longer storage or a larger number of tubes, either way a shorter pitch distance will lead to less concrete per cross-sectional area, which will increase storage prize per storage volume, as a larger fraction of total storage volume is occupied by heat transfer tubing.

Heat transfer fluid pressure has yet to be discussed. While this work does not properly model pressure or pressure loss in any component, its effect on system design should still be considered. In general, higher fluid velocities will lead to higher pressure losses throughout the storage tubing, which is not desirable. To counteract this, fluid velocities should be restricted to avoid unnecessarily large pressure losses. Which velocities are considered too fast will depend

on the heat transfer fluid in use and the system pressure. While describing the design process of a shell and tube heat exchanger, Edward (2008) proposed some velocities to be used on the tube side of a shell-and-tube heat exchanger. The thermal storage is not a shell-and-tube heat exchanger, but lessons regarding tube side pressure from that application will be used as when designing the storage all the same. Using gasses at atmospheric pressures, fluid velocities of 15-30 $\mathrm{m/s}$ was recommended, while gas velocities of 5-10 $\mathrm{m/s}$ was recommended if one were to use highly pressurized gases. The heat transfer fluid used in this work is pressurized CO_2, meaning the fluid velocity should be limited to a maximum of 10 $\mathrm{m/s}$. Another constraint was added in addition to the upper bound to fluid velocities: Heat transfer tubes should have an inner diameter of 5-10 mm, as this coincides with normal inner tube diameters in heat exchangers where pressurized CO_2 is involved.

The constraints to fluid velocities and inner diameters are in direct opposition to what was considered the best storage design from a heat transfer point of view. To comply with these restraints, while still maintaining as high a storage UA-value as possible will mean that tube diameters should be set to 10 mm, while the number of tubes should be chosen to keep fluid velocities just below 10 $\mathrm{m/s}$. This severely constrains the choice in storage layout, as is apparent in Figure 6.2: with narrow tube diameters, the number of tubes must be kept rather high to ensure proper fluid velocities, which means the optimal choice in storage design from a heat transfer perspective can no longer be considered as a possible design point.

There are some other aspects of this system that has not been further examined since the project work, but which are still important for overall system performance. One of these being the total storage heat capacity. The storage heat capacity describes the thermal energy needed to increase overall storage temperatures by 1°C. An increase in heat capacity will lead to a storage capable of storing the same amounts of thermal energy while experiencing less change in storage temperatures. This would lead to smaller cyclic changes to system temperatures, as well as smaller variations in power cycle operating conditions. In addition, a change in storage heat capacity will also lead to a change in storage UA-value, as heat capacity is tied to the mass of storage material. Assuming all other storage design parameters (pitch, inner diameter, and number of tubes) are left unchanged, a change in heat capacity will have a linear effect on storage length, i.e. it will cause a linear change to storage UA-values as well. An increase in storage heat capacity will therefore lead to a system experiencing less temperature variations, having higher UA-values, but at the same time being a bigger, more expensive storage unit.

6.3 Design of the WHRU tunnel

The design of the heat recovery tunnel will have an effect on multiple aspects of the heat recovery system. The tunnel governs heat recovery, but its design will also affect the casting conditions for the silicon molds. Thus it is important to examine how the WHRU affects both heat recovery and the silicon casting process, so that the tunnel can be designed to ensure proper silicon casting while recovering as much heat as possible.

6.3.1 Tunnel parameters' effects on silicon cooling

How the heat recovery tunnel affected the silicon solidification time was examined in detail. Multiple system parameters might affect the cooling rate, and chief among them is the mold dimensions. A shallow, long and wide mold would have a large heat transfer area, as well as

low thermal resistance through the mold, which would cause increased heat flows compared to a deeper mold with less surface area. This change in heat flows should have a noticeable effect on mold temperature profiles. In addition, the effect of air velocity through the tunnel was examined, as well as if a different fluid inlet temperature to the tunnel would cause any noticeable changes to cooling rates.

When testing for the effect of air velocity and fluid temperatures on solidification, tests were once again based on the baseline design, while changing the air velocity and tunnel HTF inlet temperature. Results from these tests are are tabulated in Tables 6.1 and 6.2. The tables show that silicon solidification times (t_s) does depend on both fluid temperature and air velocity, but neither of these parameters influences the solidification temperature in any significant manner. Tunnel HTF inlet temperatures ranging from 100°C to 700°C only caused the solidification time to increase 5 minutes. A change in air velocities would also affect the heat recovery system. While Table 6.2 shows that the solidification time will decrease with increasing air velocities, it also shows that heat recovery losses related to the tunnel air flow will balloon in size at higher air velocities, reducing the potential for heat recovery and electricity production. At low air velocities, the air within the tunnel will become very hot while air losses will be kept at low. Overall, the effect of tunnel air velocity on solidification was found to be rather minimal at sensible choices in air velocities. To achieve a noticeable reduction in solidification time, the increase in air velocity would also lead to a large increase in heat lost to the tunnel airflow, which would be counter-intuitive from an energy recovery point of view. Tunnel air velocity would affect the temperature of the tunnel air, so if there is a need to limit air temperature out of the tunnel, controlling the tunnel air flow would be the way to do so.

It is important to note that a real system would experience some air circulation as long as both sides of the heat recovery tunnel is kept, and closing the tunnel is not possible while casting molds are moved into the tunnel or away from the tunnel. Losses tied to the air flow will therefore be present for any configuration of this system. This also means that a constant air velocity of zero, or very close to zero, will not occur while the tunnel remains open.

Tables 6.1 and 6.2 showed that both the temperature of the tunnel heat transfer fluid and the air velocity would influence cooling rates to a certain extent. However, their influence was markedly less than that of the silicon surface area. In addition, the tests done with tunnel HTF inlet temperature are not applicable in an actual operational scenario. During actual operation, the tunnel HTF inlet temperature will change throughout the casting cycle alongside the storage temperature, and will therefore not be kept constant. The highest HTF inlet temperatures tested for in Table 6.1 are also not attainable in actual system simulations. In most of the simulations done in this work, tunnel inlet temperatures would at minimum be 250°C and at maximum be 450°C, and in this temperature region solidification times will not be affected much by variations in tunnel temperature.

Table 6.1: The effect of tunnel HTF inlet temperature on silicon solidification time

Property	Unit	Tunnel HTF inlet temperature (°C)						
		100	200	300	400	500	600	700
t_s	min	35.9	36.1	36.4	37.0	38.0	39.1	40.8

Mold dimensions were found to have a tremendous impact on silicon solidification times. This was tested by simulating the baseline system while changing the silicon heat transfer area by using different mold dimensions. The tests were conducted assuming 10 molds with

Table 6.2: The effect of tunnel air velocity on heat recovery and silicon solidification time.

Property	Unit	Tunnel air velocity (m/s)							
		0	0.1	0.5	1	2	5	10	20
t_s	min	37.1	36.8	36.3	36.1	35.8	35.7	34.6	32.5
$T_{air,max}$	°C	854.7	828.2	612.2	593.2	583.7	576.8	551.4	500.8
$\frac{\dot{Q}_{air}}{\dot{Q}_{mold}}$	%	0.3	3.1	11.9	16.3	19.4	21.7	31.8	49.0

quadratic silicon surface area were filled with silicon each cycle. Figure 6.6a shows how the solidification changes as total mold surface area changes, while Figure 6.6b shows how the heat recovered by the tunnel will change with total silicon surface area. Not shown here is how heat recovery can be improved by changing the width and length of each mold while keeping surface area the same. This will be shown in Subsection 6.3.2.

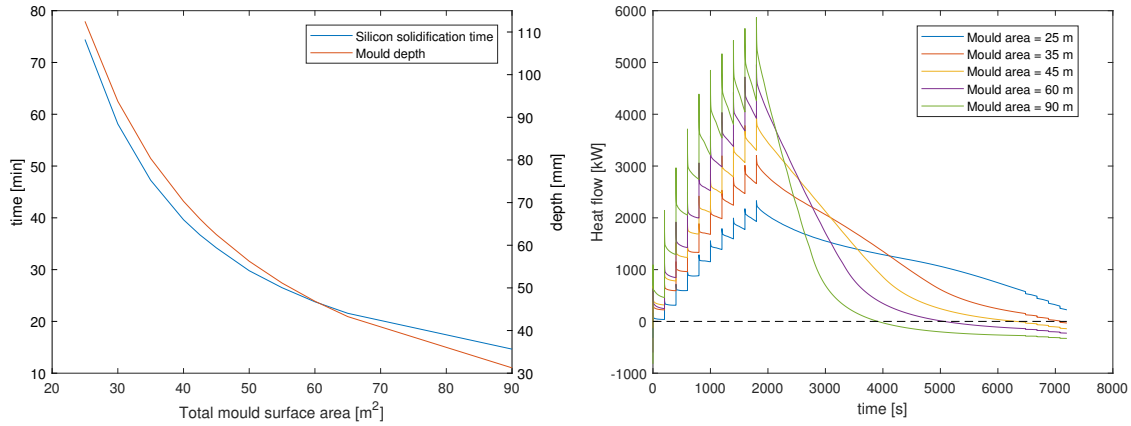

(a) Silicon solidification time with changing silicon surface areas

(b) Heat recovered from the silicon at a selection of different surface areas

Figure 6.6: Storage behaviour at various total silicon surface areas

Figure 6.6a shows how silicon cooling rates are highly dependent on the silicon surface area and the depth of silicon in each mold. The silicon depth is decided by mold dimensions and the mass of silicon in each mold. An increase in depth will increase silicon thermal resistance which will impair heat flow through the silicon. This will slow the temperature decline of the silicon towards the bottom of the mold, creating a large temperature gradient through the silicon depth. The slow temperature decline near the bottom of the mold will increase solidification times. A shallow mold will, on the other hand, reduce the thermal resistance, reducing the temperature gradient through the silicon depth, meaning the temperature toward the bottom of the mold decline faster.

Figure 6.6b shows the heat captured by the WHRU during simulations with five different silicon surface areas. Higher silicon surface areas correspond to higher initial heat flows. In turn, the higher heat flows meant a faster decrease in silicon surface temperature, which led to a faster decrease in flow rates as well. In fact, the high surface areas and heat flows led to a rapid decrease in silicon surface temperatures, which in some cases led to surface temperatures lower than that of the tunnel HTF, meaning heat transferred in the system TES will be used to heat the tunnel air or, in the most extreme cases, the silicon molds. This is the negative heat

transfer rates seen in Figure 6.6b. Low surface areas, on the other hand, meant far lower heat transfer rates, and thus it took longer for the silicon to fully solidify while the silicon heat output fluctuates far less.

The design of the heat recovery tunnel was found to have a large effect on several aspects of this system's performance and behavior. It was shown to affect the silicon cooling rates, as well as the tunnel's ability to recover heat. These are critical aspects of the system, and proper tunnel design will be important for the overall system's performance and viability. The *most* important measure of a well-designed system will be the system's ability to ensure proper silicon cooling. Any heat recovery system that is proposed must therefore first and foremost ensure that the silicon is solidified correctly. Heat recovery is secondary to this concern. As such: the tunnel should be designed to recover as much of the available heat possible, while always ensuring that the silicon achieves its intended structure and properties by solidifying at the intended rate of 36 minutes. A failure to fulfill either of these demands cannot occur if the heat recovery system ever is to be implemented.

It could prove beneficial to keep tunnel temperatures low from a heat recovery perspective, as this would increase the tunnel's ability to recover heat from silicon during the latter part of each casting cycle, when silicon temperatures are at their lowest. This could lead to a net increase in heat recovered from the silicon. However, this does not compute from an exergy point of view. The analysis of the silicon exergy content conducted in Section 5.1 showed that only a small fraction of total exergy is left to be recovered once silicon temperatures fall below 500 °C, meaning the potential benefit of recovering the very low-temperature silicon heat is slim.

The surface area of the casting molds had the greatest effect on silicon solidification time. Because of this, they must be set during the design of the tunnel to attain the desired solidification time, as neither tunnel temperature nor air velocity proved to be viable means to control the solidification time. A lower surface area was shown to be correlated to less variations in cyclic heat flows from the silicon, while a lower surface area would lead to more heat being transferred from the mold, but neither of these aspects would matter if solidification times were not as they should be. It will be shown in Subsection 6.3.2 that mold width and length can still be used to improve heat recovery without affecting solidification, however, the total area must *always* be chosen to ensure good conditions for the casting process.

Figure 6.6a described how silicon solidification time would depend on the silicon surface area while underneath the heat recovery tunnel. It also made it evident that for the solidification time and cooling rates in this new system to remain unchanged, there would be a need to increase mold surface areas and decrease mold depths when compared to the molds currently in use at Salten Elkem. It was shown that a solidification time of 36 minutes was achieved by having a total silicon surface area of 43.6 m^2, which corresponds to a 32.6% increase in silicon surface area when compared to the molds used at Salten today. The need for larger silicon surface areas while using the heat recovery system is a result of the tunnel severely reducing the silicon cooling rates relative to the cooling rates present without a tunnel. To demonstrate this fact, simulations were run to find the tunnel parameters which would ensure proper solidification time while using the original casting mold dimensions of nine molds with a silicon surface area of $2.03 \times 1.8\ \mathrm{m}^2$. A silicon solidification time of 36.4 minutes was achieved when tunnel HTF inlet temperature was set to 25°C and the air velocity set to 20 $\mathrm{m/s}$. The dimensions of the heat recovery tunnel also had to be increased: Tunnel surface area was increased 250% compared to the baseline system. The tunnel recovered 10.0% of the heat released by the mold, compared to 54.6% in the baseline system. System temperatures were also far lower. This

demonstration shows how a potential heat recovery system would *have* to use casting molds with a larger surface area than the ones currently in use at Salten, in order to ensure proper solidification times. Without larger casting molds any potential for heat recovery and power generation will be completely wiped away by the need to maintain unreasonably low system temperatures to maintain the required cooling rates.

A potential way to prevent the heat recovery unit from affecting the silicon solidification at all is to only start heat recovery once the silicon has fully solidified, i.e. start recovering silicon heat once silicon temperatures have been reduced to 1205°C. However, this would completely decimate any potential for heat recovery whatsoever. From the exergy analysis in Figure 5.1 it was shown that the majority of silicon exergy is recoverable while silicon is being solidified. By waiting to recover heat until temperatures have reached 1205°C, 65% of the exergy contained in the silicon at 1450°C has already been lost. The baseline system would only produce 131.9 kWh of electric power every casting cycle in such a system, merely 19% of what it produced with an initial silicon temperature of 1450°C. Waiting until silicon has solidified is thus not recommended, as potential energy production would plummet as a result.

6.3.2 Tunnel parameters' effect on heat recovery and heat losses

All silicon heat which is not recovered by the tunnel heat transfer fluid is referred to as heat losses, as they represent heat not collected by the system. All of these losses are associated with the WHRU tunnel. Radiation losses are thermal radiation which is radiated out of the tunnel exit or entry, thus transferring heat away from the heat recovery system. Air losses are the net heat transferred to the tunnel air flow, while wall losses are the heat transferred from the external tunnel wall to the surroundings. Tunnel losses, as well as net heat flows from the mold and to the HTF are shown for the baseline system in Figure 6.7. In this system, 54.7% of the mold heat is recovered by the system, while thermal radiation accounts for the largest fraction of the heat losses, at 25.0% of the mold heat. Heat lost to the tunnel air and through the tunnel wall corresponds to 16.1% and 4.2% of the silicon heat. Heat released from the silicon once it is removed from the mold is not part of these calculations. Only heat released from silicon while underneath the tunnel is considered.

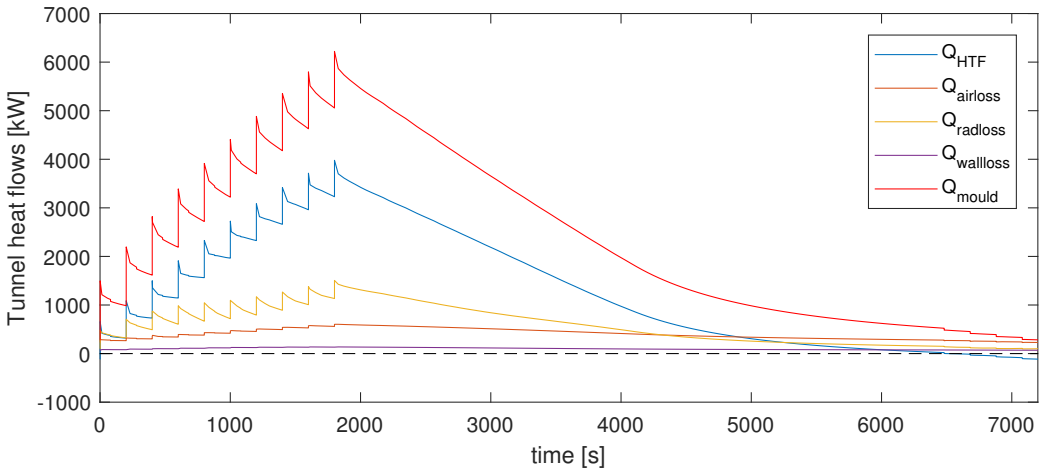

Figure 6.7: Net tunnel heat flow rates

The effect of tunnel air velocity on air losses was already tabulated in Table 6.2. It was found that increasing tunnel air flow would decrease air temperatures and increase the amount of heat transferred to the air. However, it is not really the air velocity, but rather the volumetric air flow rate which influences the air loss. This means that air losses will also be influenced by the height and width of the tunnel. Radiation losses will primarily depend on the dimensions of the storage, as surface emissivities are set constant. A tunnel designed with large openings on both sides will necessarily have a larger fraction of the total silicon radiation heat leave the heat recovery unit through said openings than a system with smaller openings. Wall losses will also be affected by tunnel dimensions, and the reason is twofold. Various tunnel layouts will lead to different tunnel temperatures depending on the rate of heat recovery, with more heat recovered leading to higher system temperatures, which will increase the temperature of the tunnel wall, increasing wall losses. In addition, a change to tunnel dimensions will change the tunnel external surface area, which will affect tunnel losses. As all these losses should be kept low to ensure a high degree of heat recovery, an investigation into how the tunnel dimensions affect heat recovery was conducted.

While total silicon surface heat transfer area must be chosen to ensure proper silicon solidification times, as seen in Subsection 6.3.1, tunnel dimensions can otherwise be chosen quite freely. When testing for how the tunnel dimensions will affect heat recovery and heat losses, total silicon surface area was kept at 43.6 m^2, similar to that of the baseline system, while the tunnel width, length, and height were varied. The casting molds in this work are thought to be placed side by side, with no spacing in-between, and an increase in tunnel width or length will therefore affect total mold surface area. An increase in tunnel width must therefore be associated with a decrease in tunnel length, and vice versa. Figure 6.8 summarizes the effect of tunnel dimensions on heat recovery and tunnel losses.

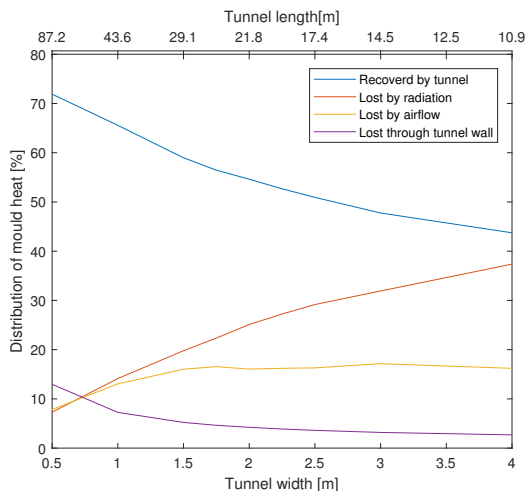

(a) Distribution of silicon heat flows at different tunnel widths, while mold surface area and tunnel height remains constant

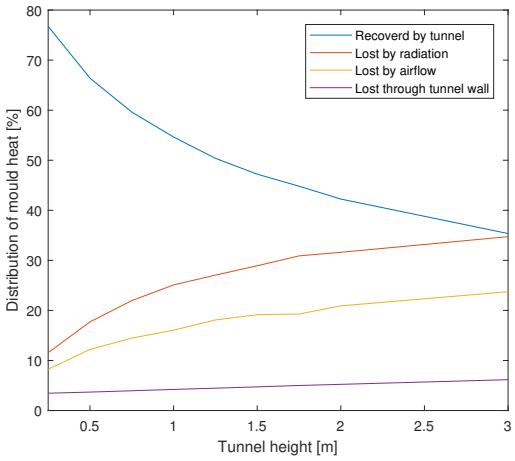

(b) Distribution of silicon heat flows at different tunnel height, while tunnel width and length remain unchanged from the baseline system

Figure 6.8: The effect of tunnel dimensions on heat recovery

Figure 6.8 shows that the choice of tunnel dimensions has a tremendous effect on heat recovery and thermal losses. Solidification times on the other hand changed very little, only changing between 35 and 37 minutes when changing tunnel width and length, with a narrow tunnel corresponding to the slowest solidification time. When changing the tunnel height, solidification

times between 35 and 38.5 minutes came to be, with high tunnels ensuring faster silicon solidification times. While these changes to solidification times are far from insignificant, they pale in comparison to the changes to solidification caused by a change in total silicon surface area.

In Figure 6.8a, it can be seen that a narrow but long tunnel will be far better at recovering heat than a wide but short tunnel. This is primarily due to the very low radiation heat loss at lower tunnel widths. At low tunnel widths, the tunnel entry and exit will be small when compared to the area of the tunnel, meaning view factors $F_{1\to3}$ and $F_{2\to3}$ will be very low, while these view factors will be substantially bigger with a wider tunnel. Of course, this view factor will be reduced as the mold moves away from the tunnel entry and in towards the middle of the tunnel insides. This means the view factors related to radiation losses will be large while silicon temperatures and radiation heat transfer are high.

During the initial part of a silicon casting molds casting cycle, view factors related to radiation losses will be high at the same time as the silicon temperature is at its highest and heat flows are at their peak. This means radiation losses will be high both due to high temperatures and due to a high $F_{1\to3}$. Then later, once silicon temperatures are lower and the mold has moved further under the tunnel, $F_{1\to3}$ will be lower, but overall silicon heat flows are lower as well. $F_{1\to3}$ will increase once the mold moves past the center, but at this point, the temperatures are much lower, and most of the silicon heat has already been transferred out of the mold. To sum up, in tunnels with large openings, more heat will be lost as radiation as silicon temperatures and heat flow are at their peak. This loss will lead to a faster fall in silicon temperatures, which will further reduce the heat available to be recovered by the tunnel. A change in mold height induces a mostly similar effect. However $F_{1\to3}$ and $F_{2\to3}$ will react a bit differently to a change in tunnel height. In addition, changing tunnel width and height will lead to different changes to tunnel surface area, which will also affect heat transfer.

When it comes to air losses, it is shown that both an increase in tunnel width and height will lead to more heat losses, since an increase to both will increase tunnel cross-sectional area, and thus increase tunnel volumetric flow rate, meaning more cold air must be heated.

In Figure 6.8b, the decrease in tunnel heat recovery at higher tunnel heights means lower tunnel temperatures. However, it also means larger tunnel surface areas. Tunnel losses are governed both by tunnel surface area and tunnel wall temperature, and the increase in tunnel area will outweigh the reduction in wall temperature when tunnel height is increased, resulting in larger wall losses. On the other hand, in Figure 6.8a, a more narrow tunnel corresponds both to an increase in tunnel surface area and higher tunnel temperatures due to better heat recovery, leading to a rapid increase in tunnel losses as tunnels become very narrow.

When validating the silicon model's behaviour in Section 4.1, cooling rates by Tveit (1988) were used in Figure 4.2. Here, 33.8% of the silicon heat would be transferred through the casting mold instead of the silicon surface. This is a substantial fraction of the total heat. In the Dymola model used to describe mold heat flow and temperatures, all heat is assumed to be transferred through the silicon surface. If this assumption is wrong, the potential for heat recovery could be far lower than estimated in this work, due to these losses. However, this work is based on the silicon casting plant at Salten, and the measurements done by Lobo (2009) and shown in Figure 4.1 has been shown to match up very well with the system results found in this work. If large fractions of the silicon heat were lost to through the mold, this would not be the case. While there will still be some heat lost through the mold, it will not be as severe as what was measured by Tveit.

6.4 System operation at various temperatures

There was an interest in examining how the temperature of the storage would affect the heat recovery system. By lowering the power cycle mass flow rate it would be possible to limit heat flow to the power cycle. In the project work, it was found that this will lead to heat accumulating in the storage, increasing loop temperatures. This will reduce the driving temperature difference in the heat recovery system, reducing the WHRU's ability to collect heat until there is a parity between cyclic heat collected by the tunnel and heat supplied to the power cycle. To achieve this increase in system and storage temperatures, less heat would be transferred from the storage to the power cycle, in order to maintain the high system temperatures. The decrease in power cycle mass flow rate will increase the temperature rise of the power cycle working fluid through the heat exchanger.

Table 6.3 shows how the system will perform at different storage temperatures. Here, all system parameters are kept equal to that of the baseline system, with the exception of the power cycle mass flow rate, which has been adjusted to attain the required system temperatures, and the heat exchanger UA-value, which has been adjusted to maintain similar driving temperature differences in the loop heat exchanger for all systems.

Table 6.3: System performance when the system is operated at different system temperatures

Property	Unit	Case			
		Very high T_{TES}	High T_{TES}	Baseline	Low T_{TES}
$\dot{m}_{WF}$	kg/s	0.75	1.75	3.00	6.00
UA_{HX}	kW/K	5.3	7.5	10.0	20.0
W	kWh	447.1	517.9	676.2	635.7
$\Delta\dot{W}$	kW	106.0	197.7	259.6	255.1
$T_{TES,avg}$	°C	567.2	455.4	383.6	283.1
$T_{turb,avg}$	°C	515.3	377.6	292.1	210.8
ΔT_{turb}	°C	134.5	124.6	106.2	90.3
η_{ex}	%	11.0	15.5	16.7	16.0
η	%	30.3	46.5	54.6	62.3
t_s	min	37.4	36.2	36.0	35.1

In Table 6.3, multiple aspects of system behaviour are listed. It shows that a rise in system temperatures, although beneficial for power cycle efficiencies, will not lead to an increase in power production. This is mainly due to the reduction in system heat flows that follows from the increase in system temperatures. This is seen by the reduction in the heat recovery efficiency (η) at higher system temperatures, as well as the low exergy efficiencies. High system temperatures did however lead to smaller variation in cyclic power production, while variations in power cycle temperatures experience a larger cyclic change. The silicon solidification time (t_s) will change with system temperatures, in accordance with the tests done in Subsection 6.3.1.

What is most interesting from these results is the notion that neither very high storage temperatures nor the largest system heat flows will lead to the most electrical power production. Instead, the baseline system was shown to produce more electrical power than all the other cases. A further investigation into this found that a mass flow rate of 3.5 $\mathrm{m/s}$ would be the optimal form a power production point of view. However, the improvement in power production was very minimal, while both the increase in UA-value and mass flow rate was substantial.

While high storage temperatures are good from a power cycle efficiency point of view, it might not be good for the concrete storage material. While it will depend on the type of concrete used, there are limits to the temperatures concrete can withstand. Concrete has been reported to be usable as a thermal storage material at temperatures up to 450°C by Hoivik et al. (2017), while Wu et al. (2016) reported the onset of cracks and poor compressive strength once concrete temperatures rose above 500°C. If higher temperatures are required, other storage materials must be considered. High storage temperatures would also be associated with higher storage heat losses, meaning there would be a need for more insulation to keep heat losses at bay.

High storage temperatures have been found to be linked to systems utilizing low power cycle mass flow rates and small heat exchanger UA-values, which could reduce system investment cost, due to smaller components. It has been found that the system will not perform its best at very high temperatures, since the heat flow through the system will be limited. Too high temperatures will also eventually make concrete not viable as storage material. On the other hand, too low storage temperatures are linked to systems utilizing high power cycle mass flow rates and high heat exchanger UA-values. Here temperatures can become so low that they will impede on power cycle performance, meaning the high heat flow rates available will not lead to the highest power production because of the poor performance of the power cycle.

Even higher temperature operation, such as the 1000°C mentioned in task 5 in the problem description of this Master's work, will be entirely unreasonable for this heat source and heat recovery system.

6.5 Control strategies

How the system is controlled is an important aspect of system operation. It was therefore of interest to examine how different system control schemes would affect system performance. However, due to the use of a single fluid loop in the recovery system, it was hard to separately control different aspect of system behavior at the same time, as a change to one operating parameter would also often affect other parts of the system. This is a drawback of this one-loop system. In a heat recovery system with one loop concerned with heat recovery and another loop concerned with delivering heat from the storage to the power cycle, one could better control the system. The mass flow of the heat recovery cycle could be controlled to maintain the desired storage temperature range, while the other loop could be controlled to achieve good operating conditions for the power cycle. As one loop controls both of these aspects in this system, this is not possible here. Some control schemes were implemented, and they will be shown below and compared, as to better understand their effect on system behavior.

Control schemes will primarily focus on further reducing system variations throughout the casting cycle. They should focus on making the power cycle operating conditions as beneficial as possible in order to ensure stable and high production of electric energy. The control scheme must concern itself with operating parameters, which can be changed throughout each cycle, and not parameters concerned with the design, as they cannot be changed during operation. This means there are limited ways a control system can influence system behavior. These include controlling air velocity inside the tunnel, controlling the time each mold spends beneath the tunnel, and the fluid flow rates in the heat recovery loop and power cycle.

From the project work, it was found that the mass flow rate on the cold side of the loop heat exchanger will have a large effect on storage temperatures, power cycle expander temperatures, and the amount of heat transferred through the heat exchanger. Thus it is well suited to be

used to control the power cycle expander inlet temperature. It is also well suited to regulate the amount of heat transferred to the power cycle. Using the loop mass flow rate to control system behavior was also examined, but this did not provide any noticeable beneficial effect on the power cycle temperatures or heat flows. It could be utilized to limit the highest temperatures out of the heat recovery tunnel, or to limit (or increase) the temperature rise through a loop component, but otherwise a PI controller changing the loop mass flow rate provided few benefits for system operation, and power cycle operation was hardly impacted by such a control scheme.

Three control systems were attempted implemented into the system, two of which involved a PI-regulator: one attempting to ensure a constant estimate for power production, and the other attempting to attain a constant cold outlet temperature from the heat exchanger. In both instances where a PI-regulator was used, it utilized the power cycle mass flow rate to induce change to the system.

PI regulators were included in this work to exemplify how the system will react to an external control scheme, but the exact tuning of these regulators will not be focused on at all. The PI-regulator constants were chosen so the system would react in a sensible way, and so it would cause a noticeable change to system behavior. The PI-regulator parameters are shown in Table 6.4. System behaviour with a PI-regulator implemented is shown in Figures 6.9 and 6.10. Here, system parameters are left unchanged from the baseline case, except for the active control scheme. The figures show the effect of the two PI-regulators on the estimated power production, heat exchanger temperatures, and mass flow rates. The figures also compare these results to the baseline system.

Table 6.4: PI-regulators used in this work

Controller objective	k_i (–)	T_i (–)	y_{min} (kg/s)	y_{max} (kg/s)
Constant estimated power	5×10^{-6}	3	1	6
Constant HX outlet temperature	-1×10^{-2}	3	1	6

Figure 6.9 shows that an active control scheme involving the power cycle mass flow rate can quite drastically reduce the fluctuations in estimated power production throughout a cycle. However, it does so by increasing variations in expander inlet temperature and working fluid mass flow rate in the power cycle. Something else to notice is how the constraints to mass flow rates limit the effectiveness of the PI-regulator. The power production estimate starts to deviate from their objective power once mass flow rates meet the system constraints listed in Table 6.4. This is very clearly shown in when comparing the PI-regulator with a target power of 325 kW and 350 kW: When the target power is 325 kW, the regulator kept mass flows within the regulator constraints most of the time, which resulted in a power production very close to the intended target during most of the system operation. However, with a target power of 350 kW, mass flow rates would be increased to increase heat flow to the power cycle, eventually reaching a point where the mass flow rates were constrained, at which point the estimate for power production would move away from the target electrical production. Once the power cycle mass flow rate could be increased no more, power cycle temperatures would experience a slower decline, since the only cause of temperature decline at this point was the steady decrease in heat delivered from the loop, while temperatures would no longer be lowered to increasing power cycle mass flow rates. This meant cyclic temperature variation in the 350 kW case were lower than in the 325 kW case, while fluctuations in estimated power were larger. None of the

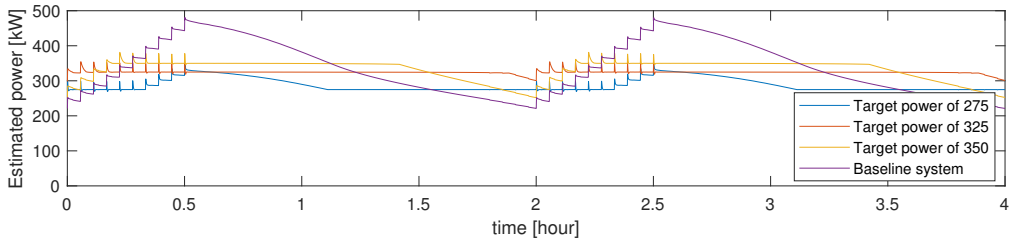

(a) Estimated power production

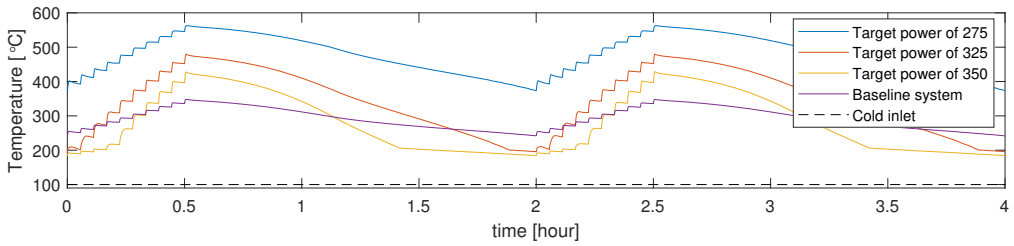

(b) Heat exchanger cold side temperatures

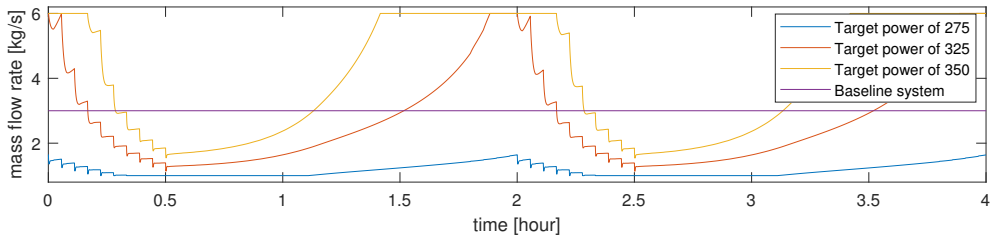

(c) Power cycle mass flow rates

Figure 6.9: Performance of the system using a PI regulator aiming for a constant estimated electric power production, alongside the baseline system for comparison

systems managed to produce more total electric energy than the baseline system without any active controls.

Figure 6.10 shows that a PI-regulator is quite successful in controlling the temperature outlet on the cold side of the heat exchanger. While not shown in the figure, a target temperature a bit higher than 350°C or lower than 250°C would lead to a mass flow rate hitting the constraints set for the controller, meaning it would not be able to maintain the power cycle temperature as well as it manages in the cases shown in the figure. The figure also shows that such a PI-regulator will induce a large change in power cycle mass flow rate and an increase to fluctuations in the estimated power produced. As with the PI-regulator controlling for constant power, there is an inverse relation between variations in power and variations to power cycle temperature, as the constant temperature led to larger variations in the electrical power conversion. Total electrical energy produced during a cycle changed very between cases when controlling for constant temperature: 677.6 kWh was produced with a target temperature of 250 °C, while a target temperature of 350°C produced 662.8 kWh. In addition, the largest fluctuations in power produced were present with the highest target temperatures, but the amount of variation stayed very similar between these three cases.

In addition to control schemes involving PI-regulators, another change to the system was attempted by changing the operation of the tunnel heat recovery unit. Subsection 6.3.1 showed how much heat was lost to air flow through the tunnel, and as radiation through the tunnel openings. In order to reduce these losses, a control scheme involving the tunnel openings were

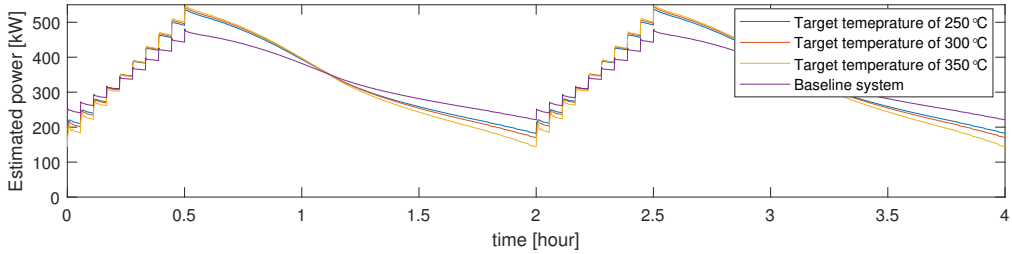

(a) Estimated power production

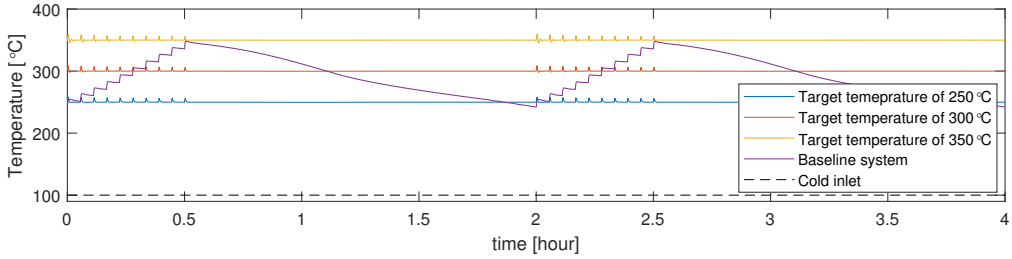

(b) Heat exchanger cold side temperatures

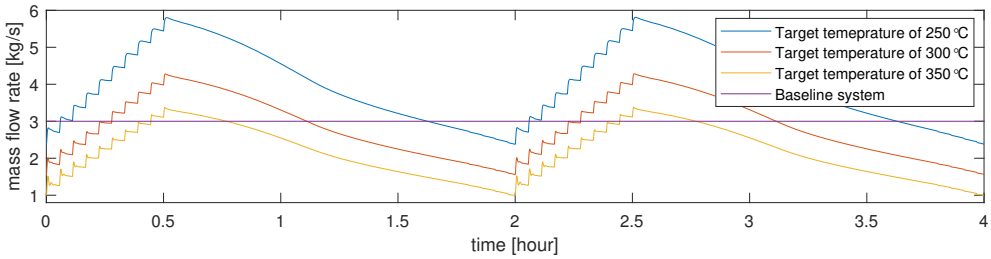

(c) Power cycle mass flow rates

Figure 6.10: Performance of the system using a PI regulator aiming for a constant temperature out of the loop heat exchanger on the power cycle side, alongside the baseline system for comparison

attempted. The WHRU was altered to enable the tunnel openings to be closed for some time during each casting cycle. This will mean that air will stagnate inside the tunnel, while radiation can no longer exit through the openings. To avoid this affecting silicon cooling rates, the tunnel would first close once all silicon beneath the tunnel was fully solidified. The tunnel would then open once the first silicon casting mold was to be removed from the tunnel. In the baseline system, this would mean that tunnel openings would close 1 hour and 6 minutes into a new casting cycle, while they would open 42 minutes later when the first silicon mold left the tunnel.

Closing the tunnel openings affected the system as suspected. Radiation and air losses would be lowered during periods where the tunnel is closed, which would increase overall heat recovery during the later part of each casting cycle. This coincided with the period in which heat flow from the molds is at their lowest. This meant heat recovery would receive a boost during the latter part of each casting cycle, enabling the system to better recover heat during the lowest temperature period of each casting cycle. The closing of the tunnel would also lead the tunnel air to be heated to temperatures far higher than during normal operation, since air at ambient temperature is not injected to the tunnel, and the hot air is not ejected from the tunnel. Using the baseline system as a reference, the implementation of the tunnel closing would lead to an 8.8% increase in heat recovery throughout each cycle, while it would experience a 12.8% reduction in total losses. The estimate for power production would increase by 9.7%. This is caused both

by the increase in heat recovered, but also due to higher storage and system temperatures to account for the improvement in energy recovery.

From both Figure 6.9 and Figure 6.10 it can be seen that this system does not allow for both power cycle temperatures and estimated power production to be controlled simultaneously. It is also important to keep in mind that this work does not properly model the power cycle. As such, there are aspects of real turbine operation that is not accounted for in this work. In a real power cycle, power cycle pressure could also be used to influence system performance. However, since neither the power cycle nor its pressure was included in this model, this method of influencing system performance was not examined. It was attempted to control power cycle temperatures through the power cycle mass flow rate, but the effects of phase change on temperature have not been considered. Even so, the implementation of PI-controller systems have demonstrated their ability to affect system performance and power conversion, and their inability to reduce cyclic fluctuations to both temperatures and heat flows at the same time. No control system managed to efficiently get rid of the variations in cyclic performance, but the implementation of tunnel openings which closes at certain intervals showed potential, as it improved heat recovery without increasing system variations or affecting solidification time.

6.6 Deciding the system design point

A good heat recovery system must satisfy a wide range of demands. It must recover an adequate amount of heat, and produce sufficient amounts of electric power. At the same time, it must not be too large, as a larger system will increase capital investment costs. It must be operated at sensible system values, i.e. not too high system temperatures, system pressures or the like. The heat recovery loop must also deliver heat to the Rankine cycle in a way which is beneficial (or at least not too detrimental) to turbine operation. Lastly, and perhaps most importantly for this specific heat recovery case: The heat recovery system must not affect the silicon casting process in a way which would prove damaging to the final silicon product. This is a heat recovery system on a silicon production process, after all, and the priority is to produce industrial grade silicon which meets the requirements of their customers. Any heat recovery system which does prove detrimental to either silicon yields or quality will most likely not be built.

Using the insight gained from the investigations conducted in this chapter, a reasonable system design point was chosen. The design point was chosen to ensure the required solidification time while recovering as much heat as possible. Care was taken to choose design parameters that would keep variations in power production low while ensuring high heat recovery and proper silicon solidification times. In the thermal storage, the focus was put on designing for a high storage UA-value to ensure satisfactory storage response, while complying with the restraints put on fluid velocity and tube diameters. The tunnel and mold dimensions were set to primarily ensure proper cooling rates, but the tunnel was made both narrower and longer than in the baseline case to ensure a reduction in radiation losses from the tunnel openings. Active control of tunnel entry and exit being opened and closed were also attempted. Heat exchanger mass flow rate and UA-value were set in accordance with Table 6.3, to ensure the highest electricity production. To further reduce cyclic variations, PI -regulators controlling power cycle temperature was also attempted. The design parameters can be seen in Table 6.5, while the performance of the baseline system, design system, and design system with active control schemes are listed in Table 6.6.

Table 6.5 shows that the dimensions of the proposed system design are somewhat larger

Table 6.5: System design parameters, compared with the parameters of the baseline system used throughout this work

Property	Unit	System	
		Basecase	Proposed design
mold time underneath tunnel	s	6480	5400
Tunnel length	m	21.8	24.3
Tunnel width	m	2	1.8
Tunnel height	m	1	0.75
Loop HTF mass flow rate	kg/s	15	15
Air mean velocity	m/s	1	1
TES storage capacity	MJ/K	50	70
TES tube inner diameter	mm	15	10
TES tube pitch	mm	90	80
TES number of HTF tubes	–	620	350
TES UA-value	kW/K	15.3	32.2
TES length	m	3.2	10.0
TES cross-section area	m^2	4.3	1.9
Rankine cycle mass flow rate	kg/s	3	3.2
Heat exchanger UA-value	kW/K	10	11.0

Table 6.6: Performance of the proposed system design, with and without further control strategies, as well as a comparison to the baseline system

System property	Unit	Baseline	Proposed system design			
Control tunnel openings		–	–	Yes	Yes	Yes
PI control: power		–	–	–	–	Yes
PI control: temperature		–	–	–	Yes	–
W	kWh	676.2	762.3	795.1	796.4	791.8
$\Delta\dot{W}$	kW	259.6	128.0	121.0	184.9	53.0
$T_{TES,avg}$	°C	383.6	396.7	405.8	407.0	398.2
$T_{TES,max}$	°C	426.6	449.2	452.2	452.8	447.6
$T_{turb,avg}$	°C	292.1	301.7	308.0	309.8	292.2
ΔT_{turb}	°C	106.2	50.0	46.7	8.0	111.6
η_{ex}	%	16.7	18.8	19.6	19.7	19.5
η	%	54.6	62.6	65.7	65.2	66.3
t_s	min	36.0	36.3	36.3	36.4	36.2

than those of the baseline system. At the same time, it can be seen that the time each mold spend underneath the tunnel is somewhat reduced. This was primarily done so that the casting carousel from the current Elkem Salten plant could be operated in a similar fashion as it is now. At the same time, the reduction in time for heat recovery will have little impact on power production, as it merely stops the system from recovering heat silicon as it is cooled from 500°C to 440°C, at which point very little exergy remains to be recovered (see Section 5.1). When implementing the control strategies, storage temperature was found to be the limiting factor for

system performance, as concrete temperatures should not exceed 450°C (Hoivik et al., 2017).

It can be seen in Table 6.6 that an improvement in system design was found to have a large positive effect on system performance, without changing the silicon solidification times away from the target time of 36 minutes. Power production has been shown to increase substantially in comparison to the baseline system, and variations in system performance through the casting cycle has been noticeably reduced. The storage and WHRU design have therefore been shown to be of utmost importance in ensuring that the variations in heat and temperature onto the power cycle are kept as low as possible. The proposed system design, with no additional control strategies, showed a 12.7% improvement in power conversion when compared to the baseline system, a less well-designed system, while variations in cyclic power production and power cycle temperature were reduced by 50.7% and 52.9%, respectively.

The increase in storage heat capacity, and reduction in number of storage tubes and tube pitch distance led to a large increase in storage UA-values, and the large UA-values and larger storage meant the system was far better at responding to the variations in silicon heat flows, which caused the reduction in system variations. This was also shown to positively affect the PI-regulators. With less variation in temperature and heat flows, they proved more successful at attaining their objectives, both when providing a constant power production and when providing constant power cycle temperatures.

The dimensions of the proposed system design are not too unreasonable. The heat recovery tunnel has dimensions similar to the casting carousel already present at Salten, meaning it should physically fit in the room available. With some adjustments to the heat recovery and tunnel, it might even fit onto the heat recovery carousel, as their dimensions match up quite well. The thermal storage will occupy a total volume of 19 m^3. It is quite narrow and long, but if the storage were to be "folded" on top of itself once, it would be nearly the same dimensions as a 20' DC shipping container.

This system, depending on the control strategy chosen, has been shown to produce nearly 800 kWh of electrical energy per two hour casting cycle, meaning the system managed to produce up towards 88.3 kWh electrical energy per tonne of silicon produced, in comparison to the 11-13 MWh needed to produce a tonne of silicon, meaning this system will recover 0.68% of the electrical energy required to produce the silicon product. The design WHRU had heat recovery efficiencies of 62.6%, which is very agreeable with the heat recovery efficiency reported by Caputo et al. (2011) in their similar heat recovery unit, although their system operated at much lower heat source surface temperatures.

Elkem recently announced that they would build a heat recovery plant at Elkem Salten to recover heat from the hot furnace off-gas. The project has an estimated investment frame of 1 billion NOK and is expected to recover upwards of 28% of the plant's total energy usage (Elkem, 2018), which is an order of magnitude larger than what will be recoverable from the system proposed in this work. This is to be expected, as the heat content in the off-gas is much higher than the heat released during cooling, as was seen in Figure 1.1. On the other hand, Børset (2015) proposed to install thermo-electric generators on a shielding wall next to the casting molds. The estimated potential of these TEGs was up towards 900 $\mathrm{W/m^2}$. While no total estimated power production was provided, the shielding wall in question has a surface area of 40 m^2, meaning potential power produced would be 36 kW, which is far lower than the estimated power produced from the system proposed in this work.

The system was found to recover an average of 1.45 MW of heat through a casting cycle, which is comparable to the heat recovery reported by Vance et al. (2019), who reported on the potential for heat recovery from some steel plants during the casting and cooling process. Here,

potential heat recovery rates ranging from 1.6 to 3 MW was reported, depending on the size of the plants, a result which seemed agreeable with the heat recovery reported from this work. Vance et al. went on to estimate that the waste heat recovery potential from such steel and iron plants are 72 TWh each year in the EU alone, meaning heat recovery from hot surfaces have real potential.

6.7 Initial economic evaluation

To gain an understanding of the economic feasibility of this waste heat recovery system, an initial economic evaluation was performed. The goal was to gain an insight into the costs associated with such a system, and examine if the system was feasible from an economic perspective. The system to be analyzed is the proposed system in Table 6.6, while controlling tunnel openings and controlling for a constant power output ($\dot{W}_{avg}$ of 396 kW).

In a system such as this, it will be difficult to find a good estimate for the capital investment cost. This is because the system is rather unconventional, making cost comparisons between this system and others difficult. It was attempted to estimate the maximum investment cost for this system when assuming different levels of subsidies and expected rates of return and use this to find acceptable system costs which would still be economically feasible.

The analysis was done using the concept of net present value (NPV). Present value is a way to discount cash flows through time, as it is believed that 1000 € today is worth more than 1000 € in ten years, as one could spend those years investing the money for further monetary gain. The net present value of the system is the sum of all yearly discounted cash flows. If the NPV is positive, the system will contribute to a net increase in value when assuming a set discount rate, thus being deemed profitable. A negative NPV will induce a loss. Eq. 6.1 describes the NPV formula:

$$NPV = -C_0 + \sum_{t=1}^{N} \frac{C_t}{(1+r)^t} \tag{6.1}$$

where C_0 is the initial capital investment, C_i is net cash flow for year t, while r is the discount rate. The profitability of a system when using the NPV method will therefore depend on whether or not the system can provide a net positive cash flow during its lifespan, while deprecating the money using a discount rate which normally represents the rate of return of an alternative investment.

During this economic evaluation, some assumptions were made. Electricity price is 45 €/MWh, while a 20-year system lifespan is assumed. The system can also be subsidized, meaning a state entity such as Enova in Norway could provide a percentage of total costs. System uptime is assumed to be 85%, meaning the system will operate 7446 hours a year, and yearly expenditures linked to operational costs (opex) of the heat recovery system is assumed to be 10 000 €. Yearly cash flows are then

$$C_i = -opex + C_w \times \dot{W}_{avg} \times t_{op,year} \tag{6.2}$$

where C_w is the assumed cost of electricity, in this case 45 €/MW, $\dot{W}_{avg}$ is the average electricity production from from the proposed heat recovery system, while $t_{op,year}$ is the amount of hours the system is operated each year.

Table 6.7 shows the total capital investment which is required to achieve a specified IRR for the assumptions made above. This table can be seen as a reference to how much this system can

cost depending on the expected rate of return by the investors. If investors expect a large return on their investment, system costs must be kept low. Also, notice that this table only includes investment costs. If the heat recovery system receives any kind of subsidy, that money will be added on top of the investment cost tabulated here, thus enabling investment into a larger or costlier system while maintaining the same IRR as before.

Table 6.7: The capital investment to achieve a specified IRR with an payback time of 20 years

	IRR (%)					
	0	5	10	15	20	25
Investment cost (€)	2 345 073	1 491 629	1 032 439	765 016	597 808	485 585

One could make a rough estimate for the costs associated with the power cycle based on the costs of power cycle on other waste heat recovery applications. Quoilin et al. (2013) collected costs from multiple ORC installations, and plotted their nominal power output up against their cost per produced power, as seen in Figure 6.11. It was previously stated that this work should use a steam Rankine cycle, not an ORC, but this is merely an estimate for costs. The figure shows that a cost per power produced of 2500 €/kW seems appropriate for this system, meaning the power cycle will cost very close to a million €. This seems to account for all system costs associated with the power cycle.

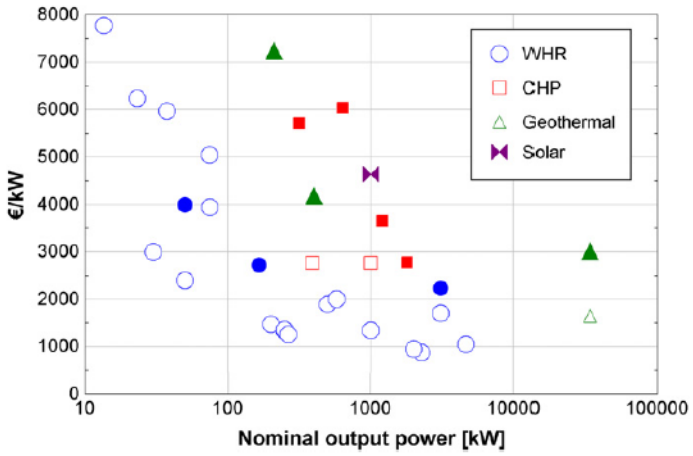

Figure 6.11: Module (empty dots) and total (plain dots) cost of ORC systems depending on the target application and on the net electrical power (Quoilin et al., 2013)

Using the dimensions from the system design (Table 6.5), one could find an approximation for the material costs for the thermal storage and WHRU. Assuming a concrete cost of 0.05 €/kg, tube cost of 3 €/kg, insulation cost of 500 €/m^3, and heat transfer tube thickness of 1 mm, and that the tubes used in the WHRU are of the same dimensions as the ones in the storage, material costs of the storage will amount to 4916 €. Tubing and insulation for the WHRU are estimated to cost 5812 €. Costs related to the support structure of the WHRU are not included. Then there are costs related to the control systems, construction, piping, working fluid, casting system retrofit, the loop circulation pump, and other overhead costs. If one were to assume material costs accounted for merely 10% of the total investment, the system, not including the power cycle, would cost approximately 161 000 €, meaning the (very) rough estimation for

total costs will be 1 151 000 €. The power cycle was estimated to account for a majority of the total costs.

A system cost of 1 151 000 € can be seen from Table 6.7 to be associated with an IRR of 7.47% if assuming no subsidies on investments and a system lifespan of 20 years. This is very low, and most investors will choose to instead invest in alternative investments with larger IRRs. However, this IRR does not include any subsidy. If subsidies are taken into account, system expenses can be higher, but the subsidizing party will stand for the increased expenses. Figure 6.12 shows the NPV of this system at different discount rates, Figure 6.12a with no Enova subsidy, while Figure 6.12b shows the NPV when 40% of total investment cost is covered by Enova. It shows that the IRR for the project will be more than doubled if the project receives 40% of total costs in subsidies, resulting in an IRR of 15.4%, thus making it a much more attractive project. But this will all depend on the validity of the assumptions made while estimating investment costs.

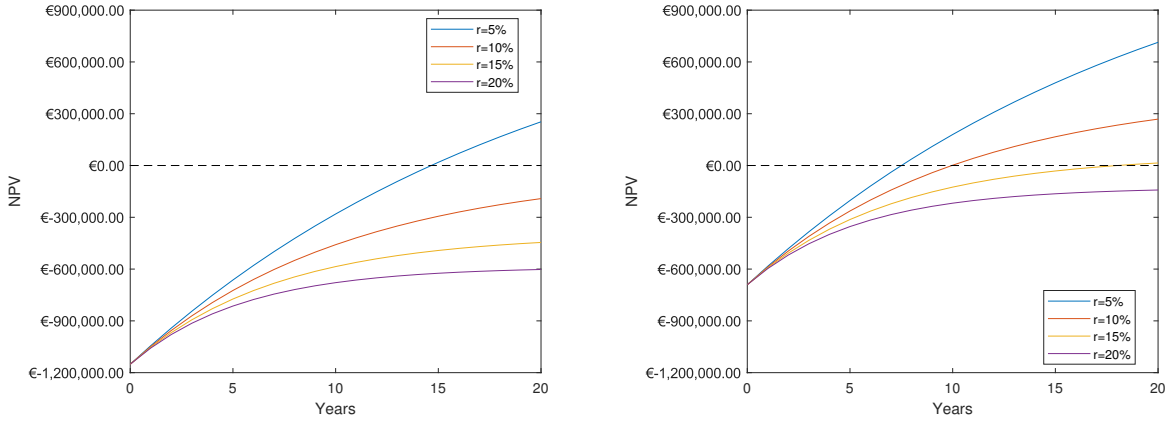

(a) No subsidy on investment

(b) 40% of investment subsidized

Figure 6.12: Net present value for the system using different discount rates and different levels of subsidized investment cost

Chapter 7

Conclusion and further work

7.1 Conclusion

This work has investigated the possibility of waste heat recovery and thermal power conversion from a highly variable waste heat source with an integrated thermal energy storage. The waste heat originated from the casting process at Salten Elkem, where hot, liquid silicon is to be cooled and solidified in a controlled manner. As the silicon is cooled, it will release large amounts of heat. This heat will be very variable, as it will decrease as silicon temperatures are lowered. The system proposed would therefore focus on recovering as much heat as possible, while counteracting the large variations in heat due to the continuous reduction in silicon temperatures, and recovering heat in a manner which does not overly affect the casting process in a negative manner.

The findings showed that it is possible to attain satisfactory cooling rates for the silicon while also recovering heat, but this would not be possible without careful design of the heat recovery system. This is because the introduction of a WHRU recovering silicon heat would severely change the cooling conditions experienced by the molds. It was found that the most effective way to control the cooling rate was to change the dimensions of the casting molds, making them longer or wider, thus increasing surface area while also making them shallower, which would counteract the worsened casting conditions induced by the WHRU. Other aspects of the WHRU would also affect solidification, but not to the same extent. Thus properly sizing the molds is paramount to ensure proper silicon casting, while other factors of the WHRU could be tuned to better optimize heat recovery.

Because the storage unit proposed in this work is based on the storing of sensible heat, it is not possible to remove all variations in heat and temperature, as sensible thermal storage is related to a change in storage temperature. All the same, the integration of a thermal storage was shown to be very effective at reducing the variations in temperature and heat experienced by the power cycle. With a well-designed heat recovery system and storage, temperature variations experienced by power cycle turbine inlet would be reduced by 88%, while the variations in estimated power production would be reduced by 87%. At the same time, the introduction of a thermal storage led to a slight reduction in total estimated power produced, which was caused by the destruction of system exergy due to the introduction of the storage. However, the loss in potential power production is more than made up by the tremendous increase in power cycle stability. The variations in power cycle conditions without a storage is far too large for any actual power cycle to utilize said heat source for power conversion, as the system would be

operated very far from its design point all the time, which would decrease system efficiencies and power cycle lifespan. This means the only realistic alternative for utilizing such a variable surplus heat source for electrical power conversion is to use a heat recovery system with an integrated thermal energy storage.

The WHRU should be designed to ensure high heat recovery efficiencies once the proper silicon casting conditions are ensured. This was primarily done by reducing the size of the tunnel openings relative to the tunnel by designing the tunnel to be of low height, while narrow and long. This would reduce radiation heat losses, which was the largest cause of heat losses. The thermal storage should be designed for large UA-values to better respond to the dynamics of the heat source. This was primarily done by reducing tube pitch distance in the storage while designing the storage to be long, narrow, with relatively few tunnels in parallel.

Some control strategies for the system was examined. Attempts to block tunnel entries at specific parts of the casting cycle showed potential, as long as it was done without affecting the silicon solidification. A PI-regulator governing the power cycle mass flow rate was shown to be capable of ensuring a more even power cycle turbine temperature or an even power production. However, the PI-regulator could not make both of these more even at the same time, as a more even power production meant more variations in temperature and vice versa.

If there is a need to actively control storage heat flows, for instance to store heat during nighttime to produce more electric power during daytime, this storage will not be effective at all, as there are very few alternatives for active control of the storage. This lack of means to control storage behavior is a disadvantage of using a one-loop system for both charging and discharging of the storage. However, the system benefits from this layout as well, as the layout enables the storage to be operated without any complicated control schemes, as only the temperature difference between the storage and loop HTF is necessary for the storage to help correct the fluctuations induced by the variable heat source. In other words, the system showed potential for the specific application area in this work, which is to reduce cyclic variations in the heat delivered from a highly variable heat source by using a simple system design. For other applications, another system layout more capable of controlling the energy stored in the storage should be considered instead.

The proposed heat recovery system design could produce up to 796 kWh of electric power every two-hour casting cycle, meaning it could recover 0.68% of net electrical input required in the silicon process. At the same time, an initial economic evaluation showed that the system could potentially be profitable, assuming investments are kept low. Here, a concrete storage is very beneficial, as the low cost of the storage will help keep system costs low. However, it is likely that other heat recovery alternatives, such as that from the furnace off-gas, should be recovered first, as the heat content and potential for power production is higher from such heat sources. But as more and more plants implement heat recovery for the off-gas heat, the casting heat will become a potential target for heat recovery, not just in silicon plants, but other high-temperature industries as well, such as the casting and cooling processes in iron and steel making industries.

7.2 Further work

While this model is a decent description of the heat recovery system, it does not model the power cycle in a satisfying manner. The largest improvement to this model would be to properly model the power cycle. This would both mean the heat exchanger would behave more as it should, meaning loop behavior would be more correct, but more importantly it would give a better understanding of how a power cycle would behave when producing power from heat delivered by the heat recovery system. The implementation of a proper power cycle would introduce other areas of interest for further studies, such as how one should decide the power cycle design point to ensure the best cyclic operation. A better description of the power cycle would also mean one could attain a better estimate for the actual power production possible form this system, and a better understanding of how a reduction in heat source variations would help reduce losses related to the off-design operation of the power cycle.

It would also be of interest to investigate how a different choice in storage technology would affect system performance. Other storages examined could for instance be a different concrete storage concept or an entirely different storage technology. When it comes to different concrete concepts, it would be of interest to examine the effects of a system where storage charging and discharging would not be controlled through the same fluid loop, instead having one part of the system transferring heat from the heat source to the storage, while another would transfer heat from the storage to the power cycle, is in Figure 3.3. Other options, except other similar solid state sensible storage technologies, would be the use of steam accumulators or active storage concepts, where the heat transfer fluid would also act as the storage medium, such as molten salts or thermal oils. By introducing different storage concept alternatives, one could make a comparison to better decide on the best one. Other storage concepts are often reported as being better storage options than concrete, with concrete having the benefit of very low investment cost and very simple storage and system designs. It would be of interest to see if potential improvements from other storage concepts would outweigh the simplicity and low cost of the system proposed in this work.

Bibliography

Benham, G., Hildal, K., Please, C., Van Gorder, R., 2016. Solidification of silicon in a one-dimensional slab and a two-dimensional wedge. International Journal of Heat and Mass Transfer 98.

Bergan, P. G., Greiner, C. J., 2014. A new type of large scale thermal energy storage. Energy Procedia 58, 152 – 159, renewable Energy Research Conference, RERC 2014.

Bianchi, G., Panayiotou, G., Aresti, L., Argyrou, M. C., Georgiou, G. S., Tassou, S. A., Jouhara, H., Kalogirou, S. A., Florides, G. A., Christodoulides, P., 2019. Waste heat recovery in the eu industry and proposed new technologies. Energy Procedia 161, 489 – 496.

Buehler, R., , Ordonez, J. C., Oct 2016. Heat transfer fluids for parabolic trough solar collectors - a comparative study. In: 2016 IEEE Conference on Technologies for Sustainability (SusTech). pp. 68–75.

Børset, M. T., 2015. Energy dissipation and recovery in the context of silicon production: Exergy analysis and thermoelectricity. Ph.D. thesis, Norwegian University of Science and Technology.

Caputo, A. C., Pelagagge, P. M., Salini, P., 2011. Performance modeling of radiant heat recovery exchangers for rotary kilns. Applied Thermal Engineering 31 (14), 2578 – 2589.

Delpech, B., Axcell, B., Jouhara, H., 2019. Experimental investigation of a radiative heat pipe for waste heat recovery in a ceramics kiln. Energy 170, 636 – 651.

Doretti, L., Martelletto, F., Mancin, S., 2019. A simplified analytical approach for concrete sensible thermal energy storages simulation. Journal of Energy Storage 22, 68 – 79.

Du, W.-J., Yin, Q., Cheng, L., 2018. Experiments on novel heat recovery systems on rotary kilns. Applied Thermal Engineering 139, 535 – 541.

Edward, J. E., 2008. Design and rating shell and tube heat exchangers. P&I Design Ltd.

Elkem, May 2018. Energy recovery plant decided at Elkem Salten.
URL www.elkem.com/media/news-articles/energy-recovery-plantdecided-at-elkem-salten/

Gundersen, T., 2009. An introduction to the concept of exergy and energy quality. Tech. rep., Department of Energy and Process Engineering - NTNU.

Ho, C. K., 2017. Advances in central receivers for concentrating solar applications. Solar Energy 152, 38 – 56.

Ho, C. K., Iverson, B. D., 2014. Review of high-temperature central receiver designs for concentrating solar power. Renewable and Sustainable Energy Reviews 29, 835 – 846.

Hoivik, N., Greiner, C., Tirado, E. B., Barragan, J., Bergan, P., Skeie, G., Blanco, P., Calvet, N., 2017. Demonstration of EnergyNest thermal energy storage (TES) technology. AIP Conference Proceedings 1850 (1), 080011.

Incorpera, F. P., Dewitt, D. P., Bergman, T. L., Lavine, A. S., 2005. Fundamentals of Heat and Mass Transfer, 6th Edition. John Wiley & Sons.

Jian, Y., Bai, F., Falcoz, Q., Xu, C., Wang, Y., Wang, Z., 2015. Thermal analysis and design of solid energy storage systems using a modified lumped capacitance method. Applied Thermal Engineering 75, 213 – 223.

Jouhara, H., Almahmoud, S., Chauhan, A., Delpech, B., Bianchi, G., Tassou, S. A., Llera, R., Lago, F., Arribas, J. J., 2017. Experimental and theoretical investigation of a flat heat pipe heat exchanger for waste heat recovery in the steel industry. Energy 141, 1928 – 1939.

Kalogirou, S. A., 2014. Solar Energy Engineering, second edition Edition. Academic Press, Boston.

Lingaas, S., Dec. 2018. Heat-to-power conversion from variable surplus heat sources.

Lobo, S., 2009. Study of the energy lost through radiation during the casting of metallurgical silicon at Elkem Salten. Master's thesis, Norwegian University of Science and Technology.

Qiu, Y., Li, M.-J., He, Y.-L., Tao, W.-Q., 2017. Thermal performance analysis of a parabolic trough solar collector using supercritical CO2 as heat transfer fluid under non-uniform solar flux. Applied Thermal Engineering 115, 1255 – 1265.

Quoilin, S., Broek, M. V. D., Declaye, S., Dewallef, P., Lemort, V., 2013. Techno-economic survey of organic rankine cycle (orc) systems. Renewable and Sustainable Energy Reviews 22, 168 – 186.

Sarbu, I., Sebarchievici, C., 2017. Solar Heating and Cooling Systems. Academic Press.

Schei, A., 1998. Production of high silicon alloys. Tapir, Trondheim.

Tveit, H., 1988. Størkning av 75% ferrosilisium : forløp, struktur og styrke. Ph.D. thesis, Norges tekniske høgskole, Trondheim.

Vance, D., Nimbalkar, S., Thekdi, A., Armstrong, K., Wenning, T., Cresko, J., Jin, M., 2019. Estimation of and barriers to waste heat recovery from harsh environments in industrial processes. Journal of Cleaner Production 222, 539 – 549.

Wu, C., Pan, J., Zhong, W., Jin, F., 09 2016. Testing of high thermal cycling stability of low strength concrete as a thermal energy storage material. Applied Sciences 6, 271.

Zaversky, F., Seubert, B., Lu, J., Karl, M., Muller, R., Fluri, T., Montenon, A., Guerreiro, L., Canavarro, D., Pereira, M. C., 2014. Project deliverable 7.12: Performance comparison of advanced thermal energy storage systems through simulations. Report, Stage-STE.

Appendix A

Appendix

A.1 Draft scientific article

One of the tasks of this thesis was to make a draft scientific paper based on the work performed in this thesis. The draft is included below. The paper should be kept short, and therefore could not be a complete summary of the entire work. Instead, the article focused on describing the proposed system with integrated thermal storage, presenting the chosen case study, and listing the main results found. The article is shown below.

Heat-to-power conversion from variable surpluss heat sources utilizing a thermal energy storage

Simon Johan Nilsen Lingaas
NTNU: Norwegian University of Science and Technology

Petter Nekså, Trond Andresen & Brede Hagen
SINTEF Energy Research

Abstract

The goal of this work was to explore the potential benefit of thermal buffering in surplus heat recovery systems. The work examined the possibility to integrate a form of thermal storage into a heat recovery system to better handle heat sources of a highly variable nature. The heat source in focus will be the heat released as silicon is cooled from 1450°C at the Elkem Salten silicon plant, where both temperatures and heat output will experience large variations as the silicon is cooled.

This work proposes a system to recover this casting heat, where a sensible concrete storage is integrated to buffer the silicon heat in order to counteract the variations in heat throughput due to the variable waste heat source. The recovered heat is to be used in an electric power conversion system. Care was taken to ensure that the introduced heat recovery system would not interfere or disturb the silicon production system, as a change in the silicon cooling process can affect the quality of the product silicon. The work found that a well-designed heat recovery system would be able to recover the waste heat with little change to the silicon process, while the storage would reduce variations in heat loads onto the conversion system, enabling power production from the variable waste heat source.

1 Introduction

In order to reduce greenhouse gas emissions and lessen the effects of climate change, it is vital to improve upon the energy usage in the industrial sector. This sector accounts for a large part of the global energy usage and is therefore a large contributor of emissions that may harm the environment. One way to reduce energy usage in the industrial sector is to recover industrial waste heat. This work has examined the possibility to use a highly variable industrial waste heat source as the heat source for an electric power conversion system. However, the variable nature of this heat source is disadvantageous, as it will complicate the operation of the power cycle, increase system costs and increase system losses due to off-design system operation. To reduce the variations in temperature and heat output from the heat source to the power cycle, a thermal energy storage was integrated into the heat recovery system. It was meant to act as a buffer, storing heat during periods of high heat load, which will be delivered to the power cycle during periods with lower heat loads.

One variable waste heat source is the heat released from metal industry as the product metal is cooled after the furnace. The heat released will decline as the metal temperatures are lowered, meaning both the hot output and the temperature of the waste heat source will be variable. The waste heat recovery potential from the cooling processes at iron and steel works amount to 72 $\mathrm{TW\,h}$ of heat each year in the EU alone [11]. There have been some attempts to

recover this heat in the literature. A flat heat pipe recovery system was meant to recover radiant heat in the steel making industry [8]. A pilot system was built and tested, and in the steel wire cooling process it recovered heat from, it was believed to be able to recover 700 kW of heat. Others have examined the possibility to recover heat from other surfaces, such as the ceramics industry [4] or from rotary kilns [3, 5]. However, all these studies operated on hot surfaces with little variability, and none utilized the waste heat in a power conversion system, instead opting to use the recovered heat for process heating or for district heating. The heat sources were also far less variable, unlike the focus of this work.

This work will be based on a case study of heat recovery from the Salten Elkem silicon plant, where silicon in a batch process is cooled from 1450°C. This case fits the requirements of a variable heat source, as heat source temperatures will decline as the silicon is cooled, while the casting process is a batch process, where new, hot silicon is only added for cooling every second hour, meaning the heat released by the cooling silicon will fluctuate a lot during every two hour period. The silicon process is very energy intensive, most plants use 11-13 kW h of electrical energy per kilogram of silicon produced [2]. This corresponds to 45% of the total energy supplied to the process, while the energy contained in the raw materials and electrodes accounts for the rest. 32% of the input energy is contained in the product silicon, while the rest leaves the process as heat (Fig. 1). The waste heat is mostly contained in the off-gas, but this heat source is often already utilized for heat recovery. Instead, the heat source used will be the heat released from the product silicon as during the casting process, as it is a much less utilized heat source, and it is much more variable. The casting heat accounts for 7.3% of the electric energy input to the system, or 3.3% the total energy required to produce the silicon.

To examine the potential of this heat source, an exergy analysis were conducted. Assuming the product "silicon" was not pure silicon, but instead a high purity ferrosilicon [1], it was found that 5.6 MW h of heat would be released as 9000 kg of silicon was cooled from 1450°C to 25°C. Using a gliding temperature

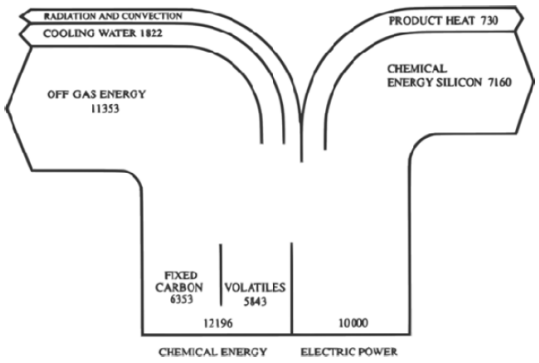

Figure 1: Sankey diagram for the energy flows in a 10 MW silicon furnace [9]

Carnot efficiency to find an estimate for silicon exergy content, it was found that 71.8% of the heat released could be considered exergy. 65% of the exergy would be released from the silicon before it solidified at 1205°C, while 90% of available exergy would already be released once silicon temperatures reached 500°C.

The primary product from Elkem Salten is industrial silicon, and the casting heat from this silicon is the heat source in this work. However, the installation of a WHRU above the solidifying silicon will cause a change in the casting conditions. This will affect the product silicon, as the silicon grain size is affected by how long it takes for silicon to solidify. It will therefore be of utmost importance to design this system in a way which ensures that the solidification time is not affected by the silicon, as the quality of the product silicon is the first priority, and any heat recovery will only occur if it does not negatively affect cooling rates. This work found that the solidification time at Elkem Salten is currently approximately 36 minutes, meaning the proposed heat recovery design will aim at ensuring a solidification time of 36 minutes as well.

[1] More specifically the silicon properties was assumed to be those of FeSi 75 0.025 Ti High Purity Ferrosilicon, a silicon product produced at Elkem: www.matweb.com

2 System description

In order to better utilize the heat released as silicon is cooled, a heat recovery system was proposed. In it, silicon casting heat will act as the heat source for a Rankine cycle. The system is based on a waste heat recovery unit (WHRU), a thermal energy storage (TES) and a power cycle connected in a closed loop. A heat transfer fluid (HTF) flows through the loop, transferring heat between the system components. Heat is first transferred to the loop by a WHRU meant to capture the radiation and convective heat released by the silicon. Then, the HTF passes through a thermal storage, before depositing heat onto a power cycle, which utilizes the captured silicon heat to generate power. A concept sketch of the system is shown in Fig. 2.

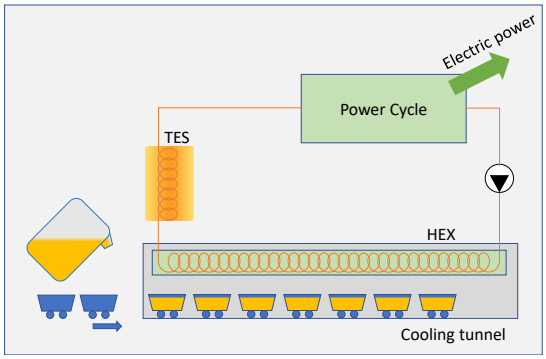

Figure 2: Simple concept diagram of the heat recovery and conversion system

The WHRU is inspired by the design of [3], where radiant heat is collected by a heat shield placed around the hot surface. The WHRU was imagined as a heat shield, or tunnel, placed above the casting molds, with the loop HTF fluid flowing through an array of pipes inside the tunnel walls. The molds would move through the tunnel either by a carousel, as is currently the case at Salten, or in a straight path, as described by [8]. Radiation and convection heat from the mold would heat the tunnel walls, which would in turn heat the fluid inside the pipe array.

To mitigate the fluctuations caused by the heat source, a thermal energy storage (TES) was included in the heat recovery loop. It is meant to store excess heat delivered to the loop as silicon heat transfer rates are high, which can then be deposited to the power cycle once silicon temperatures and heat transfer rates have declined. By using the thermal storage as a buffer, it will help reduce fluctuations in both temperature and heat transfer rates onto the power cycle, ensuring a more stable power production, and smaller variations in the power produced.

The thermal storage chosen in this project was a sensible storage with high-temperature concrete as the storage material. It consists of a bundle of steel tubes encased in concrete. The loop HTF will flow through the storage immediately after the WHRU. If silicon heat output is high, the temperature of the HTF will be higher than the concrete, thus transferring some of the surplus heat to the storage. If instead HTF temperatures are low, due to low silicon heat outputs, concrete temperatures will be higher than the HTF, thus some of the storage heat will be transferred to the HTF. The storage will in both cases help reduce the thermal variations caused by a variable heat source. As can be seen from Fig. 2, there is only one loop for both heat supply and extraction between the loop and the TES, meaning the rate of heat transferred to or from the storage is entirely dependent on the temperature of the concrete and the heat transfer fluid, meaning there are few to no means of actively controlling when the storage should store or deposit heat. On the other hand, the primary function of this storage, reducing thermal variations encountered by the power cycle, will be achieved without a need for any active storage control.

The electric power conversion system will be a Rankine cycle.

The proposed system utilizes one loop for both charging and discharging of the thermal energy storage, unlike most other sensible storage solutions, where separate loops for charging and discharging are present. In such a system, one can more easily control the system behavior, by cutting of storage charging at a set storage temperature, or stopping storage discharge once the heat transfer fluid goes below a set temperature. In addition, the fluid flowing through the storage will change directions during charging and discharging periods, which enables better thermal stratification, thus it will maintain a hot and cold side in the storage material. A one loop

solution simplifies modeling and operation and reduces the number of control systems necessary for proper operation of the system. The loop will also help maintain a higher loop temperature, which will be beneficial in regards to the power cycle, where higher temperatures are associated with higher cycle efficiencies. Higher temperatures in the loop could also lead to less heat recovery, as the temperature difference between the silicon heat source and casting molds and loop heat transfer fluid is smaller.

3 Methodology

A dynamic model of the heat recovery system was developed using a dynamic model formulation in the programming language Modelica,with Dymola being used as the interface for modeling, compiling and simulation. Modelica is a high-level declarative language for describing mathematical behavior. It is often applied to engineering systems and can be used to describe the behavior of different type of engineering components. These component models can then be connected into larger systems, enabling easy modeling of complex physical systems. As a declarative modeling language, Modelica does not require the user to implement numerical solvers for the numerous equations necessary to model every component in a system. The user needs only focus on the mathematical description of the component, while Dymola will handle the numerics. The basics of the model will be described, and an overview of the governing equations used will be provided

All fluid flow in this model is modeled with constant fluid parameters, and using simple control volumes, as described in Eq. 1

$$\dot{m}(h_{in} - h_{out}) + \sum_i \dot{Q}_i = \frac{dU}{dt} = m_{cv} c_v \frac{dT}{dt} \quad (1)$$

where $\sum_i \dot{Q}_i$ is the total heat *input* to the control volume.

3.1 WHRU

The WHRU is modelled as a heat source, i.e. the silicon, transferring heat to a heat transfer fluid by convective and radiation heat, were air flow will be the flowing in between the silicon and tunnel wall. Air flow will also be modelled using Eq. 1, where the Gnielinski's correlation willl be used to decide the convective heat transfer coefficient. For the tunnel heat transfer fluid, total heat input is

$$\begin{aligned} \sum_i \dot{Q}_i &= \dot{Q}_c + \dot{Q}_w + \dot{Q}_{rad,2} \\ &= A_w\big(h_a(T_a - T_{HTF}) \\ &\quad - h_{loss}(T_{HTF} - T_{amb})\big) + \dot{Q}_{rad,2} \end{aligned} \quad (2)$$

while the total heat input to the air flow will be

$$\begin{aligned} \sum_i \dot{Q}_i = \dot{Q}_{c,s} + \dot{Q}_{c,w} &= A_s\big(h_a(T_s - T_a) \\ &\quad + A_w(h_a(T_{HTF} - T_a)\big) \end{aligned} \quad (3)$$

Radiation heat transfer is modelled using the radiation heat transfer network method [6]. Three surfaces are considered here: the silicon surface (surface 1), the WHRU tunnel wall (surface 2), and the surroundings, i.e. radiation not impacting the tunnel walls, instead being lost (surface 3). The surroundings are assumed to be a blackbody ($\varepsilon_3 = 1$), since very little heat is radiated from the surroundings to the other surfaces. The radiation heat transfer network is summarized in the radiation energy balances seen in Eqs. 4-7.

$$\frac{\sigma T_1^4 - J_1}{\frac{1-\varepsilon_1}{\varepsilon_1 A_1}} = \frac{J_1 - J_2}{\frac{1}{A_1 F_{1\to2}}} + \frac{J_1 - J_3}{\frac{1}{A_1 F_{1\to3}}} \quad (4)$$

$$\frac{\sigma T_2^4 - J_2}{\frac{1-\varepsilon_2}{\varepsilon_2 A_2}} = \frac{J_2 - J_1}{\frac{1}{A_1 F_{1\to2}}} + \frac{J_2 - J_3}{\frac{1}{A_2 F_{2\to3}}} \quad (5)$$

$$\frac{\sigma T_3^4 - J_3}{\frac{1-\varepsilon_3}{\varepsilon_3 A_3}} = \frac{J_3 - J_1}{\frac{1}{A_1 F_{1\to3}}} + \frac{J_3 - J_2}{\frac{1}{A_2 F_{2\to3}}} \quad (6)$$

Because the surface radiative resistance is zero at surface 3, Eq. 6 is simplified by multiplying both sides of the equation with $\frac{1-\varepsilon_3}{\varepsilon_3 A_3} = 0$, which results in Eq. 7.

$$\sigma T_3^4 - J_3 = 0 \quad (7)$$

The temperature of each surface is T_1, T_2, and T_3, while the net radiation heat flow from each surface is defined as:

$$\dot{Q}_{rad,1} = \frac{\sigma T_1^4 - J_1}{\frac{1-\varepsilon_1}{\varepsilon_1 A_1}} \quad (8)$$

$$\dot{Q}_{rad,2} = \frac{\sigma T_2^4 - J_2}{\frac{1-\varepsilon_2}{\varepsilon_2 A_2}} \tag{9}$$

$$\dot{Q}_{rad,3} = \frac{J_3 - J_1}{\frac{1}{A_1 F_{1\to 3}}} + \frac{J_3 - J_2}{\frac{1}{A_2 F_{2\to 3}}} \tag{10}$$

Here, $Q_{rad,1}$ is the radiation heat out of the silicon heat source, $Q_{rad,2}$ is the radiation heat impacting the WHRU tunnel wall, while $Q_{rad,3}$ is the radiation heat lost from the system. $\dot{Q}_{rad,3}$ was calculated differently due to it being a blackbody.

3.2 Silicon

The silicon is modelled as a thermal capacitor, where temperature decreases as heat is released from the silicon. To include the additional heat released by the silicon due to the phase change occurring, i.e. the heat of fusion, the thermal capacitance was modified to increase in the casting interval, by assuming the heat of fusion is released in a uniform manner across the solidification interval. Then, to include the thermal gradient in the silicon through the silicon, the silicon was modelled as several thermal capacitances in series, with a thermal resistor in-between. Heat transfer was modeled assuming heat was only released from the topmost surface of the silicon, and assuming 1-D heat transfer through the silicon depth, in accordance with other simple silicon solidification models [1, 10].

3.3 Thermal energy storage

The thermal energy storage (TES) was modeled using an approach described by [7], where a concrete storage is modelled using the lumped capacitance assumption while defining an effective heat transfer coefficient to describe heat transfer from the heat transfer fluid to the concrete material. To simplify the model, a single heat transfer tube with its surrounding concrete material was modelled, and the model was scaled up to properly represent the true size of the storage. As with the WHRU, the fluid flow through the storage was described by Eq. 1, while the concrete heat balance was

$$(mc_p)_{TES}\frac{dT_{TES}}{dt} = h_E A_{TES}(T_{HTF} - T_{TES}) \tag{11}$$

The net heat input into the storage material will also be the net heat output from the fluid passing through the storage, while h_E is the effective storage heat transfer coefficient, found by:

$$\frac{1}{h_E} = \frac{1}{h} + \frac{1}{k}\frac{4ab^4 \ln\frac{b}{a} - 3ab^4 + 4a^3b^2 - a^5}{4(b^2 - a^2)^2} \tag{12}$$

where a is the inner radius of the heat transfer pipe, b is the radius of the concrete medium surrounding pipe, while h is the convective heat transfer coefficient of the heat transfer fluid.

The power cycle was not properly modeled in this work, to keep the scope of the work at bay. A simple counter flow heat exchanger was included to include a heat sink for the loop, while the potential electrical power production from the recovered heat was estimated to be 50% of the available exergy transferred through this heat exchanger. This is a rough estimate, and will still give a somewhat tolerable estimate for the potential for the system to produce electric power. However, an estimate will not account for losses introduced due to off-design operation, or be used to verify that a power cycle could be utilized for said heat source if variations were to large.

3.4 Others

The sections above describe the main components of the proposed system. Several other components was also made to properly model the movement of the silicon through the tunnel, among others. In addition, some components were made to implement system control schemes. One such component would how the WHRU tunnel would open and close, in order to reduce radiation losses, while another was a PI-regulator meant to control the power cycle mass flow rate to examine if such a regulator could ensure less variable operating conditions for the power cycle.

4 Results and discussion

Table 1 describes the main characteristics of the system, both how it would operate without a storage system, and with it, as well as how different control systems would affect operation. The integration of a storage was found to be very effective at reducing

Table 1: Performance of the proposed system, with and without further control strategies

System property	Unit	No storage	Proposed system design			
Control tunnel openings		–	–	Yes	Yes	Yes
PI control: power		–	–	–	–	Yes
PI control: temperature		–	–	–	Yes	–
W	kW h	819.8	762.3	795.1	796.4	791.8
$\Delta\dot{W}$	kW	1128.7	128.0	121.0	184.9	53.0
$T_{TES,avg}$	°C	–	396.7	405.8	407.0	398.2
$T_{TES,max}$	°C	–	449.2	452.2	452.8	447.6
$T_{turb,avg}$	°C	293.8	301.7	308.0	309.8	292.2
ΔT_{turb}	°C	487.3	50.0	46.7	8.0	111.6
η_{ex}	%	20.3	18.8	19.6	19.7	19.5
η	%	60.3	62.6	65.7	65.2	66.3
t_s	min	37.2	36.3	36.3	36.4	36.2

the variations in operating conditions encountered by the power cycle. Variations in the estimate for power production and power cycle expander inlet temperature decreased by 88.7% and 89.7% respectively, by adding a 19 m^3 TES, roughly the size of a small shipping container.

From Table 1, it can be seen that the inclusion of the storage reduced the potential for power production by 7%. This loss is associated with the exergy destruction which happens due to the loss of temperature during heat transfer to and from the storage. The loss in potential power production is an acceptable loss in potential power production to reduce variations as much as was done, as no real power cycle would be operated while experiencing variations in expander inlet temperature of nearly 500°C.

Also shown is how some different system control schemes would affect system performance. Controlling the openings of the WHRU tunnel showed potential, as it was shown to improve energy recovery while not affecting solidification. Using the power cycle working fluid flow rate as part of a PI-regulator scheme was also examined. Both controlling for an even expander inlet temperature and an even estimate for power production was possible, but both of these instances showed that reduction in variations in either one of these system characteristics would lead to an increase in variations in the other.

The system with no control scheme was found to produce 762.3 $\mathrm{kW\,h}$ of electric power every two-hour casting cycle, which is 0.65% of the electric energy required to produce the silicon. The system would recover 62.6% of the waste heat released by the silicon as it was placed beneath the WHRU tunnel, while it would convert 18.8% of the exergy contained as heat in the hot silicon to electric energy.

It was found that the WHRU system would affect the cooling conditions of the silicon. Multiple aspects of the WHRU design and operation would affect it, but the design of the casting molds was found the affect it the most. The WHRU would reduce the cooling rates, prolonging the solidification time, which meant an increase in mold surface area, and a decrease in the silicon depth in the mold could counteract some of this change. Increasing surface areas would increase heat transfer area, and thus initial heat transfer rates, while shallower silicon would reduce the thermal resistance through the mold, which would be beneficial for a more even solidification. Other aspects of the WHRU which would also affect solidification included the temperature of the WHRU heat transfer fluid and walls and the flow rate of air through the tunnel, but neither was capable of ensuring proper solidification times on their own without removing any potential for heat recovery simultaneously. In the design system, the mold size would be

increased by 33% compared to the molds currently in use at Salten. The extent of the effect of mold dimensions on solidification time is shown in Fig. 3.

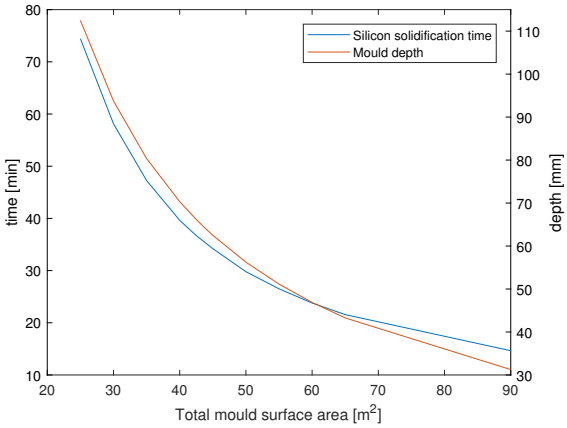

Figure 3: Silicon solidification time with changing mould surface areas

The TES was designed to ensure as high a storage-HTF heat transfer as possible. A large heat transfer area would be ensured by designing for few parallel heat transfer tubes, short tube pitch distance, and large inner tube diameters. Large storage heat transfer coefficients were shown to result in a storage better able to react to the large changes to storage temperature and heat loads, thus being more effective at reducing cyclic variations. The storage material, concrete, would also mean the cost of the storage would be manageable, compared to other more expensive storage alternatives.

Using the decided upon system layout with one loop for both storage charge and discharge, it was found that the storage was quite effective at reducing cyclic variations caused by the variable silicon heat source. However, it was also found that the system would not be viable if there was a need to more manually control the charge or discharge from the storage. This because the one loop system makes it difficult to decouple the charging and discharge. At the same time, this one loop system would be beneficial for the purpose of this work, where the intention was not to store heat for extended periods of time, but instead to reduce variations without the need for complex system control, as it will primarily be the temperature difference between the storage and loop heat transfer fluid which will regulate how the storage absorbs or releases heat.

5 Conclusion

This work has investigated the integration of a sensible thermal energy storage in a waste heat recovery system for the recovery of a variable waste heat source. A dynamic model of the system was proposed and a case study was examined, being the heat released from the silicon casting process. The model primarily showed the potential of utilizing storage to recover heat from a variable heat source, which could pave the way for power conversion from heat sources which until now has been difficult to utilize.

The results show that the system proposed would prove capable of reducing storage variations to a very large extent. Estimated power production and power cycle expander inlet temperature would experience a reduction in variation of well above 85%, which would simplify the operation of any power cycle. This reduction in variations was achieved without the need of storage control systems, due to the storage layout proposed. This also meant that the system was effective for this exact purpose, but less so for other applications where more direct control of the storage would be necessary.

The system was shown capable of recovering heat from the hot silicon, producing upwards of 800 kW h of electric energy every two-hour casting cycle. It was also shown that with careful design of the WHRU it would be possible to recover silicon heat in a way which did not negatively impact the casting process.

References

[1] BENHAM, G., HILDAL, K., PLEASE, C., AND VAN GORDER, R. Solidification of silicon in a one-dimensional slab and a two-dimensional wedge. *International Journal of Heat and Mass Transfer 98* (02 2016).

[2] BØRSET, M. T. *Energy Dissipation and Recovery in the Context of Silicon Production: Exergy Anal-*

ysis and Thermoelectricity. PhD thesis, Norwegian University of Science and Technology, 2015.

[3] CAPUTO, A. C., PELAGAGGE, P. M., AND SALINI, P. Performance modeling of radiant heat recovery exchangers for rotary kilns. *Applied Thermal Engineering 31*, 14 (2011), 2578 – 2589.

[4] DELPECH, B., AXCELL, B., AND JOUHARA, H. Experimental investigation of a radiative heat pipe for waste heat recovery in a ceramics kiln. *Energy 170* (2019), 636 – 651.

[5] DU, W.-J., YIN, Q., AND CHENG, L. Experiments on novel heat recovery systems on rotary kilns. *Applied Thermal Engineering 139* (2018), 535 – 541.

[6] INCORPERA, F. P., DEWITT, D. P., BERGMAN, T. L., AND LAVINE, A. S. *Fundamentals of Heat and Mass Transfer*, 6th ed. John Wiley & Sons, 2005.

[7] JIAN, Y., BAI, F., FALCOZ, Q., XU, C., WANG, Y., AND WANG, Z. Thermal analysis and design of solid energy storage systems using a modified lumped capacitance method. *Applied Thermal Engineering 75* (2015), 213 – 223.

[8] JOUHARA, H., ALMAHMOUD, S., CHAUHAN, A., DELPECH, B., BIANCHI, G., TASSOU, S. A., LLERA, R., LAGO, F., AND ARRIBAS, J. J. Experimental and theoretical investigation of a flat heat pipe heat exchanger for waste heat recovery in the steel industry. *Energy 141* (2017), 1928 – 1939.

[9] SCHEI, A. *Production of high silicon alloys*. Tapir, Trondheim, 1998.

[10] TVEIT, H. *Størkning av 75% ferrosilisium : forløp, struktur og styrke*. PhD thesis, Norges tekniske høgskole, Trondheim, 1988.

[11] VANCE, D., NIMBALKAR, S., THEKDI, A., ARMSTRONG, K., WENNING, T., CRESKO, J., AND JIN, M. Estimation of and barriers to waste heat recovery from harsh environments in industrial processes. *Journal of Cleaner Production 222* (2019), 539 – 549.

Nomenclature

Abbreviations

HTF	Heat transfer fluid
TES	Thermal energy storage
WHRU	Waste heat recovery unit

Symbols

A	Area, m^2
c	Specific heat capacity, $\mathrm{J}/(\mathrm{kg\,K})$
h	Specific enthalpy, J/kg
h	Convection coefficient, $\mathrm{J\,K}/\mathrm{m}^2$
k	Conductivity, $\mathrm{J}/(\mathrm{m\,K})$
m	Mass, kg
$\dot{m}$	Mass flow, kg/s
$\dot{Q}$	Heat flow rate, kW
T	Temperature, K

Greek symbols

Δ	Difference
η	Efficiency
ε	Emissivity
σ	Steffan Boltsmanns constant

Subscripts

a	Air
avg	Time average
amb	Ambient
c	Convection
cv	Control volume
ex	Exergy
in	Control volume inlet
$loss$	Heat loss
out	Control volume outlet
rad	Radiation
s	Silicon
$turb$	Inlet of power cycle expander
w	WHRU wall

A.2 Modelica code

All relevant code will be attached. The MSL libraries `Modelica.Thermal` and `Modelica.Blocks` will be necessary libraries in addition the attached code.

A.2.1 Silicon heat source components

```
record SiliconParameters
  extends Modelica.Icons.Record;
  parameter Modelica.SIunits.Density rho = 3200 "Density";
  parameter Modelica.SIunits.SpecificHeatCapacity cp_gliding =
    812
    "Specific heat capacity when not solidifying";
  parameter Modelica.SIunits.SpecificEnthalpy h_latent = 1100e3
    "latent heat released when solidifying";
  parameter Modelica.SIunits.Temperature T_solidus = 1205+273.15
    "End point of solidification";
  parameter Modelica.SIunits.Temperature T_liquidus = 1350+273.15
    "Start point of solidification";
  parameter Modelica.SIunits.ThermalConductivity k = 23.5
    "Thermal conductivity of solid phase";
  parameter Modelica.SIunits.ThermalConductivity k_liq = 44
    "Thermal conductivity before solidification";
end SiliconParameters;

model HeatCapSilicon
public
  parameter SiliconParameters s=SiliconParameters();
  parameter Modelica.SIunits.Temperature T_new "Temperature when
     reinitializing the element";
  parameter Modelica.SIunits.Mass         m "mass of capacitance";
  Modelica.SIunits.SpecificHeatCapacity   cp "Heat capacity of
     element (= cp*m)";
  Modelica.SIunits.Temperature            T(start=293.15,
     displayUnit="degC") "Temperature of element";
  Modelica.SIunits.HeatCapacity           C "heat capacity of
     element";
  Modelica.Thermal.HeatTransfer.Interfaces.HeatPort_a port;
  Modelica.Blocks.Interfaces.BooleanInput reStart;
equation
  when reStart then
    reinit(T, T_new);
  end when;
  cp = specificHeat(T, s);
  C = m*cp;
  T = port.T;
  C*der(T) = port.Q_flow;
end HeatCapSilicon;
```

```
model Mould
protected
  parameter Modelica.SIunits.ThermalConductance       G = s.k*A/(d
     /N);
public
  parameter SiliconParameters s=SiliconParameters();
  parameter Modelica.SIunits.Temperature              T0 =
     1450+273.15 "Initial temperature of the element";
  parameter Modelica.SIunits.Mass                     m = 1000 "
     mass of silicon";
  parameter Integer                                   N(min=1) "
     Number of discrete capacitances";
  parameter Modelica.SIunits.Area                     A "surface
     area of mould";
  final parameter Modelica.SIunits.Length             d = m/(s.rho
     *A) "depth of mould";
  Modelica.Thermal.HeatTransfer.Interfaces.HeatPort_a port_a;
  Modelica.Thermal.HeatTransfer.Components.ThermalConductor
     thermalConductor[N - 1](each G=G);
  Modelica.Blocks.Interfaces.BooleanInput reStart;
  HeatCapSilicon heatCapSilicon[N](
    each m=m/N,
    each T_new=T0,
    each s=s,
    T(each start=T0, each fixed=true));
equation
  for i in 1:N-1 loop
    connect(heatCapSilicon[i].port, thermalConductor[i].port_a);
    connect(thermalConductor[i].port_b, heatCapSilicon[i+1].port)
       ;
  end for;
  connect(heatCapSilicon[N].port,port_a);
  for i in 1:N loop
    connect(reStart,heatCapSilicon[i].reStart);
  end for;
end Mould;

model ThermalConductor
  "Thermal conductor with variable conductanceLumped thermal
     element transporting heat without storing it"
  parameter SiliconParameters s=SiliconParameters();
  extends Modelica.Thermal.HeatTransfer.Interfaces.Element1D;
  parameter Modelica.SIunits.Area A;
  parameter Modelica.SIunits.Length L;
  Modelica.SIunits.ThermalConductance G;
  Modelica.SIunits.ThermalConductivity k;
  Modelica.SIunits.Temperature T_avg;
equation
  T_avg = (port_a.T+port_b.T)/2;
  k = if T_avg>s.T_solidus then s.k_liq else  s.k;
```

```
    G = k*A/L;
    Q_flow = G*dT;
  end ThermalConductor;

  function specificHeat
    "Approximation of the specific heat of silicon, including the
       enthalpy of fusion"
    input Modelica.SIunits.Temperature            T;
    input SiliconParameters s;
    output Modelica.SIunits.SpecificHeatCapacity  cp;
  algorithm
    if T<s.T_solidus then
      cp := s.cp_gliding;
    elseif T>=s.T_solidus and T<=s.T_liquidus then
      cp := s.h_latent/(s.T_liquidus-s.T_solidus)+s.cp_gliding;
    else
      cp :=s.cp_gliding;
    end if;
  end specificHeat;
```

A.2.2 WHRU conponents

```
  model Radiation
    "View factors are given as a continuous input.  Also inclused a
       possibility to block tunnel entrances"
  protected
    parameter Real sigma = Modelica.Constants.sigma;
  public
    Modelica.SIunits.HeatFlux J1, J2, J3;
    Modelica.SIunits.HeatFlowRate q12,q13,q23;
    parameter Modelica.SIunits.Area A1;
    parameter Modelica.SIunits.Area A2;
    parameter Modelica.SIunits.Area A3;
    parameter Real e1(min=0,max=1), e2(min=0,max=1), e3(min=0,max
       =1);
    Real F12new(min=0,max=1), F13new(min=0,max=1), F23new(min=0,max
       =1);
    Modelica.Thermal.HeatTransfer.Interfaces.HeatPort_a port_1;
    Modelica.Thermal.HeatTransfer.Interfaces.HeatPort_a port_2;
    Modelica.Thermal.HeatTransfer.Interfaces.HeatPort_a port_3;
    Modelica.Blocks.Interfaces.BooleanInput isBlocked;
    Modelica.Blocks.Interfaces.RealInput F12;
    Modelica.Blocks.Interfaces.RealInput F13;
    Modelica.Blocks.Interfaces.RealInput F23;
  equation
    if isBlocked then
      F12new = 0.95;
      F13new = 0.05;
      F23new = 0.05;
    else
```

```
    F12new = F12;
    F13new = F13;
    F23new = F23;
  end if;
  (sigma*port_1.T^4-J1)/((1-e1)/(e1*A1)) = (J1-J2)/(1/(A1*F12new)
    ) + (J1-J3)/(1/(A1*F13new));
  (sigma*port_2.T^4-J2)/((1-e2)/(e2*A2)) = (J2-J1)/(1/(A1*F12new)
    ) + (J2-J3)/(1/(A2*F23new));
  (sigma*port_3.T^4-J3)/((1-e3)/(e3*A3)) = (J3-J1)/(1/(A1*F13new)
    ) + (J3-J2)/(1/(A2*F23new));
  q12 = (J1-J2)/(1/(A1*F12new));
  q13 = (J1-J3)/(1/(A1*F13new));
  q23 = (J2-J3)/(1/(A2*F23new));
  port_1.Q_flow = (sigma*port_1.T^4-J1)/((1-e1)/(e1*A1));
  port_2.Q_flow = (sigma*port_2.T^4-J2)/((1-e2)/(e2*A2));
  port_3.Q_flow = (sigma*port_3.T^4-J3)/((1-e3)/(e3*A3));
end Radiation;

model TunnelSegment
  "Tunnel view factors depend on time and relative positioning,
    but with the possibility of blocking of tunnel entry and
    exit to ensure all radiation impacts the tunnel wall. Also,
    optional wall-loss"
protected
  parameter Modelica.SIunits.Mass m_air = length*A3/2*air.rho "
    Total air in entire tunnel segment";
  parameter Modelica.SIunits.Mass m_HTF = length*
    Modelica.Constants.pi*d^2/4*HTF.rho "Total HTF in entire
    tunnel segment";
  // tunnel view factors
  parameter Real F12=ViewFactorParallelRectangles(
        width,
        length,
        height) + 2*ViewFactorPerpendicularRectangles(
        width,
        height,
        length);
  parameter Real F13=2*ViewFactorPerpendicularRectangles(
        length,
        height,
        width);
  parameter Real F32=1 - ViewFactorParallelRectangles(
        height,
        width,
        length) - ViewFactorPerpendicularRectangles(
        height,
        length,
        width);
  parameter Real F23 = F32*A3/A2;
public
```

```
parameter Modelica.Thermal.FluidHeatFlow.Media.Medium HTF=
    Modelica.Thermal.FluidHeatFlow.Media.Medium() "Heat Transfer
     FLuid";
parameter Modelica.Thermal.FluidHeatFlow.Media.Medium air=
    Modelica.Thermal.FluidHeatFlow.Media.Medium() "air used in
    forced convection inside tunnel";
final parameter Modelica.SIunits.Area      A1 = length*width;
final parameter Modelica.SIunits.Area      A2 = length*width +
    2*length*height;
final parameter Modelica.SIunits.Area      A3 = 2*width *
    height;
parameter Real e1, e2, e3;
parameter Integer                          N(min=2) "Number of
    partitions in segment";
parameter Modelica.SIunits.Temperature T0_HTF, T0_air;
parameter Modelica.SIunits.Length      length, width, height;
parameter Real startTime "position of tunnelSegment in discrete
     tunnel, i_mould/N_mould";
parameter Real active(min=0, max=100);
parameter Real period(min=0);
parameter Real pouring(min=0, max=period);
parameter Modelica.SIunits.Diameter    d "diameter of HTF pipe"
    ;
parameter Boolean useWallLoss=false "Enable / disable volume
    flow input";
parameter Modelica.SIunits.CoefficientOfHeatTransfer h_free;
parameter Modelica.SIunits.ThermalConductivity k_ins;
parameter Modelica.SIunits.Length L_ins;
Boolean blocked;
Modelica.SIunits.HeatFlowRate Q_mould, Q_airloss, Q_HTF,
    Q_radloss, Q_wallloss;
Modelica.SIunits.Temperature Tair_a, Tair_b, Thtf_a, Thtf_b;
Modelica.Thermal.FluidHeatFlow.Interfaces.FlowPort_a flowPort_a
    (medium=air);
Modelica.Thermal.FluidHeatFlow.Interfaces.FlowPort_b flowPort_b
    (medium=air);
Modelica.Thermal.FluidHeatFlow.Interfaces.FlowPort_a
    flowPort_a1(medium=HTF);
Modelica.Thermal.FluidHeatFlow.Interfaces.FlowPort_b
    flowPort_b1(medium=HTF);
Modelica.Thermal.HeatTransfer.Interfaces.HeatPort_a port_mould;
Radiation radiation[N](
  each A1=A1/N,
  each A2=A2/N,
  each A3=A3/N,
  each e1=e1,
  each e2=e2,
  each e3=e3);
Modelica.Thermal.HeatTransfer.Components.Convection convection[
    N];
```

```
Modelica.Thermal.HeatTransfer.Components.Convection convection1
    [N];
Modelica.Thermal.FluidHeatFlow.Components.HeatedPipe HTFflow[N
    ](
  each medium=HTF,
  each V_flowLaminar=1,
  each V_flowNominal=2,
  each h_g=0,
  each T0fixed=true,
  each T0=T0_HTF,
  each m=m_HTF/N,
  each dpLaminar=100,
  each dpNominal=2000);
Modelica.Thermal.FluidHeatFlow.Components.HeatedPipe airFlow[N
    ](
  each medium=air,
  each V_flowLaminar=1,
  each V_flowNominal=2,
  each h_g=0,
  each T0fixed=true,
  each T0=T0_air,
  each m=m_air/N,
  each dpLaminar=100,
  each dpNominal=2000);
Modelica.Thermal.HeatTransfer.Interfaces.HeatPort_b
    port_ambient;
Modelica.Blocks.Interfaces.RealInput convectionCoefficient(unit
    ="W/(m2.K)");
Modelica.Blocks.Math.Gain Gc1(k(unit="m2")=A2/N, y(unit="W/K"))
    ;
Modelica.Blocks.Math.Gain Gc(k(unit="m2")=A1/N, y(unit="W/K"));
Modelica.Thermal.HeatTransfer.Components.ThermalResistor [N]
    wallLoss(
  each R=1/(h_free*A2/N)+1/(k_ins*A2/N/L_ins)) if useWallLoss;
ViewFactor viewFactorF12(
  pouring=pouring,
  active=active,
  period=period,
  startTime=startTime,
  offset=F12,
  amplitude=1 - F12 - 0.01);
ViewFactor viewFactorF13(
  pouring=pouring,
  active=active,
  period=period,
  startTime=startTime,
  offset=F13,
  amplitude=-F13 + 0.01);
ViewFactor viewFactorF23(
  pouring=pouring,
```

```
      active=active,
      period=period,
      startTime=startTime,
      offset=F23,
      amplitude=-F23 + 0.01);
  equation
    blocked = if abs(flowPort_a.m_flow)>0.1*height*width then false
        else true;
    Q_mould = port_mould.Q_flow;
    Q_airloss = sum(airFlow[1:N].heatPort.Q_flow);
    Q_HTF = sum(HTFflow[1:N].heatPort.Q_flow);
    Q_radloss = -sum(radiation[1:N].port_3.Q_flow);
    Q_wallloss = -port_ambient.Q_flow-Q_radloss;
    Tair_a = airFlow[1].T_a;
    Tair_b = airFlow[end].T_b;
    Thtf_a = HTFflow[1].T_a;
    Thtf_b = HTFflow[end].T_b;
    connect(convectionCoefficient, Gc1.u);
    connect(convectionCoefficient, Gc.u);
    connect(flowPort_a, airFlow[1].flowPort_a);
    connect(flowPort_b, airFlow[end].flowPort_b);
    connect(flowPort_a1, HTFflow[1].flowPort_a);
    connect(flowPort_b1, HTFflow[end].flowPort_b);
    for i in 1:N-1 loop
      connect(airFlow[i].flowPort_b, airFlow[i+1].flowPort_a);
      connect(HTFflow[i].flowPort_b, HTFflow[i+1].flowPort_a);
    end for;
    for i in 1:N loop
      //convection connections first
      connect(Gc.y,convection[i].Gc);
      connect(Gc1.y, convection1[i].Gc);
      connect(port_mould, convection[i].solid);
      connect(convection[i].fluid, airFlow[i].heatPort);
      connect(airFlow[i].heatPort, convection1[i].fluid);
      connect(convection1[i].solid, HTFflow[i].heatPort);
      //radiation connections
      connect(port_mould, radiation[i].port_1);
      connect(radiation[i].port_2, HTFflow[i].heatPort);
      connect(radiation[i].port_3, port_ambient);
      radiation[i].isBlocked=blocked;
      connect(viewFactorF12.y, radiation[i].F12);
      connect(viewFactorF13.y, radiation[i].F13);
      connect(viewFactorF23.y, radiation[i].F23);
      //tunnel losses
      connect(wallLoss[i].port_a, HTFflow[i].heatPort);
      connect(wallLoss[i].port_b, port_ambient);
    end for;
  end TunnelSegment;
  model TunnelDiscrete
    "Same as TunnelDiscrete2, but with the possibility of blocking
```

```
    of tunnel entry and exit to ensure all radiation impacts the
     tunnel wall"
  parameter Modelica.Thermal.FluidHeatFlow.Media.Medium air=
    Modelica.Thermal.FluidHeatFlow.Media.Air_70degC();
  parameter Modelica.Thermal.FluidHeatFlow.Media.Medium HTF=
    Modelica.Thermal.FluidHeatFlow.Media.Medium();
  parameter SiliconParameters s=
     SiliconParameters();
  parameter Integer N_moulds(min=2)=2 "Number of discrete moulds
    in the tunnel";
  parameter Integer N_partitions(min=1)=1 "Number of tunnel
    partitions per mould";
  parameter Integer N_mouldlayers(min=1)=1 "Number of layers in
    moulds";
  parameter Real active(min=0, max=100)=50 "The fraction of the
    period in which the mould is heating the cycle, in
    percentage, 0-100";
  parameter Real period(min=0) = 7200 "Time in seconds for one
    melting cylce";
  parameter Real pouring(min=0, max=period)=1800 "Time to pour
    one ladle into 9 moulds";
  parameter Real e1(min=0, max=1) = 0.4;
  parameter Real e2(min=0, max=1) = 0.5;
  parameter Real e3(min=0, max=1) = 0.9999;
  parameter Modelica.SIunits.Temperature  T_amb "ambient
    temperature=air inlet temperature";
  parameter Modelica.SIunits.Temperature  T0_mould "mould initial
     temperature";
  parameter Modelica.SIunits.Temperature  T0_HTF "HTF intial
    temperature";
  parameter Modelica.SIunits.Mass m_silicon = 9000 "Total mass of
     silicon";
  parameter Modelica.SIunits.Length length = N_moulds*2.03 "Total
     length of tunnel";
  parameter Modelica.SIunits.Length width = 1.8 "width of tunnel"
    ;
  parameter Modelica.SIunits.Length height = 1 "height of tunnel,
     mould surface to roof";
  parameter Modelica.SIunits.Diameter d = 0.1 "diameter of HTF
    pipe";
  parameter Modelica.SIunits.Velocity v_air = 1 "air-velocity
    through tunnel";
  parameter Modelica.SIunits.CoefficientOfHeatTransfer h_free = 6
     "air free convection coefficient";
  parameter Modelica.SIunits.ThermalConductivity k_ins = 0.09;
  parameter Modelica.SIunits.Length L_ins = 0.01;
  parameter Boolean useVolumeFlowInput=false "Enable / disable
    volume flow input";
  parameter Boolean useWallLoss=false "Enable / disable tunnel
    wall heat loss";
```

```
parameter Boolean measureSolidification=false "Measure the
    innermost temperature of last silicon mould";
Modelica.SIunits.Temperature Tair_a, Tair_b, Thtf_a, Thtf_b;
Modelica.SIunits.HeatFlowRate Q_mould, Q_HTF, Q_airloss,
    Q_radloss, Q_wallloss;
Modelica.SIunits.Heat E_mould(start=0), E_HTF(start=0),
    E_airloss(start=0), E_radloss(start=0), E_wallloss(start=0);
TunnelSegment tunnelSegment[N_moulds](
  each HTF=HTF,
  each air=air,
  each N=N_partitions,
  each T0_HTF=T0_HTF,
  each T0_air=T_amb,
  each width=width,
  each height=height,
  each e1=e1,
  each e2=e2,
  each e3=e3,
  each d=d,
  each length=length/N_moulds,
  each h_free=h_free,
  each useWallLoss=useWallLoss,
  startTime=linspace(
        1,
        pouring,
        N_moulds),
  each active=active,
  each period=period,
  each pouring=pouring,
  each k_ins=k_ins,
  each L_ins=L_ins);
Mould mould[N_moulds](
  each m=m_silicon/N_moulds,
  each N=N_mouldlayers,
  each A=length/N_moulds*width,
  each s=s,
  each T0=T0_mould);
Modelica.Blocks.Sources.Constant volumeFlow(k=v_air*height*
    width) if not
  useVolumeFlowInput;
Modelica.Thermal.FluidHeatFlow.Interfaces.FlowPort_a flowPort_a
    (medium=HTF);
Modelica.Thermal.FluidHeatFlow.Interfaces.FlowPort_b flowPort_b
    (medium=HTF);
ForcedConvection forcedConvection(
  medium=air,
  width=width,
  height=height,
  h_free=h_free);
Modelica.Thermal.FluidHeatFlow.Sources.Ambient airInlet(
```

```
    constantAmbientPressure=0,
    medium=air,
    constantAmbientTemperature=T_amb);
  Modelica.Thermal.FluidHeatFlow.Sources.Ambient airOutlet(
    medium=air,
    constantAmbientPressure=0,
    constantAmbientTemperature=T_amb);
  Modelica.Thermal.FluidHeatFlow.Sources.VolumeFlow pump1(
    m=0,
    useVolumeFlowInput=true,
    constantVolumeFlow=1,
    medium=air);
  Modelica.Thermal.HeatTransfer.Sources.FixedTemperature ambient(
     T=T_amb);
  Modelica.Blocks.Sources.BooleanPulse booleanMultiple[N_moulds](
    each width=active,
    each period=period,
    startTime=linspace(
        1,
        pouring,
        N_moulds)) if      N_moulds >= 2;
  HeatBlocker heatBlocker[N_moulds];
  Modelica.Blocks.Interfaces.RealInput airVolumeFlow if
     useVolumeFlowInput;
  Modelica.Blocks.Interfaces.RealOutput lastMouldTemp;
  Modelica.Blocks.Interfaces.RealOutput firstMouldTemp;
equation
  //summary:
  Tair_a = tunnelSegment[1].airFlow[1].T_a;
  Tair_b = tunnelSegment[end].airFlow[end].T;
  Thtf_a = tunnelSegment[1].HTFflow[1].T_a;
  Thtf_b = tunnelSegment[end].HTFflow[end].T;

  Q_mould = sum(tunnelSegment[1:N_moulds].Q_mould);
  Q_HTF = sum(tunnelSegment[1:N_moulds].Q_HTF);
  Q_airloss = sum(tunnelSegment[1:N_moulds].Q_airloss);
  Q_radloss = sum(tunnelSegment[1:N_moulds].Q_radloss);
  Q_wallloss = sum(tunnelSegment[1:N_moulds].Q_wallloss);
  der(E_mould) = Q_mould;
  der(E_HTF) = Q_HTF;
  der(E_airloss) = Q_airloss;
  der(E_radloss) = Q_radloss;
  der(E_wallloss) = Q_wallloss;
  lastMouldTemp = mould[end].heatCapSilicon[1].T;
  firstMouldTemp = mould[1].heatCapSilicon[1].T;
  //connections
  for i in 1:N_moulds-1 loop
    connect(tunnelSegment[i].flowPort_b, tunnelSegment[i+1].
       flowPort_a);
    connect(tunnelSegment[i].flowPort_b1, tunnelSegment[i+1].
```

```
        flowPort_a1);
    end for;
    for i in 1:N_moulds loop
      // connect(mould[i].port_a, tunnelSegment[i].port_mould);
      connect(mould[i].port_a, heatBlocker[i].port_a);
      connect(heatBlocker[i].port_b, tunnelSegment[i].port_mould);
      connect(tunnelSegment[i].port_ambient, ambient.port);
      connect(forcedConvection.y, tunnelSegment[i].
        convectionCoefficient);
      connect(booleanMultiple[i].y, mould[i].reStart);
      connect(booleanMultiple[i].y, heatBlocker[i].u);
    end for;
    connect(flowPort_a, tunnelSegment[1].flowPort_a1);
    connect(tunnelSegment[end].flowPort_b1, flowPort_b);
    connect(tunnelSegment[end].flowPort_b, airOutlet.flowPort);
    connect(pump1.flowPort_b, forcedConvection.flowPort_a);
    connect(forcedConvection.flowPort_b, tunnelSegment[1].
      flowPort_a);
    connect(volumeFlow.y, pump1.volumeFlow);
    connect(airInlet.flowPort, pump1.flowPort_a);
    connect(airVolumeFlow, pump1.volumeFlow);
  end TunnelDiscrete;

  model HeatBlocker "heat can only pass through if boolean=true"
    Modelica.Thermal.HeatTransfer.Interfaces.HeatPort_a port_a;
    Modelica.Thermal.HeatTransfer.Interfaces.HeatPort_b port_b;
    Modelica.Blocks.Interfaces.BooleanInput u;
    Modelica.SIunits.HeatFlowRate Q_flow;
    Modelica.SIunits.TemperatureDifference dT;
  equation
    dT = port_a.T - port_b.T;
    port_a.Q_flow = Q_flow;
    port_b.Q_flow = -Q_flow;
    if u then
      dT=0;
    else
      Q_flow=0;
    end if;
  end HeatBlocker;
  function ViewFactorParallelRectangles "l and w is the size of
    each rectangle, d is the distance between them, as
  described on http://www.thermalradiation.net/calc/sectionc/
    C-11.html"
    input Modelica.SIunits.Length a;
    input Modelica.SIunits.Length b;
    input Modelica.SIunits.Distance c;
    output Real F;
  protected
    Real X,Y,p1,p2,p3,p4;
  algorithm
```

```
  X :=a/c;
  Y :=b/c;
  p1 :=log(sqrt(((1 + X^2)*(1 + Y^2))/(1 + X^2 + Y^2)));
  p2 :=X*sqrt(1 + Y^2)*atan(X/sqrt(1 + Y^2));
  p3 :=Y*sqrt(1 + X^2)*atan(Y/sqrt(1 + X^2));
  p4 :=-X*atan(X) - Y*atan(Y);
  F :=2/(Modelica.Constants.pi*X*Y)*(p1+p2+p3+p4);
end ViewFactorParallelRectangles;

function ViewFactorPerpendicularRectangles "l and w is th esize
    of each rectangle, d is the distance between them, as
described on http://www.thermalradiation.net/calc/sectionc/
    C-11.html"
  input Modelica.SIunits.Length w;
  input Modelica.SIunits.Length h;
  input Modelica.SIunits.Distance l;
  output Real F;
protected
  Real H,W,p1,p2,p3,p4;
algorithm
  H :=h/l;
  W :=w/l;
  p1 :=W*atan(1/W) + H*atan(1/H) - (H^2 + W^2)^0.5*atan(1/sqrt(H
      ^2 + W^2));
  p2 :=((1 + W^2)*(1 + H^2))/(1 + W^2 + H^2);
  p3 :=((W^2*(1 + W^2 + H^2))/((1 + W^2)*(W^2 + H^2)))^(W^2);
  p4 :=((H^2*(1 + H^2 + W^2))/((1 + H^2)*(H^2 + W^2)))^(H^2);
  F :=1/(Modelica.Constants.pi*W)*(p1 + 1/4*log(p2*p3*p4));
end ViewFactorPerpendicularRectangles;
block ViewFactor
  parameter Real amplitude=0.5 "Amplitude of trapezoid";
  parameter Modelica.SIunits.Time pouring(final min=0) "Pouring
      time";
  parameter Real active(final min=0, final max=100) "active in
      percentage";
  parameter Modelica.SIunits.Time period(final min=
      Modelica.Constants.small, start=1) "Time for one period";
  parameter Integer nperiod=-1 "Number of periods (< 0 means
      infinite number of periods)";
  parameter Real offset=0.5 "Offset of output signal";
  parameter Modelica.SIunits.Time startTime(final max=pouring)=0
      "Output = offset for time < startTime";
  extends Modelica.Blocks.Interfaces.SO;
  Real dy;
  Modelica.SIunits.Time T_ref "reference pouint for dy";
protected
  parameter Modelica.SIunits.Time T_active=period*active/100
    "End time of active phase in one period";
  parameter Modelica.SIunits.Time T_startconstant =
      pouring-startTime;
```

```
  parameter Modelica.SIunits.Time T_stopconstant =
     T_active-startTime;
  Modelica.SIunits.Time T_start "Start time of current period";
  Integer count "Period count";
  Real x;
initial algorithm
  count := integer((time - startTime)/period);
  T_start := startTime + count*period;
  T_ref := startTime + count*period;
  y :=offset;
equation
  dy = amplitude/(pouring/2);
  when integer((time - startTime)/period) > pre(count) then
    count = pre(count) + 1;
    T_start = time;
  end when;
  when {y>=offset+amplitude, y<=offset+amplitude, integer((time -
      startTime)/period) > pre(count)} then
    T_ref = time;
  end when;
  x = if (time>=T_start+T_startconstant and time <=T_start+
     T_stopconstant) then 0 else 1;
  der(y) = (
   if time < startTime then
     0
   else
     if (time < (T_start+T_active)) then
       if time>=T_start+T_startconstant and time <=T_start+
          T_stopconstant then
         0
       elseif (T_ref<=T_start) then
         dy
       else
          -dy
     else
         0);
end ViewFactor;

model ForcedConvection
  "Gnielsky-correlation for forced convection coefficient"
  extends
     Modelica.Thermal.FluidHeatFlow.Interfaces.Partials.FlowSensor
     (y(unit="W/(m2.K)")
      "Volume flow as output signal");
  parameter Modelica.SIunits.Length width, height;
  parameter Modelica.SIunits.CoefficientOfHeatTransfer h_free;
  Real Re, Pr, Nu, f;
  Modelica.SIunits.Diameter d_hyd;
  Modelica.SIunits.CoefficientOfHeatTransfer h_final, h_forced;
  Modelica.SIunits.Velocity v_air;
```

```
equation
  d_hyd = 4*(width*height)/(2*(width+height)); //=4*A/P
  v_air = V_flow/(width*height);
  Re = abs(v_air*d_hyd/medium.nue);
  Pr = medium.cp*medium.rho*medium.nue/medium.lamda;
  if Re <= 2300 then
    f=0;
    Nu=0;
    h_forced=0;
  else
    f = (0.79*log(Re)-1.64)^(-2); //Darcy friction factor, smoot
       tube friction factor by petukhov
    Nu = ((f/8)*(Re-1000)*Pr)/(1+12.7*(f/8)^0.5*(Pr^(2/3)-1));
    h_forced = Nu*medium.lamda/d_hyd;
  end if;
  h_final = max(h_forced, h_free);
  y = h_final;
end ForcedConvection;
```

A.2.3 Thermal energy storage components

```
model StorageHeatTransfer "heat transfer according to Yian"
  extends
     Modelica.Thermal.FluidHeatFlow.Interfaces.Partials.FlowSensor
     (y(unit="W/(m2.K)")
      "Volume flow as output signal");
  parameter Modelica.SIunits.Diameter di;
  parameter Modelica.SIunits.Diameter do;
  parameter Modelica.SIunits.ThermalConductivity k;
  parameter Real N_pipes;
  Real Re, Pr, Nu, f, Bi;
  Modelica.SIunits.CoefficientOfHeatTransfer h_forced, h_E;//
     h_geo;
  Modelica.SIunits.Velocity v;
  Modelica.SIunits.Diameter a,b;
equation
  //calculating forced convection heat transfer coefficient
  v = V_flow/(Modelica.Constants.pi*di^2/4*N_pipes);
  Re = abs(v*di/medium.nue);
  Pr = medium.cp*medium.rho*medium.nue/medium.lamda;
  if Re <= 2300 then
    f = 0;
    Nu = 4.36 "Uniform surface heat flux"; //=3.66 "uniform
       surface temperature";
    h_forced = Nu*medium.lamda/di;
  else
    f = (0.79*log(Re)-1.64)^(-2); //Darcy friction factor, smoot
       tube friction factor by petukhov
    Nu = ((f/8)*(Re-1000)*Pr)/(1+12.7*(f/8)^0.5*(Pr^(2/3)-1));
    h_forced = Nu*medium.lamda/di;
```

```
    end if;
    //calculating TES heat transfer coefficient
    a = di/2;
    b = do/2;
    1/h_E = 1/h_forced + 1/k*(4*a*b^4*log(b/a)-3*a*b^4+4*a^3*b^2-a
        ^5)/(4*(b^2-a^2)^2);
    y = h_E;
    Bi = h_E/medium.lamda*(b^2-a^2)/(2*a);
  end StorageHeatTransfer;

  model TES
    "not modeling the steel pipe itself, as the heat transfer
       through the concrete will be the limiting factor of this
       heat transfer"
  public
    parameter Modelica.Thermal.FluidHeatFlow.Media.Medium medium=
       Modelica.Thermal.FluidHeatFlow.Media.Medium()
      "Medium in the component";
    parameter Modelica.SIunits.Temperature  T0_HTF "starting
       temperature of the pipe";
    parameter Modelica.SIunits.Temperature  T0_first "starting
       temperature of the first storage module";
    parameter Modelica.SIunits.Temperature  T0_last "starting
       temperature of the last storage module";
    parameter Integer  N(min=1) "Number of discretizations";
    parameter Integer  N_pipes(min=1) "Number of pipes in pipe
       bundle";
    parameter Modelica.SIunits.HeatCapacity     C_tot;
    final parameter Modelica.SIunits.Length     L =  (C_tot/cp)/(
       N_pipes*Modelica.Constants.pi*(do^2-di^2)/4*rho) "Length of
       storage unit";
    parameter Modelica.SIunits.Length           D(min=di) "storage
       unit utilizes triangular tube pitch, D meter between pipe
       center axises";
    parameter Modelica.SIunits.Diameter         di "inner
       pipediameter/inner diameter of the energy storage unit";
    final parameter Modelica.SIunits.Diameter  do = sqrt(2*sqrt(3)*
      D^2/Modelica.Constants.pi) "outer pipediameter in the
       equivalent cylindrical storage";
    //hentet disse verdiene fra yian
    parameter Modelica.SIunits.SpecificHeatCapacity  cp = 1180 "
       specific heat capacity of the storage material";
    parameter Modelica.SIunits.Density                rho = 3100 "
       specific density of storage material";
    parameter Modelica.SIunits.ThermalConductivity    k = 2.65 "
       thermal conductivity of storage material";
    final parameter Modelica.SIunits.Mass m_HTF =
       Modelica.Constants.pi*di^2/4*L*N_pipes*medium.rho;
    Modelica.SIunits.HeatFlowRate         Q_tot "Total heat flux
       flowing into the TES";
```

```
  Modelica.SIunits.Energy                E_TES "Total stored heat";
  Modelica.SIunits.Temperature           T_in, T_out, T_first,
    T_last;
  Modelica.SIunits.ThermalConductance    UA;
  Modelica.SIunits.Mass                  m "Total mass of storage
    material";
  Modelica.Thermal.HeatTransfer.Components.HeatCapacitor
    heatCapacitor[N](each C=C_tot/N);
  Modelica.Thermal.FluidHeatFlow.Components.HeatedPipe HTFflow[N
    ](
    each medium=medium,
    each T0=T0_HTF,
    each V_flowLaminar=1,
    each V_flowNominal=2,
    each m=m_HTF/N,
    each h_g=0,
    each T0fixed=true,
    each dpLaminar=100,
    each dpNominal=2000);
  Modelica.Thermal.HeatTransfer.Components.Convection
    heatTransfer[N];
  StorageHeatTransfer storageHeatTransfer(
    di=di,
    do=do,
    k=k,
    medium=medium,
    N_pipes=N_pipes);
  Modelica.Blocks.Math.Gain gain(k(unit="m2")=
    Modelica.Constants.pi*di*N_pipes*L/N, y(unit="W/K"));
  Modelica.Thermal.FluidHeatFlow.Interfaces.FlowPort_a flowPort_a
    (medium=medium);
  Modelica.Thermal.FluidHeatFlow.Interfaces.FlowPort_b flowPort_b
    (medium=medium);
initial equation
  for i in 1:N loop
    heatCapacitor[i].T=T0_first+(i-1)*(T0_last-T0_first)/(N-1);
  end for;
equation
  //equations
  Q_tot = sum(heatCapacitor[1:N].port.Q_flow);
  T_in =HTFflow[1].T_a;
  T_out =HTFflow[end].T_b;
  T_first = heatCapacitor[1].T;
  T_last = heatCapacitor[end].T;
  m = C_tot/cp;
  UA = storageHeatTransfer.y*Modelica.Constants.pi*di*L*N_pipes;
  der(E_TES) = Q_tot;
  //connectors
  for i in 1:N-1 loop
    connect(HTFflow[i].flowPort_b, HTFflow[i + 1].flowPort_a);
```

```
    end for;
    for i in 1:N loop
      connect(gain.y, heatTransfer[i].Gc);
      connect(heatCapacitor[i].port, heatTransfer[i].solid);
      connect(heatTransfer[i].fluid, HTFflow[i].heatPort);
    end for;
    connect(storageHeatTransfer.flowPort_a, flowPort_a);
    connect(storageHeatTransfer.y, gain.u);
    connect(storageHeatTransfer.flowPort_b, HTFflow[1].flowPort_a);
    connect(HTFflow[end].flowPort_b, flowPort_b);
  end TES;
```

A.2.4 Power cycle and tunnel control

```
  model HeatExchanger
    parameter Modelica.Thermal.FluidHeatFlow.Media.Medium hotMedium
       =Modelica.Thermal.FluidHeatFlow.Media.Medium()
      "Medium in hot side";
    parameter Modelica.Thermal.FluidHeatFlow.Media.Medium
       coldMedium=Modelica.Thermal.FluidHeatFlow.Media.Medium()
      "Medium in cold side";
    parameter Modelica.SIunits.Temperature          T0_hot, T0_cold;
    parameter Integer                               N(min=1) = 2;
    parameter Modelica.SIunits.Mass                 m_hot, m_cold;
    //parameter Modelica.SIunits.ThermalResistance  R "Total
       thermal resistance";
    parameter Modelica.SIunits.ThermalConductance UA;
    parameter Boolean measureTcoldout=true "Measure the cold
       temperature outlet";
    Modelica.SIunits.HeatFlowRate                   Q_tot;
    Modelica.SIunits.Temperature                    T_hot_in,
       T_hot_out, T_cold_in, T_cold_out;
    Modelica.SIunits.Energy                         E_HX;
    Modelica.Thermal.FluidHeatFlow.Interfaces.FlowPort_a hotPort_a(
       medium=hotMedium);
    Modelica.Thermal.FluidHeatFlow.Interfaces.FlowPort_b hotPort_b(
       medium=hotMedium);
    Modelica.Thermal.FluidHeatFlow.Interfaces.FlowPort_a coldPort_a
       (medium=coldMedium);
    Modelica.Thermal.FluidHeatFlow.Interfaces.FlowPort_b coldPort_b
       (medium=coldMedium);
    Modelica.Thermal.FluidHeatFlow.Components.HeatedPipe coldPipe[N
       ](each medium=coldMedium,
      each T0=T0_cold,
      each V_flowLaminar=1,
      each V_flowNominal=2,
      each h_g=0,
      each m=m_cold/N,
      each T0fixed=false,
      each dpLaminar=100,
```

```
      each dpNominal=2000);
    Modelica.Thermal.FluidHeatFlow.Components.HeatedPipe hotPipe[N
      ](each medium=hotMedium,
      each T0=T0_hot,
      each V_flowLaminar=1,
      each V_flowNominal=2,
      each h_g=0,
      each m=m_hot/N,
      each T0fixed=false,
      each dpLaminar=100,
      each dpNominal=2000);
    Modelica.Thermal.HeatTransfer.Components.ThermalResistor
      thermalResistor[N](each R=N/UA);
    Modelica.Blocks.Interfaces.RealOutput Q_HX;
    Modelica.Blocks.Interfaces.RealOutput T_hotin;
    Modelica.Blocks.Interfaces.RealOutput T_hotout;
    Modelica.Blocks.Interfaces.RealOutput T_coldout;
  equation
    Q_tot = sum(coldPipe[1:N].heatPort.Q_flow);
    T_hot_in = hotPipe[end].T_b;
    T_hot_out = hotPipe[1].T_a;
    T_cold_in = coldPipe[1].T_a;
    T_cold_out = coldPipe[end].T_b;
    Q_HX = Q_tot;
    T_hotin = T_hot_in;
    T_hotout = T_hot_out;
    T_coldout = T_cold_out;
    der(E_HX) = Q_tot;
    connect(coldPort_a, coldPipe[1].flowPort_a);
    connect(coldPipe[N].flowPort_b, coldPort_b);
    connect(hotPort_a, hotPipe[N].flowPort_b);
    connect(hotPort_b, hotPipe[1].flowPort_a);
    for i in 1:N-1 loop
      connect(coldPipe[i].flowPort_b, coldPipe[i+1].flowPort_a);
      connect(hotPipe[i].flowPort_b, hotPipe[i+1].flowPort_a);
    end for;
    for i in 1:N loop
      connect(coldPipe[i].heatPort, thermalResistor[i].port_a);
      connect(thermalResistor[i].port_b, hotPipe[i].heatPort);
    end for;
  end HeatExchanger;
model CarnotPower
  parameter Real                  fraction(min=0,max=1)=0.5;
  parameter Modelica.SIunits.Temperature T_amb;
  Modelica.SIunits.Power      W_carnot,W_produced;
  Modelica.SIunits.Energy     E_carnot, E_produced;
  Real                        eta_carnot;
  Modelica.Blocks.Interfaces.RealInput Q;
  Modelica.Blocks.Interfaces.RealInput T_hotout;
  Modelica.Blocks.Interfaces.RealInput T_hotin;
```

```
  Modelica.Blocks.Interfaces.RealOutput W_prod annotation;
equation
  if noEvent(T_hotin > T_hotout) then
    eta_carnot = 1-T_amb/(T_hotin-T_hotout)*log(T_hotin/T_hotout);
  elseif noEvent(T_hotin < T_hotout) then
    eta_carnot = 1-T_amb/(T_hotout-T_hotin)*log(T_hotout/T_hotin);
  else
    eta_carnot = 0;
  end if;
  W_carnot = Q*eta_carnot;
  W_produced = fraction*W_carnot;
  W_prod = W_produced;
  der(E_carnot) = W_carnot;
  der(E_produced) = W_produced;
end CarnotPower;
```

A.2.5 System

```
  model System
    extends Modelica.Icons.Example;
  public
    parameter Modelica.Thermal.FluidHeatFlow.Media.Medium HTF =
       Modelica.Thermal.FluidHeatFlow.Media.Medium(rho = 55.13, cp
       = 1156, cv = 934, nue = 5.39e-7, lamda = 0.0467);
    parameter Modelica.Thermal.FluidHeatFlow.Media.Medium air =
       Modelica.Thermal.FluidHeatFlow.Media.Medium(rho = 0.736, cp
       = 1027, cv = 739, nue = 3.5e-5, lamda = 0.0378);
    parameter Modelica.Thermal.FluidHeatFlow.Media.Medium WF =
       Modelica.Thermal.FluidHeatFlow.Media.Medium(rho = 6.30, cp =
        2245, cv = 1659, nue = 3.17e-6, lamda = 0.0484);
    parameter SiliconParameters silicon=SiliconParameters() "
       silicon parameters";
    //moulds and tunnel
    parameter Modelica.SIunits.Length height = 0.75;
    parameter Modelica.SIunits.Length width =  1.8;
    parameter Modelica.SIunits.Length length = area/width;
    final parameter Modelica.SIunits.Area area = 2*2.18*10*1.003;
    parameter Modelica.SIunits.Velocity v_air = 1;
    parameter Modelica.SIunits.MassFlowRate m_htf = 15;
    parameter Modelica.SIunits.CoefficientOfHeatTransfer h_free=10;
    parameter Real  active(min=0, max=100) = 75;
    parameter Real  period(min=0) = 7200;
    parameter Real  pouring(min=0,max=period) = 1800;
    parameter Integer N_moulds = 10;
    parameter Integer N_partitions(min=1) = 3;
    parameter Integer N_mouldlayers(min=1)= 15;
    parameter Modelica.SIunits.Mass m_silicon = 9000;
    parameter Real e1 = 0.55 "emissivity of  cooling silicon";
    parameter Real e2 = 0.8 "emissivity of tunnel wall";
    parameter Real e3 = 0.99 "emissivity of surroundings, backbody"
```

```
    ;
parameter Modelica.SIunits.Temperature T0_HTF = 273.15+280;
parameter Modelica.SIunits.Temperature T_amb = 273.15+25;
parameter Modelica.SIunits.Temperature T0_mould = 273.15+1450;
parameter Modelica.SIunits.ThermalConductivity k_ins = 0.055;
parameter Modelica.SIunits.Length L_ins = 0.01;
//TES
parameter Modelica.SIunits.Temperature T0_TESfirst =
   353.4+273.15;
parameter Modelica.SIunits.Temperature T0_TESlast =
   384.3+273.15;
parameter Integer N_TES = 10;
parameter Integer N_TES_pipes = 350;//620;
parameter Modelica.SIunits.HeatCapacity C_tot = 7e7;
parameter Modelica.SIunits.Length   D = 80e-3;
parameter Modelica.SIunits.Diameter di = 10e-3;
//HX
parameter Integer N_HX = 10;
parameter Modelica.SIunits.ThermalConductance UA_HX = 1.1e4;
parameter Modelica.SIunits.MassFlowRate m_WF = 3.2;
parameter Modelica.SIunits.Temperature T0_WF = 100+273.15;
TunnelDiscrete tunnelDiscrete(
  air=air,
  HTF=HTF,
  N_moulds=N_moulds,
  N_partitions=N_partitions,
  N_mouldlayers=N_mouldlayers,
  active=active,
  period=period,
  pouring=pouring,
  e1=e1,
  e2=e2,
  e3=e3,
  T_amb=T_amb,
  T0_mould=T0_mould,
  T0_HTF=T0_HTF,
  length=length,
  width=width,
  height=height,
  m_silicon=m_silicon,
  v_air=v_air,
  s=silicon,
  h_free=h_free,
  useWallLoss=true);
TES tES(
  medium=HTF,
  T0_HTF=T0_HTF,
  N=N_TES,
  N_pipes=N_TES_pipes,
  C_tot=C_tot,
```

```
      D=D,
      di=di,
      T0_first=T0_TESfirst,
      T0_last=T0_TESlast);
    HeatExchanger heatExchanger(
      T0_hot=T0_HTF,
      T0_cold=T0_WF,
      N=N_HX,
      hotMedium=HTF,
      coldMedium=WF,
      UA=UA_HX,
      m_hot=45,
      m_cold=45,
      measureTcoldout=true);
    CarnotPower carnotPower(T_amb=T_amb);
    Modelica.Thermal.FluidHeatFlow.Sources.VolumeFlow volumeFlow(
       medium=HTF,
      m=0,
      useVolumeFlowInput=false,
      constantVolumeFlow=m_htf/HTF.rho);
    Modelica.Thermal.FluidHeatFlow.Sources.AbsolutePressure
       referencePressure(medium=
          HTF, p=100000);
    Modelica.Thermal.FluidHeatFlow.Sources.VolumeFlow volumeFlow1(
      medium=WF,
      m=0,
      useVolumeFlowInput=false,
      constantVolumeFlow=m_WF/WF.rho);
    Modelica.Thermal.FluidHeatFlow.Sources.Ambient RC_1(
      medium=WF,
      constantAmbientTemperature=T0_WF,
      constantAmbientPressure=100000);
    Modelica.Thermal.FluidHeatFlow.Sources.Ambient RC_2(
      medium=WF,
      constantAmbientTemperature=T_amb,
      constantAmbientPressure=100000);
  equation
    connect(tunnelDiscrete.flowPort_b, tES.flowPort_a);
    connect(tES.flowPort_b, heatExchanger.hotPort_a);
    connect(volumeFlow.flowPort_b, tunnelDiscrete.flowPort_a);
    connect(referencePressure.flowPort, tES.flowPort_a);
    connect(carnotPower.T_hotout, heatExchanger.T_hotout);
    connect(carnotPower.Q, heatExchanger.Q_HX);
    connect(heatExchanger.T_hotin, carnotPower.T_hotin);
    connect(volumeFlow1.flowPort_b, heatExchanger.coldPort_a);
    connect(heatExchanger.coldPort_b, RC_2.flowPort);
    connect(RC_1.flowPort, volumeFlow1.flowPort_a);
    connect(heatExchanger.hotPort_b, volumeFlow.flowPort_a);
  end System;
```